Fixed-time nonlinear homogeneous sliding mode approach for robust tracking control of multirotor aircraft: Experimental validation

Omar Mechali[a, b], Limei Xu[a, b], Jamshed Iqbal[c], Xiaomei Xie[a, b, *]

[a] *School of Aeronautics and Astronautics, University of Electronic Science and Technology of China, Chengdu, 611731, China*

[b] *Aircraft Swarm Intelligent Sensing and Cooperative Control Key Laboratory of Sichuan Province, University of Electronic and Technology of China, Chengdu 611731, China*

[c] *Department of Computer Science and Technology, Faculty of Science and Engineering, University of Hull, HU6 7RX, UK*

Abstract

This paper presents a robust scheme for fixed-time tracking control of a multirotor system. The aircraft is subjected to matched lumped disturbances, i.e., unmodeled dynamics, parameters uncertainties, and external perturbations besides measurement noise. Firstly, a novel Nonlinear Homogeneous Continuous Terminal Sliding Manifold (NHCTSM) based on the weighted homogeneity theory is presented. The sliding manifold is designed with prescribed dynamics featuring Global Asymptotic Stability (GAS) and fixed-time convergence. Then, a novel Fixed-time Non-switching Homogeneous Nonsingular Terminal Sliding Mode Control (FNHNTSMC) is proposed for the position and attitude loops by employing the developed NHCTSM and an appropriate reaching law. Moreover, the control framework incorporates a disturbance observer to feedforward and compensate for the disturbances. The designed control scheme can drive the states of the system to the desired references in fixed-time irrespective of the values of the Initial Conditions (ICs). Since the existing works on homogeneous controllers rely on the bi-limit homogeneity concept in the convergence proofs, the estimate of the settling-time or its upper-bound cannot be given explicitly. In contrast, this study employs Lyapunov Quadratic Function (LQF) and Algebraic Lyapunov Equation (ALE) in the stability analysis of both controller and observer. Following this method, an expression of the upper-bound of the settling-time is explicitly derived. Furthermore, to assure the Uniform Ultimate Boundedness (UUB) of all signals in the feedback system, the dynamics of the observer and controller are jointly analyzed. Simulations and experiments are conducted to quantify the control performance. The proposed approach achieves superior performance compared with recent literature on fixed-time/finite-time control and a commercially available PID controller. The comparative results witness that the developed control scheme improves the convergence-time, accuracy, and robustness while overcoming the singularity issue and mitigating the chattering effect of conventional SMC.

Keywords: Quadrotor aircraft; Trajectory tracking control; Fixed-time stability; Bounded settling-time; Weighted homogeneity; Nonsingular terminal sliding mode control; Real-time experiment.

Nomenclature

General-purpose mathematical symbols and notations	
$\approx, \stackrel{\text{def}}{=}, \equiv$	Is approximately equal to, is by definition equal to, is equivalent to
$\mathbb{R}, \mathbb{R}^n$	Set of the real numbers, n-dimensional state space
$\mathbb{R}_+$	$\mathbb{R}_+ \stackrel{\text{def}}{=} \{\mathrm{x} \in \mathbb{R}: \mathrm{x} > 0\}$, is the set of positive real numbers
$\dot{f}, \ddot{f}$	First and second derivatives of a given entity f
$\mathcal{C}^1$	Space of continuously differentiable functions
$\lvert\cdot\rvert$	Absolute value in $\mathbb{R}$
$\lVert\cdot\rVert_p, \lVert\cdot\rVert$	p-norm on $\mathbb{R}^n$ defined for a vector $\mathrm{v} \in \mathbb{R}^n$ as $\lVert\mathrm{v}\rVert_p \stackrel{\text{def}}{=} (\sum_{i=1}^{n} \lvert\mathrm{v}_i\rvert^p)^{1/p}$. In particular, $\lVert\mathrm{v}\rVert$ stands for the 2-norm
$\mathrm{x}(0) = \mathrm{x}_0$	Initial Condition (IC) of a given system at $t = 0$
$\exp(\cdot)$	Exponential function. $\forall \mathrm{x} \in \mathbb{R}, \exp(\mathrm{x}): \mathbb{R} \to \mathbb{R}, \mathrm{x} \mapsto e^{\mathrm{x}}$, where the base $e = 2.71828\ldots$
sx, cx, tx	$\mathrm{sx} \stackrel{\text{def}}{=} \sin \mathrm{x}$, $\mathrm{cx} \stackrel{\text{def}}{=} \cos \mathrm{x}$, and $\mathrm{tx} \stackrel{\text{def}}{=} \tan \mathrm{x}$
$\mathrm{x} \mapsto \mathrm{sign}^{\alpha}(\mathrm{x})$	$\mathrm{sign}^{\alpha}(\mathrm{x}) \stackrel{\text{def}}{=} \lvert\mathrm{x}\rvert^{\alpha}\mathrm{sign}(\mathrm{x})$ for any $\mathrm{x} \in \mathbb{R}$ and $\alpha \in \mathbb{R}_+$
$\mathrm{sign}(\cdot)$	Standard signum function, where $\mathrm{sign}(\mathrm{x}) = 1$ if $\mathrm{x} > 0$, $\mathrm{sign}(\mathrm{x}) = 0$ if $\mathrm{x} = 0$, and $\mathrm{sign}(\mathrm{x}) = -1$ if $\mathrm{x} < 0$
I	Identity matrix
$\lambda_{\min}(M), \lambda_{\max}(M)$	Minimum and maximum eigenvalues of a matrix $M \in \mathbb{R}^{n \times n}$
$\mathrm{diag}(\mathrm{a}_1, \mathrm{a}_2, \ldots, \mathrm{a}_n)$, $\mathrm{a}_n \in \mathbb{R}$	Diagonal matrix
t, τ, t_0, t_f	Time variables
i	Subscript indicating the i-th element of a given vector quantity
$i = \overline{1, n}$	Denotes a sequence of n element $i = 1, \ldots, n$
Notation for the rest of the manuscript	
$\mathrm{E} \stackrel{\text{def}}{=} (\mathcal{O}_E, x_E, y_E, z_E)$	Earth-fixed (inertial) frame 'E-frame'
$\mathrm{B} \stackrel{\text{def}}{=} (\mathcal{O}_B, x_B, y_B, z_B)$	Body-fixed frame 'B-frame'
$\xi^E \stackrel{\text{def}}{=} [x \quad y \quad z]_E^T$	Aircraft position in E-frame, m
$\mathcal{V}^E \stackrel{\text{def}}{=} [v_x \quad v_y \quad v_z]_E^T$	Linear velocities of the vehicle, m/s
$\Theta^B \stackrel{\text{def}}{=} [\Phi \quad \theta \quad \psi]_B^T$	Aircraft attitude (Euler angles) in B-frame, rad
$\dot{\Theta}^B \stackrel{\text{def}}{=} [\dot{\Phi} \quad \dot{\theta} \quad \dot{\psi}]_B^T$	Attitude rates, rad/s
$\zeta^B \stackrel{\text{def}}{=} [p \quad q \quad r]_B^T$	Angular velocities, rad/s
$W_{\zeta^B \to \dot{\Theta}^B}^{-1}(\Theta^B) \in \mathbb{R}^{3\times3}$	Skew-symmetric matrix, i.e., $W_{\zeta^B \to \dot{\Theta}^B}^T = -W_{\zeta^B \to \dot{\Theta}^B}$, describing the relationship between $\dot{\Theta}^B$ and ζ^B
$\mathrm{R}_{B \to E} \in \mathbb{R}^{3\times3}$	Rotation matrix from B-frame to E-frame
$F_l^B, F_{\mathrm{g}}^E, F_a^E \in \mathbb{R}^3$	Total lift force, gravity force, and aerodynamic drag force, respectively, N

$\tau_m^B, \tau_a^B, \tau_g^B \in \mathbb{R}^3$	Motors torque, aerodynamic friction torque, and gyroscopic torque, respectively, N.m
$F_d^E \triangleq d_\xi^{\text{ext}}, \tau_d^B \triangleq d_\theta^{\text{ext}} \in \mathbb{R}^3$	External acceleration disturbances acting on the quadrotor's translational and rotational accelerations dynamics, respectively, e.g., wind, m/s^2, rad/s^2
$J \triangleq \text{diag}(J_{xx}, J_{yy}, J_{zz}) \in \mathbb{R}_+^{3\times3}$	Moments of inertia matrix, kg.m^2
$\text{g} = 9.81\ \text{m/s}^2$	Gravitational acceleration constant
m	Total mass of the quadrotor, kg
$K_a \triangleq \text{diag}(k_x, k_y, k_z) \in \mathbb{R}_+^{3\times3}$	Diagonal aerodynamic drag matrix
$u_\theta \triangleq [u_\Phi \quad u_\theta \quad u_\psi]_B^T$	Control inputs (control torques) for Euler angles, i.e., roll, pitch, and yaw, N.m
u_z	Thrust control (total lift force), N
$J_r \in \mathbb{R}_+$	Inertia of the rotor, kg.m^2
$c_\Phi, c_\theta, c_\psi \in \mathbb{R}_+$	Aerodynamic friction coefficients
$\Omega_i, i = \overline{1,4}$	Angular speed of the rotors, rad/s
$c_d, c_t \in \mathbb{R}_+$	Air-drag and thrust coefficients, N/(m/s)^2, N/(rad/s)^2
$l \in \mathbb{R}_+$	Length of the quadrotor arm, m
$f_i \in \mathbb{R}_+, i = \overline{1,4}$	Thrust force of the i-th rotor, N
$\bar{\omega} \triangleq \Omega_1 - \Omega_2 + \Omega_3 - \Omega_4$	Overall residual angular velocity of the rotor, rad/s
$\mathcal{P}$	Notation symbolizes the system's parameters
$\mathcal{N}, \Delta$	Superscripts indicating nominal and uncertain parts of the system's parameters $\mathcal{P}$
$d_\theta^{\text{unm}}, d_\xi^{\text{unm}} \in \mathbb{R}^3$	Internal unmodeled dynamics
$d_\theta^{\text{lum}}, d_\xi^{\text{lum}} \in \mathbb{R}^3$	Total lumped disturbances, including unmeasurable external disturbances and internal disturbances (unmodeled dynamics and parametric uncertainties)
$\text{x}, X_\theta, X_\xi, \chi_1, \chi_2, \bar{\text{x}}, x$	State vectors
$\mathcal{Y}_1, \mathcal{Y}_2$	Vectors of the controlled states, $\mathcal{Y}_1 \triangleq [\Phi \quad \theta \quad \psi]_B^T, \mathcal{Y}_2 \triangleq [x \quad y \quad z]_E^T$
$f_\theta^{\mathcal{N}}(\chi_2, \mathcal{P}_1^{\mathcal{N}}, t)$, $g_\theta^{\mathcal{N}}(\mathcal{P}_2^{\mathcal{N}}, t)$	Nonlinear functions characterizing attitude dynamics
$F_\xi \triangleq [F_x \quad F_y \quad F_z]^T$	Function that describes the coupling between rotational and translational motions
$\Theta_d(t), \xi_d(t)$	Desired reference signals
$e_1^\theta(t), e_1^\xi(t)$	Attitude and position tracking errors
$e_2^\theta(t), e_2^\xi(t)$	Tracking errors dynamics
T_θ, T_ξ	Convergence-time of attitude and position tracking errors, s
$T_\theta^{\max}, T_\xi^{\max}$	Upper-bounds on T_θ and T_ξ, respectively
$T_x, T_x^{\max}$	Convergence-time of the roll states and its upper bound
$T_0, T_0^{\max}$	Convergence-time and its upper bound
$T_1, T_1^{\max}$	Convergence-time and its upper bound
$T_{\text{r}}, T_{\text{r}}^{\max}$	Convergence-time and its upped bound during the reaching phase of the sliding motion
$T_{\text{sm}}, T_{\text{sm}}^{\max}$	Sliding-time during the sliding mode
$(T_{\text{ob},\xi}, T_{\text{ob},\xi}^{\max})$, $(T_{\text{ob},\theta}, T_{\text{ob},\theta}^{\max})$	Convergence-time of the observers and related upped-bounds
$\mathcal{S}$	Sliding manifold
$s, s_{\text{x}_1}, s_\theta, s_\xi, \mathfrak{s}$	Sliding surfaces
$\mathcal{v}, \mathcal{w}, \mathcal{v}_\theta, \mathcal{w}_\theta, \mathcal{v}_\xi, \mathcal{w}_\xi$	Intermediate variables
$k_1^{\text{x}_1}, k_2^{\text{x}_1}, \bar{k}_1^{\text{x}_1}, \bar{k}_2^{\text{x}_1}, k_1^\theta, k_2^\theta, \bar{k}_1^\theta, \bar{k}_2^\theta, k_1^\xi, k_2^\xi, \bar{k}_1^\xi, \bar{k}_2^\xi, \gamma_1, \gamma_2, \bar{\gamma}_1, \bar{\gamma}_2, \gamma, \bar{\gamma}, \varepsilon_1, \varepsilon_2, k_i^{\bar{\text{x}}_i}, \bar{k}_i^{\bar{\text{x}}_i}$	Positive control design parameters
$k_1^{s\theta}, k_2^{s\theta}, k_1^{s\xi}, k_2^{s\xi}$	Positive control design parameters of the reaching law
A, B	Matrices to represent a linear system in state-space form, $A \in \mathbb{R}^{n\times n}, B \in \mathbb{R}^n$
$u_x, u_{\bar{\text{x}}}, u_z$	Control inputs for some given systems
Ξ, x, z, Ξ_z	Variables of Lyapunov Functions (LFs)
$V_1(\Xi), V_1(x), V_2(\Xi), V_2(x), V_\theta(s_\theta), V(s_\theta, e_1^\theta, e_2^\theta), V_z(z), V_z(\Xi_z)$	LFs
$A_1, P_1^x, Q_1^x, A_2, P_2^x, Q_2^x, A_z, P_z^\xi, Q_z^\xi, P_z^\theta, Q_z^\theta, P_1^{\bar{\text{x}}}, Q_1^{\bar{\text{x}}}, P_2^{\bar{\text{x}}}, Q_2^{\bar{\text{x}}}$	Matrices for constructing the ALEs
$l_1, l_2, l_3, \kappa_1, \kappa_2, \kappa_3, \kappa_z$	Degrees of homogeneity
$r_i, r_{i,z}, (i = \overline{1,n})$	Weights of homogeneity
$c_1, c_2, c_z \in \mathbb{R}_+$	Positive constant
$\beth \in \mathbb{R}_+$	Positive number
$\delta \in \mathbb{R}_+$	Arbitrarily small positive constant
u_{r}^θ	Reaching control
u_{eq}^θ	Equivalent control
$\alpha, \beta \in \mathbb{R}_+$	Positive exponents
$\bar{\alpha}, \bar{\beta} \in \mathbb{R}_+$	Positive constants
$\hat{d}_\theta^{\text{lum}}, \hat{d}_\xi^{\text{lum}} \in \mathbb{R}^3$	Estimates of the lumped disturbances $d_\theta^{\text{lum}}, d_\xi^{\text{lum}}$
$F_\xi^d \in \mathbb{R}^3$	Desired virtual controls of the position states
$e_1^{\text{ob}}, e_2^{\text{ob}}, e_3^{\text{ob}}$	Observation error
$K_V, L_V \in \mathbb{R}$	Bounded positive constants
$\bar{d}_\theta, \bar{d}_\xi \in \mathbb{R}_+$	Upper-bounds on the lumped disturbances $d_\theta^{\text{lum}}, d_\xi^{\text{lum}}$
$\Lambda(t)$	Switching function defined as $\Lambda(t): [0,\infty) \to \{0.1\}$, $\Lambda(t) = 0$ if $t \le T_u$, $\Lambda(t) = 1$ if $t > T_u$, where T_u is switching time
$\bar{\tau}$	Small positive time constant
$\Gamma_1^\xi, \Gamma_2^\xi, \Gamma_3^\xi$	Estimates of $\xi, \mathcal{V}$ and d_ξ^{lum}, respectively, i.e., $\Gamma_1^\xi \equiv \hat{\xi}, \Gamma_2^\xi \equiv \hat{\mathcal{V}}, \Gamma_3^\xi \equiv \hat{d}_\xi^{\text{lum}}$
$\sigma_i, \varrho_i, \rho_i^\xi, \bar{\rho}_i^\xi, (i = \overline{1,3}), \bar{\sigma}, \bar{\varrho}, \varepsilon_3, \varepsilon_4$	Positive parameters for observer design
A_{ob}^ξ	A Hurwitz matrix used for observer's gains selection
$v_{w,\xi}, k_d^\xi$	Velocity of the Dryden wind model. Coefficient related to the Dryden wind

1 Introduction

1.1 Background Motivations and Context of the Study

Quadrotors are the most popular and useful kind of Unmanned Aerial Vehicles (UAVs) owing to their particular flight mode, variety of sizes, and high maneuverability. These aircraft have been widely used for solving complex missions [1] [2] [3]. The research related to the quadrotors and their applications is an active and emerging domain in the scientific community related to aerospace, robotics, mechatronics, and control engineering practice. Nevertheless, despite the numerous merits and advantages of the quadrotors UAVs, they have some critical drawbacks related to stabilization and control. In practice, these aircraft are inevitably affected by various disturbances induced by parametric uncertainties, unmodeled dynamics, wind gusts, and load perturbations [4] [5]. This leads to great difficulties in tracking and control. Notably, Cartesian trajectory tracking is a fundamental task for the operation of the autonomous quadrotors. Substantially, since the quadrotor exhibits underactuated dynamics, the control of the position states is realized through the stabilization of the attitude states. The strongly coupled and highly nonlinear nature of the quadrotor's dynamics further makes the design of the control system challenging [6]. Hence, the autonomous flight of

quadrotor aircraft requires an adequate and reliable flight control algorithm to achieve stability and high performance, thus, fulfilling the mission requirements. Convergence-time, disturbance rejection, and control precision are primary decisive features for the control algorithm during flight missions [1]. Substantially, convergence-time should be carefully addressed in the control design since it is a crucial factor for some applications of the quadrotors. This distinguishing feature is more prominent in the cooperative control of multi-agent systems, notably for the formation control of the quadrotors required to converge to the desired spatial formation pattern quickly. Up to date, fixed-time convergence is considered as the ultimate convergence rate for dynamical systems [7]. Unfortunately, linear control seems unable to achieve fixed-time convergence, robustness, and precision at the same time. Thus, it is natural to discuss which control methodology can achieve all these features simultaneously. To this end, this study aims to investigate the combination of the weighted homogeneity theory and SMC theory. Such procedure allows attaining the foregoing objective while avoiding chattering and singularity problems inherent in classical SMC. Ultimately, the homogeneity property allows preserving the fast (finite/fixed) convergence feature besides robustness and chattering alleviation.

However, another pertinent problem consists in estimating the settling-time for the homogeneous-based control laws. Mathematical proofs based on the bi-limit homogeneity approach are widely used [8] [9] [10] [11] [12]. Nevertheless, these proofs are limited since the bi-limit homogeneity concept cannot estimate the convergence-time or its upper bound. Besides the above crucial problems, another critical issue should be addressed. SMC is known to be robust against parameters uncertainties, modeling errors, and matching disturbances. Nonetheless, the control performance may be threatened in the presence of strong external disturbances acting on the quadrotor. Hence, to deal with this shortcoming, an Active Disturbance Rejection Control (ADRC) approach is developed in this study to reject the strong lumped disturbances and thus preserve the nominal control performance.

As a result, the present manuscript investigates the design of a novel flight-control system that is based on homogeneous SMC. This aims to address the robust tracking control problem for the four-rotor aircraft while ensuring good flight performance regarding the convergence-time, disturbance rejection, and control precision.

1.2 Literature Review of Related Works

Scientific literature reports various linear control laws for trajectory tracking of a quadrotor aircraft, such as Proportional Integral Derivative (PID) and Linear Quadratic Regulator (LQR) [13]. However, linear control laws are known to demonstrate adequate performance only in the close vicinity of the equilibrium point around which the quadrotor model is linearized. Moreover, linear controllers are sensitive to model nonlinearities and strong disturbances. In reality, the quadrotor operates in challenging flight environments and may perform aggressive movements leading to exhibit a strong nonlinear response. Thus, the linear control laws are incapable of ensuring the desired performance consistently during flight operating modes. Fortunately, modern control has the ability to address shortcomings of the linear control counterpart by designing nonlinear control laws to ensure stable and safer flights for the aircraft throughout the mission.

Recently, Variable Structure Control (VSC) such as SMC has attracted considerable interest in designing robust controllers for a quadrotor system. Given the nonlinear, uncertain, and perturbated quadrotor dynamics, the SMC control laws are considered efficient and appropriate candidates [14] [15]. Such a method is known for its unparalleled advantages, such as design simplicity and robust treatment of disturbances and modeling uncertainties [16]. SMC-based control law consists of two key steps. The first step involves the design of a sliding manifold as per the desired dynamics, while the control law is designed in the second step. The control law is designed in such a way that the states of the system approach the sliding surface and remain there, finally converging to the origin [17]. Many research works recently reported in the literature deal with the disturbances on a quadrotor aircraft using SMC-based robust controllers [18]. Research in [19] proposes an SMC-based control law for a quadrotor's attitude control system. Backstepping SMC-based laws are presented in [20] and [21] to stabilize the inner attitude loop of a multirotor aircraft. However, these works utilize traditional (conventional, linear) SMC which suffers from the so-called chattering effects. This phenomenon deteriorates the control performance by introducing abnormal switching frequencies in the control input [22]. Such a control signal may lead to system instability. Furthermore, it can inevitably damage the brushless motors of the multirotor. In addition, the sliding surface of the traditional SMC is linear which implies that the states are guaranteed to converge asymptotically to the origin. Therefore, the settling-time being unpredictable cannot be estimated or adjusted in advance and the maximum limit of the settling-time is unknown [23].

In an attempt to improve the tracking performance, finite-time control is considered a promising solution [24]. For example, authors of [25] present a finite-time distributed resilient control of multiple heterogeneous battery energy storage under denial-of-service attacks. Ning *et al.* proposed a finite-time bipartite tracking control for networked systems described by double-integrator dynamics in [26]. Compared to infinite-time SMC, finite-time SMC exhibits better control performance, notably faster convergence [14]. Several research works have employed finite-time SMC for a quadrotor control. Among these works, a terminal SMC-based law for a quadrotor featuring finite-time convergence is designed in [27]. The work in [28] proposed a flatness-based adaptive SMC law to deal with the tracking control problem of a quadrotor in finite-time. Finite-time stabilization of a quadrotor aircraft subjected to time-dependant disturbances employing a modified nonlinear super twisting fast SMC is discussed in [29]. In general, the systems demonstrating finite-time stability exhibit superior performance as compared to their infinite-time counterparts; however, the finite-time control has an unavoidable drawback. The ICs deviating from the equilibrium point result in

unbounded settling-time growth, leading to a slow convergence-rate [30]. Besides, it is difficult, in some cases impossible, to obtain the ICs of dynamical systems in practice. Fixed-time stabilization has been introduced to address the slow convergence-rate problem. The fixed-time notion has been proposed as an extension of the finite-time stabilization in [31] and then formally defined in [32]. Fixed-time stability offers pre-definition and adjustment of a settling-time. This method stabilizes the states of the system in fixed-time irrespective of the values of the ICs. This distinguishing feature is pertinent in real-world flight operations of the quadrotor aircraft. Such temporal feature is instrumental in providing deep insight for both single quadrotor control and cooperative control of multi-quadrotor systems. Particularly in the case of the formation control of the quadrotors required to converge to the desired formation pattern in a uniform short time [33]. Fixed-time consensus is addressed in [7] for multiple wheeled mobile robots under leader-follower configuration with practical results. The work [34] comes up with a new fixed-time protocol that can avoid saturation problems, save energy, and ensure practical fixed-time leader-following consensus and practical fixed-time leaderless consensus. An edge-based fixed-time consensus approach is investigated in [35] to address the problem of distributed optimization for multiagent systems while ensuring state agreement in a fixed-time. The authors indicate that the results can be used for drone rendezvous within a required time. Few studies have investigated the fixed-time control for the quadrotor system. Also, since the reported works have witnessed some drawbacks, more efforts are required to fill in the gap while dealing with the stated issues. Research in [36] presented the design of a backstepping fixed-time control law exploiting the potential of adaptive neural control. Although this work treated model uncertainties, external disturbances are not considered. Also, the inherent issue of backstepping control law, i.e., "*explosion of complexity*", is not considered. The work in [8] proposed a robust homogeneous fixed-time control law for attitude and position variables while considering the disturbances acting on a quadrotor aircraft. But, the graphs of the attitude variables, i.e., roll and pitch angles, are not provided. The work [9] provides a fixed-time trajectory following for multi-quadrotors. Unfortunately, the convergence proofs of the fixed-time controllers in [8] and [9] are based on the bi-limit homogeneity analysis, which cannot estimate the convergence-time or its upper-bound. Another study in [37] considered the faults occurring in a quadrotor's actuators in addition to external disturbances and proposed a fixed-time homogeneous sliding mode active fault-tolerant law for attitude tracking. In this work, the fixed-time convergence is proved only for the reaching phase of the sliding manifold, and the global convergence-time, including the sliding phase is not provided. The work in [38] countered external disturbances acting on the quadrotor for trajectory tracking in fixed-time using a differential flatness-based SMC. Inspired by [39], this work introduces a homogeneous-based virtual control law in the recursive backstepping design to achieve fixed-time stability. However, the disturbances are not considered on the attitude dynamics, besides model uncertainties and parameters variation are not addressed. On the other hand, the works [8] [37] [38] have considered a high-fidelity model for the quadrotor with accurate awareness of the system's parameters. In reality, it is hard to identify the accurate values of the physical parameters precisely. Moreover, in most cases, the identification devices and equipment are not available in some laboratories. In addition, model uncertainties are unavoidably existing in the dynamic model. In contrast to the works [8] [37] [38], internal parametric and nonparametric uncertainties have been considered in our study besides external disturbances. Substantially, although the works [8] [9] [36] [37] [38] provide prominent simulation results, the experiment on a real hardware setup is not conducted to verify the theoretical findings. A recent motivating work that presents real experimental results on fixed-time tracking control of a quadrotor in the presence of disturbances is reported in [39]. However, the fixed-time convergence property has not been verified for different ICs. It is known that the fixed-time stability offers a prescribed convergence-time (within the physical limits of the system's velocity) because it is independent of the values of the ICs. It would have been more interesting if research in [39] provided at least simulation results to corroborate the theoretical understanding for the convergence property of the fixed-time stability. Unlike [39], our work provides a detailed control methodology including theoretical design and analysis besides practical technological implementation. Similar to [8] and [37], the work [39] is limited to fixed-time stabilization of the 3- Degrees of Freedom (DoF) attitude dynamics. These works have not investigated fixed-time control for the complete 6-DoF dynamics of the vehicle. The attitude states are fully actuated making the control design much easier. Unlike that, we have investigated fixed-time control of the attitude and position loops simultaneously, where the underactuated problem inherent in the quadrotor dynamics has been addressed. To the best of the authors' knowledge, few works reported in the literature (e.g. [8] [9] [36] [37] [38] and [39]) address the design of fixed-time control laws for a quadrotor. Moreover, these works have some shortcomings that need to be stressed.

As has been mentioned above, SMC is an efficient control method to achieve superior control performance. However, it still suffers from some shortcomings [14] that limit its application to a quadrotor system. Therefore, to take advantage, i.e., fast convergence rate and robustness, of the SMC and simultaneously avoiding chattering and singularity problems, we here employ homogeneity theory to design a fixed-time continuous nonsingular and chattering-free SMC controller. The homogeneity concept has been introduced by Andrieu *et al*. in [31]. It has been shown that if the origins of the two approximating functions in the bi-limit, i.e., 0-limit and ∞-limit, of a given system are GAS with a negative and positive degree of homogeneity, respectively, then the system's origin demonstrates stability in fixed-time. The analyses based on the bi-limit homogeneity concept have been used as the basis of many proofs of fixed-time stability for homogeneous dynamical systems. For instance, in our previous work [10] and the works reported in [8] [9] [11] [12]. However, these mathematical proofs based on the bi-limit homogeneity approach are limited since they cannot estimate the convergence-time or its upper

bound. The motivating work proposed by Basin *et al*. in [40] provides interesting results on the fixed-time stability of homogeneous controllers by engaging another alternative.

A fundamental conclusion deduced from the previous research works and analyses is that persistent and thorough efforts are required on the practical aspect of fixed-time stability and homogeneous systems. Particularly in the context of quadrotor aircraft to thoroughly exploit the potential of these advanced concepts. Owing to the importance and emerging nature of the fixed-time robust control laws, further real-time studies on experimental platforms need to be conducted. These experimental investigations are highly suggested as they serve the purpose of bridging the gap between mathematical foundations and technological innovations, which is essentially the key purpose of this research.

1.3 Theoretical and Practical Contributions

Motivated by the above studies and the work [40], the present research investigates a robust nonlinear control scheme for the quadrotor system. The aircraft is subjected to parametric variations, modeling uncertainties, and time-dependent disturbances externally acting on the aircraft. The following theoretical and practical aspects demonstrate the main contributions of the present research:

(i) Inspired by the weighted homogeneity theory, a novel NHCTSM with prescribed dynamics featuring fixed-time convergence and GAS is designed. Next, a general methodology is established for designing fixed-time stabilization feedback controllers for uncertain nonlinear n -th order systems. Following the proposed design procedure, a novel control law is synthesized to deal with the robust tracking control of a multirotor aircraft. The chattering phenomenon is mitigated since the designed control scheme is continuous by nature. Moreover, the control law avoids the singularity problem since the design does not require the derivative of terms with fractional powers.

(ii) The fixed-time convergence proof of the feedback-loop system is conducted using LQF and ALE. In contrast to the works [8] [9] [10] [11] [12] [41], the present research provides an explicit expression of the convergence-time for the proposed homogeneous-SMC-based controller. To the best of our knowledge, this is the first attempt to provide an explicit settling-time expression of a homogeneous SMC control law being designed for the nonlinear, coupled, and underactuated quadrotor system. Besides, the observer-controller dynamics are jointly analyzed to assure the Uniform Ultimate Boundedness (UUB) of all signals in the feedback system.

(iii) A quadrotor hardware platform is built and comparative analyses with other robust fixed/finite-time controllers are carried out based on real-time experimental tests. To the best of the authors' knowledge, few reported works address the practical implementation of the fixed-time control laws for quadrotor aircraft.

This manuscript is organized into six sections: Section 2 presents preliminary foundations and problem statement. The main results of the work are presented in Section 3. Simulation and hardware-based results are presented and critically discussed in Section 4 and Section 5, respectively. Finally, Section 6 concludes the manuscript.

2 Preliminary Foundations and Problem Statement

2.1 Preliminaries

This section introduces related terminologies and mathematical lemmas required for the design of the control law and stability analysis conducted in the present research.

Consider the following ordinary differential equation describing a nonlinear autonomous system

$$\dot{\mathrm{x}}(t) = f(t,\mathrm{x}),\ \mathrm{x}(0) = \mathrm{x}_0,\ \mathrm{x} \in \mathbb{R}^n \text{ and } t \in \mathbb{R}_+. \tag{1}$$

where x is the state and $f: \mathbb{R}_+ \times \mathbb{R}^n \to \mathbb{R}$ is a nonlinear continuous function (or vector field: $f: \mathbb{R}_+ \times \mathbb{R}^n \to \mathbb{R}^n$) on an open neighborhood $\mathfrak{O} \subseteq \mathbb{R}^n$ of the origin such that the set $f(t,\mathrm{x})$ is non-empty for any $\mathrm{x} \in \mathfrak{O}$, and $f(t,0) = 0$ for all $t > 0$. The point $\mathrm{x}(0) = \mathrm{x}_0$ is the IC of system (1). The solutions of system (1) are understood in the Filippov sense [42] if $f(t,\mathrm{x})$ is discontinuous. Suppose that the origin $\mathrm{x} = 0$ is an equilibrium point of (1). The following subsection introduces some interesting notions on the stability of the system (1).

2.1.1 Notions on Finite-Time Stability, Fixed-Time Stability, and Weighted Homogeneity

Definition 1. ([10]). (Finite-time stability). The origin $\mathrm{x} = 0$ of system (1) is said to be globally finite-time stable if it is GAS and there are an open neighborhood $\mathfrak{U} \subseteq \mathfrak{O}$ of the origin and a function $T_{\mathrm{x}}(\mathrm{x}_0): \mathfrak{U}\backslash\{0\} \to \mathbb{R}_+ \cup \{0\}$ such that every solution $\mathrm{x}(t,\mathrm{x}_0)$ of system (1) starting from the initial point $\mathrm{x}_0 \in \mathfrak{U}\backslash\{0\}$ is well-defined for $t \in [0, T_{\mathrm{x}}(\mathrm{x}_0))$, and $\lim_{t \to T_{\mathrm{x}}(\mathrm{x}_0)} \mathrm{x}(t,\mathrm{x}_0) = 0$. $T_{\mathrm{x}}(\mathrm{x}_0)$ denotes the settling-time function (w.r.t. x_0) or a function corresponding to the time of convergence. If $\mathfrak{U} = \mathfrak{O} = \mathbb{R}^n$, the origin is said to exhibit global stability in finite-time.

Definition 2. ([32]). (Fixed-time stability). The equilibrium point $\mathrm{x} = 0$ of the system (1) is said to be globally fixed-time stable if it is globally finite-time stable and the settling-time function $T_{\mathrm{x}}(\mathrm{x}_0)$ is bounded independently w.r.t. IC x_0, i.e., $\exists T_{\mathrm{x}}^{\max} \in \mathbb{R}_+$, such that $T_{\mathrm{x}}(\mathrm{x}_0) \leq T_{\mathrm{x}}^{\max}$, $\forall \mathrm{x}_0 \in \mathbb{R}$.

Definition 3. ([31]). (Weighted homogeneity). Let $r = [r_1, r_2, \ldots, r_n]^T \in \mathbb{R}_+^n$ be the weight vector. The dilation mapping is defined by $\Lambda_\lambda^r(\mathrm{x}) = [\lambda^{r_1}\mathrm{x}_1, \lambda^{r_2}\mathrm{x}_2, \ldots, \lambda^{r_n}\mathrm{x}_n]^T$ for $\forall \lambda > 0$ and $\forall \mathrm{x} \in \mathbb{R}^n$. A function $f_i(\mathrm{x}): \mathbb{R}^n \to \mathbb{R}$ is said to be r- homogeneous with degree $\kappa \in \mathbb{R}$ if for $\forall \mathrm{x} \in \mathbb{R}^n$ and $\forall \lambda > 0$, $f_i\big(\Lambda_\lambda^r(\mathrm{x})\big) = \lambda^\kappa f_i(\mathrm{x})$ holds. A vector field $f(\mathrm{x}): \mathbb{R}^n \to \mathbb{R}^n$, where $f(\mathrm{x}) = [f_1(\mathrm{x}), f_2(\mathrm{x}), \ldots, f_n(\mathrm{x})]^T$ is said to be r -

homogeneous with degree $\kappa \in \mathbb{R}$ if the component $f_i(\mathrm{x})$ is r-homogeneous with degree of $\kappa + r_i$, i.e., $f_i\left(\Lambda_\lambda^r(\mathrm{x})\right) = \lambda^{\kappa+r_i} f_i(\mathrm{x})$ for $\forall \lambda > 0$.

Definition 4. ([43]). ($p = \{0, \infty\}$-limit homogeneity). Let r_p be a generalized weight, $\kappa_p \in \mathbb{R}$ and $f_p(\mathrm{x})$ be a function (resp. a vector field). A function (resp. a vector field) $f(\mathrm{x})$ is said to be homogeneous in the p-limit with associated triples (r_p, κ_p, f_p) if $\lim_{\lambda \to p} \sup_{\mathrm{x} \in \mathrm{C}} \left\| \lambda^{-\kappa_p} f\left(\Lambda_\lambda^{r_p} \mathrm{x}\right) - f_p(\mathrm{x}) \right\| = 0, \forall \lambda > 0$ (resp. if $\lim_{\lambda \to p} \sup_{\mathrm{x} \in \mathrm{C}} \left\| \lambda^{-\kappa_p} \left(\Lambda_\lambda^{r_p}\right)^{-1} f\left(\Lambda_\lambda^{r_p} \mathrm{x}\right) - f_p(\mathrm{x}) \right\| = 0$) for all compact subsets $\mathrm{C} \in \mathbb{R}^n \backslash \{0\}$. A function or a vector field is said to be homogeneous in the bi-limit if it is homogeneous in the 0-limit and the ∞-limit simultaneously.

2.1.2 Mathematical Lemmas

Lemma 1. ([1]). Suppose there exists a continuous positive-definite Lyapunov function $V(t, \mathrm{x}): \mathbb{R}_+ \times \mathbb{R}^n \to \mathbb{R}_+ \cup \{0\}$, and its derivative satisfying $\dot{V}(t, \mathrm{x}) \leq -k_1 V^{\wp} - k_2 V^{q}$, where $k_1, k_2 > 0, \wp > 1$, and $q < 1$ are some positive constants, then the origin of system (1) is fixed-time stable. The settling-time function T_{x} is bounded as $T_{\mathrm{x}} \leq T_{\mathrm{x}}^{\max} \triangleq \frac{1}{k_1(\wp - 1)} + \frac{1}{k_2(1-q)}$.

Lemma 2. ([44]). Suppose V_1 and V_2 are continuous real-valued functions on $\mathbb{R}^n$, homogeneous of degrees $\kappa_1 > 0$ and $\kappa_2 > 0$, respectively, and V_1 is positive definite. Then, for every $\mathrm{x} \in \mathbb{R}^n$

$$\left[\min_{\{\bar{z}: V_2(\bar{z})=1\}} V_2(\bar{z})\right] V_1^{\frac{\kappa_2}{\kappa_1}}(\mathrm{x}) \leq V_2(\mathrm{x}) \leq \left[\max_{\{\bar{z}: V_2(\bar{z})=1\}} V_2(\bar{z})\right] V_1^{\frac{\kappa_2}{\kappa_1}}(\mathrm{x}).$$

Lemma 3. ([45] [46]). (Rayleigh-Ritz). Let $\boldsymbol{A} = \boldsymbol{A}^{\boldsymbol{T}} \in \mathbb{R}^{\boldsymbol{n} \times \boldsymbol{n}}$ be a square symmetric matrix and $\mathbf{x} \in \mathbb{R}^{\boldsymbol{n}}$ be any $\boldsymbol{n}$-dimensional real vector satisfying $\mathbf{x} \neq \mathbf{0}$. The Rayleigh quotient of the vector $\mathbf{x}$ is defined as

$$\mathcal{R}(\mathrm{x}) \triangleq \frac{\mathrm{x}^T A \mathrm{x}}{\mathrm{x}^T \mathrm{x}}.$$

Let the eigenvalues of A be labelable according to the increasing (non-decreasing size) as: $\lambda_1 = \lambda_{\min} \leq \lambda_2 \leq \cdots \leq \lambda_{n-1} \leq \lambda_n = \lambda_{\max}$. The smallest and largest eigenvalues are characterized as a solution to the constrained minimum-maximum problem as

$$\max_{\mathrm{x} \in \mathbb{R}^n : \mathrm{x} \neq 0} \mathcal{R}(\mathrm{x}) = \lambda_{\max}(A),$$
$$\min_{\mathrm{x} \in \mathbb{R}^n : \mathrm{x} \neq 0} \mathcal{R}(\mathrm{x}) = \lambda_{\min}(A).$$

2.2 Problem Statement

2.2.1 Mathematical Modeling of the Quadrotor System

The quadrotor's (Fig. 1) motion in space can be described by two 3-D coordinate frames as illustrated in Fig. 2, namely, B-frame and E-frame. The rotational motion is described by B-frame, i.e., Euler angles $\Theta^B = [\Phi \quad \theta \quad \psi]_B^T$, while the translational motion is represented by E-frame $\xi^E = [x \quad y \quad z]_B^T$.

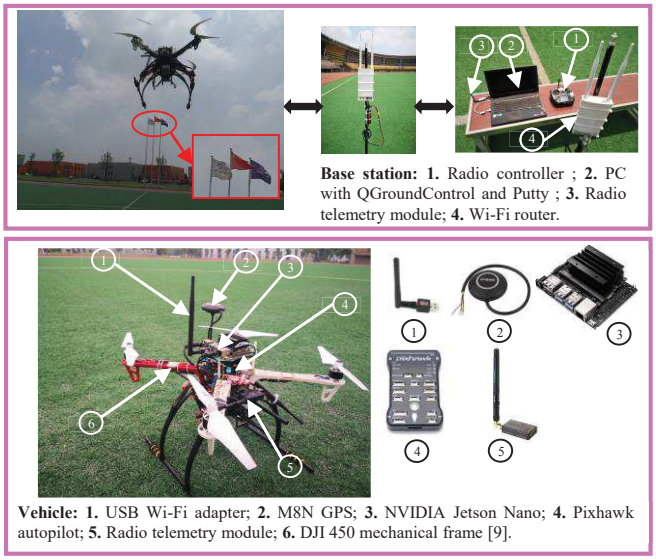

Fig. 1. Experimental setup for the real outdoor flight of the quadrotor aircraft. The experiment is conducted in a windy outdoor area.

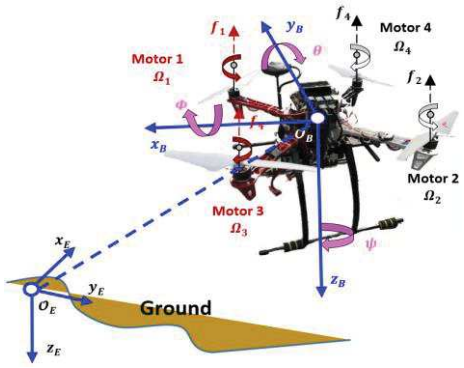

Fig. 2. Representation of the quadcopter in both E-frame and B-frame.

The attitude rates $\dot{\Theta}^B$ and the angular velocities ζ^B are related by the following relationship [47]

$$[\dot{\Phi} \quad \dot{\theta} \quad \dot{\psi}]_B^T \triangleq W_{\zeta^B \to \dot{\Theta}^B}^{-1}(\Theta^B)[p \quad q \quad r]_B^T. \tag{2}$$

where $W_{\zeta^B \to \dot{\Theta}^B}^{-1}$ is defined as in [48]

$$W_{\zeta^B \to \dot{\Theta}^B}^{-1}(\Theta^B) \triangleq \begin{bmatrix} 1 & s\Phi t\theta & c\Phi t\theta \\ 0 & c\Phi & -s\Phi \\ 0 & s\Phi/c\theta & c\Phi/c\theta \end{bmatrix}. \tag{3}$$

By employing the Newton-Euler formalism in the body and inertial frames, the complete 6-DoF dynamics governing the position and attitude motions are obtained as [10]

$$\begin{cases} m\ddot{\xi}^E \triangleq \mathrm{R}_{B \to E} F_l^B + F_{\mathrm{g}}^E + F_a^E + F_d^E, \\ J\dot{\zeta}^B \triangleq -[(\zeta^B)^T \times J\zeta^B] + \tau_m^B + \tau_g^B + \tau_a^B + \tau_d^B. \end{cases} \tag{4}$$

The symbol $\times$ on the right-hand side of the second equation of (4) stands for the cross product (vector product). The forces F_{g}^E, F_a^E are defined as

$$\begin{cases} F_{\mathrm{g}}^{E} \overset{\text{def}}{=} [0 \quad 0 \quad mg]^{T}, \\ F_{a}^{E} \overset{\text{def}}{=} -K_{a}\dot{\xi}^{E}. \end{cases} \tag{5}$$

The force F_l^B is defined hereafter in equation (7). The torques related to the attitude motion are given as

$$\begin{cases} \tau_{m}^{B} \overset{\text{def}}{=} [u_{\Phi} \quad u_{\theta} \quad u_{\psi}]_{B}^{T}, \\ \tau_{g}^{B} \overset{\text{def}}{=} -\sum_{i=1}^{4} (\zeta^{B})^{T} \times J_{r}[0 \quad 0 \quad (-1)^{i+1}\Omega_{i}]^{T}, \\ \tau_{a}^{B} \overset{\text{def}}{=} -\mathrm{diag}(c_{\Phi}, c_{\theta}, c_{\psi})[\dot{\Phi}^{2} \quad \dot{\theta}^{2} \quad \dot{\psi}^{2}]_{B}^{T}. \end{cases} \tag{6}$$

On the other hand, $F_d^E \overset{\text{def}}{=} [d_x^{\text{ext}} \quad d_y^{\text{ext}} \quad d_z^{\text{ext}}]^T$, $\tau_d^B \overset{\text{def}}{=} \left[d_{\Phi}^{\text{ext}} \quad d_{\theta}^{\text{ext}} \quad d_{\psi}^{\text{ext}}\right]^T$. Besides, the thrust control (total lift force) F_l^B is defined by the angular speeds $\Omega_i, (i = \overline{1,4})$ of the four rotors. Hence, the quadrotor's actuators produce a total lift force given as [49]

$$F_{l}^{B} \overset{\text{def}}{=} u_{z} = \textstyle\sum_{i=1}^{4} f_{i} = c_{t} \sum_{i=1}^{4} \Omega_{i}^{2}. \tag{7}$$

Besides, the torques u_Θ are related to the angular speeds of the rotors by the following expression [50]

$$u_{\Theta} \overset{\text{def}}{=} \begin{bmatrix} u_{\Phi} \\ u_{\theta} \\ u_{\psi} \end{bmatrix} = \begin{bmatrix} lc_{t}(-\Omega_{1}^{2} + \Omega_{2}^{2} + \Omega_{3}^{2} - \Omega_{4}^{2}) \\ lc_{t}(\Omega_{1}^{2} - \Omega_{2}^{2} + \Omega_{3}^{2} - \Omega_{4}^{2}) \\ c_{d}(-\Omega_{1}^{2} - \Omega_{2}^{2} + \Omega_{3}^{2} + \Omega_{4}^{2}) \end{bmatrix}. \tag{8}$$

Besides, the angular velocities of the four propellers, i.e., $\Omega_i, (i = \overline{1,4})$, are related to u_Θ (control torques) and u_z (thrust control force) as [51]

$$\begin{bmatrix} u_{z} \\ u_{\Theta} \end{bmatrix} \overset{\text{def}}{=} \begin{bmatrix} u_{z} \\ u_{\Phi} \\ u_{\theta} \\ u_{\psi} \end{bmatrix} = \begin{bmatrix} c_{t} & c_{t} & c_{t} & c_{t} \\ -lc_{t} & lc_{t} & lc_{t} & -lc_{t} \\ lc_{t} & -lc_{t} & lc_{t} & -lc_{t} \\ -c_{d} & -c_{d} & c_{d} & c_{d} \end{bmatrix} \begin{bmatrix} \Omega_{1}^{2} \\ \Omega_{2}^{2} \\ \Omega_{3}^{2} \\ \Omega_{4}^{2} \end{bmatrix}. \tag{9}$$

From (2) and (4), it yields

$$\begin{cases} \dot{\Theta}^{B} = W_{\zeta^{B} \to \dot{\Theta}^{B}}^{-1}(\Theta^{B})\zeta^{B}, \\ J\dot{\zeta}^{B} = -[(\zeta^{B})^{T} \times J\zeta^{B}] + \tau_{m}^{B} + \tau_{g}^{B} + \tau_{a}^{B} + \tau_{d}^{B}. \end{cases} \tag{10}$$

Remark 1. (Small-Angle Approximation (SAA)). Note that for small Euler angles $\boldsymbol{\Theta^B}$ (in rad), i.e., in the limit where the angles approach zero, it results that $\boldsymbol{\tan\theta \approx \theta, \sin\Phi \approx \Phi, \cos\theta \approx 1 - \frac{\theta^2}{2} (\approx 1), \cos\Phi \approx 1 - \frac{\Phi^2}{2} (\approx 1)}$ [49] [52]. The SAA is commonly used in quadrotor modeling and control as in [10] [53] [54]. Furthermore, in real flight missions without flips such as payload transportation, mapping, and inspection, the vehicle is intended to fly along with a dynamically feasible, i.e., continuous, and sufficiently smooth, Cartesian trajectory to ensure a safe flight mission. Consequently, abrupt reference changes leading to aggressive maneuvers that require large roll and pitch angles can be avoided [55] [56]. Thus, from (2) and considering SAA, we can get that $\boldsymbol{W_{\zeta^B \to \dot{\Theta}^B}^{-1}(\Theta^B) \approx I}$. Thus, $\boldsymbol{\dot{\Theta}^B \approx \zeta^B}$.

Accordingly, we get the resulting approximative relationship between $\ddot{\Theta}^B$ and $\dot{\zeta}^B$ as

$$\ddot{\Theta}^{B} = [\ddot{\Phi} \quad \ddot{\theta} \quad \ddot{\psi}]_{B}^{T} \approx [\dot{p} \quad \dot{q} \quad \dot{r}]_{B}^{T}. \tag{11}$$

Then, the six differential equations governing the rotational and translational dynamics of the quadcopter aircraft in the presence of external disturbances are obtained as

$$\begin{cases} \ddot{\Phi} = J_{xx}^{-1}[(J_{yy} - J_{zz})\dot{\theta}\dot{\psi} - c_{\Phi}\dot{\Phi}^{2} - J_{r}\bar{\omega}\dot{\theta} + u_{\Phi} + d_{\Phi}^{\text{ext}}], \\ \ddot{\theta} = J_{yy}^{-1}[(J_{zz} - J_{xx})\dot{\Phi}\dot{\psi} - c_{\theta}\dot{\theta}^{2} + J_{r}\bar{\omega}\dot{\Phi} + u_{\theta} + d_{\theta}^{\text{ext}}], \\ \ddot{\psi} = J_{zz}^{-1}[(J_{xx} - J_{yy})\dot{\Phi}\dot{\theta} - c_{\psi}\dot{\psi}^{2} + u_{\psi} + d_{\psi}^{\text{ext}}], \end{cases} \tag{12}$$

and

$$\begin{cases} \ddot{x} = -m^{-1}[(c\Phi s\theta c\psi + s\Phi s\psi)u_{z} - k_{x}\dot{x} + d_{x}^{\text{ext}}], \\ \ddot{y} = -m^{-1}[(c\Phi s\theta s\psi - s\Phi c\psi)u_{z} - k_{y}\dot{y} + d_{y}^{\text{ext}}], \\ \ddot{z} = -m^{-1}[(c\Phi c\theta)u_{z} - k_{z}\dot{z} + d_{z}^{\text{ext}}] + \mathrm{g}. \end{cases} \tag{13}$$

Remark 2. In reality, it is out of reach to precisely identify the physical parameters of an aerial vehicle such as the quadrotor aircraft. Moreover, the physical parameters such as aerodynamic coefficients, mass, and moments of inertia vary over time, making it difficult even far to obtain an accurate model of the system [57] [58]. Therefore, the dynamics of a quadrotor inevitably include parametric and nonparametric uncertainties. Unlike many reported works, e.g., [8] [37] [38], considering an ideal model with all parameters known, the present work takes into account time-dependent external disturbances as well as internal parametric and nonparametric uncertainties. Therefore, the following assumption is made for the dynamics representing the quadrotor system in (12) and (13).

Assumption 1. The physical parameters of the quadrotor can be represented by the sum of two parts; the nominal part indicated by $\mathcal{N}$ superscript and the uncertain part indicated by Δ superscript.

(i) Attitude dynamics. The uncertainties on the moments of inertia are defined as

$$\begin{cases} J_{xx}^{-1}(J_{yy} - J_{zz}) \overset{\text{def}}{=} \mathcal{P}_{1}^{xx} = \left(\mathcal{P}_{1}^{\mathcal{N},xx} \pm \mathcal{P}_{1}^{\Delta,xx}\right), \\ J_{yy}^{-1}(J_{zz} - J_{xx}) \overset{\text{def}}{=} \mathcal{P}_{1}^{yy} = \left(\mathcal{P}_{1}^{\mathcal{N},yy} \pm \mathcal{P}_{1}^{\Delta,yy}\right), \\ J_{zz}^{-1}(J_{xx} - J_{yy}) \overset{\text{def}}{=} \mathcal{P}_{1}^{zz} = \left(\mathcal{P}_{1}^{\mathcal{N},zz} \pm \mathcal{P}_{1}^{\Delta,zz}\right), \\ J_{xx}^{-1} \overset{\text{def}}{=} \mathcal{P}_{2}^{xx} = \left(\mathcal{P}_{2}^{\mathcal{N},xx} \pm \mathcal{P}_{2}^{\Delta,xx}\right), \\ J_{yy}^{-1} \overset{\text{def}}{=} \mathcal{P}_{2}^{yy} = \left(\mathcal{P}_{2}^{\mathcal{N},yy} \pm \mathcal{P}_{2}^{\Delta,yy}\right), \\ J_{zz}^{-1} \overset{\text{def}}{=} \mathcal{P}_{2}^{zz} = \left(\mathcal{P}_{2}^{\mathcal{N},zz} \pm \mathcal{P}_{2}^{\Delta,zz}\right), \\ J_{xx} \overset{\text{def}}{=} J_{xx}^{\mathcal{N}} \pm J_{xx}^{\Delta}, \\ J_{yy} \overset{\text{def}}{=} J_{yy}^{\mathcal{N}} \pm J_{yy}^{\Delta}, \\ J_{zz} \overset{\text{def}}{=} J_{zz}^{\mathcal{N}} \pm J_{zz}^{\Delta}. \end{cases} \tag{14}$$

The uncertainty on the rotor's inertia is described as

$$J_{r} \overset{\text{def}}{=} \mathcal{P}_{3} = \left(\mathcal{P}_{3}^{\mathcal{N}} \pm \mathcal{P}_{3}^{\Delta}\right) = J_{r}^{\mathcal{N}} \pm J_{r}^{\Delta}. \tag{15}$$

The uncertainties on the aerodynamic friction coefficients are described as

$$\begin{cases} c_\Phi \overset{\text{def}}{\equiv} \mathcal{P}_4^\Phi = \left(\mathcal{P}_4^{\mathcal{N},\Phi} \pm \mathcal{P}_4^{\Delta,\Phi}\right) = c_\Phi^{\mathcal{N}} \pm c_\Phi^{\Delta}, \\ c_\theta \overset{\text{def}}{\equiv} \mathcal{P}_4^\theta = \left(\mathcal{P}_4^{\mathcal{N},\theta} \pm \mathcal{P}_4^{\Delta,\theta}\right) = c_\theta^{\mathcal{N}} \pm c_\theta^{\Delta}, \\ c_\psi \overset{\text{def}}{\equiv} \mathcal{P}_4^\psi = \left(\mathcal{P}_4^{\mathcal{N},\psi} \pm \mathcal{P}_4^{\Delta,\psi}\right) = c_\psi^{\mathcal{N}} \pm c_\psi^{\Delta}. \end{cases} \tag{16}$$

Then, for instance, we can obtain the roll dynamics from (12) as

$$\ddot{\Phi} = \mathcal{P}_1^{\mathcal{N},xx}\dot{\theta}\dot{\psi} + \mathcal{P}_2^{\mathcal{N},xx}u_\Phi + \mathcal{P}_1^{\Delta,xx}\dot{\theta}\dot{\psi} - \mathcal{P}_2^{xx}\mathcal{P}_4^\Phi\dot{\Phi}^2 - \mathcal{P}_2^{xx}\mathcal{P}_3\bar{\omega}\dot{\theta} + \mathcal{P}_2^{\Delta,xx}u_\Phi + \mathcal{P}_2^{xx}d_\Phi^{\text{ext}}, \tag{17}$$

We assume that the unmodeled internal dynamics denoted by d_Φ^{unm} include the aerodynamic and gyroscopic effects defined as: $d_\Phi^{\text{unm}} \overset{\text{def}}{\equiv} -J_{xx}^{-1}c_\Phi\dot{\Phi}^2 - J_{xx}^{-1}J_r\bar{\omega}\dot{\theta}$, i.e., $d_\Phi^{\text{unm}} \overset{\text{def}}{\equiv} -\mathcal{P}_2^{xx}\mathcal{P}_4^\Phi\dot{\Phi}^2 - \mathcal{P}_2^{xx}\mathcal{P}_3\bar{\omega}\dot{\theta}$. Then, we can obtain the adequate control model, which is composed of a nominal part and an uncertain part as

$$\ddot{\Phi} = \mathcal{P}_1^{\mathcal{N},xx}\dot{\theta}\dot{\psi} + \mathcal{P}_2^{\mathcal{N},xx}u_\Phi + d_\Phi^{\text{lum}}. \tag{18}$$

where the uncertain part represents the lumped disturbances, which are defined as

$$d_\Phi^{\text{lum}} \overset{\text{def}}{\equiv} \mathcal{P}_1^{\Delta,xx}\dot{\theta}\dot{\psi} + d_\Phi^{\text{unm}} + \mathcal{P}_2^{\Delta,xx}u_\Phi + \mathcal{P}_2^{xx}d_\Phi^{\text{ext}}. \tag{19}$$

(ii) Position dynamics. The uncertainty on the mass is defined as

$$\begin{cases} m^{-1} \overset{\text{def}}{\equiv} \mathcal{P}_5 = \left(\mathcal{P}_5^{\mathcal{N}} \pm \mathcal{P}_5^{\Delta}\right), \\ m = m^{\mathcal{N}} \pm m^{\Delta}. \end{cases} \tag{20}$$

The uncertainties on the drag coefficients are defined as

$$\begin{cases} k_x \overset{\text{def}}{\equiv} \mathcal{P}_6 = \left(\mathcal{P}_6^{\mathcal{N}} \pm \mathcal{P}_6^{\Delta}\right) = k_x^{\mathcal{N}} \pm k_x^{\Delta}, \\ k_y \overset{\text{def}}{\equiv} \mathcal{P}_7 = \left(\mathcal{P}_7^{\mathcal{N}} \pm \mathcal{P}_7^{\Delta}\right) = k_y^{\mathcal{N}} \pm k_y^{\Delta}, \\ k_z \overset{\text{def}}{\equiv} \mathcal{P}_8 = \left(\mathcal{P}_8^{\mathcal{N}} \pm \mathcal{P}_8^{\Delta}\right) = k_z^{\mathcal{N}} \pm k_z^{\Delta}, \end{cases} \tag{21}$$

Then, for instance, we can obtain the x position dynamics from (13) as

$$\ddot{x} = -\mathcal{P}_5^{\mathcal{N}}(c\Phi s\theta c\psi + s\Phi s\psi)u_z - \mathcal{P}_5^{\Delta}(c\Phi s\theta c\psi + s\Phi s\psi)u_z + \mathcal{P}_5\mathcal{P}_6\dot{x} - \mathcal{P}_5 d_x^{\text{ext}}, \tag{22}$$

We assume that the internal unmodeled dynamics denoted d_x^{unm}, is the aerodynamic drag force defined as $d_x^{\text{unm}} \overset{\text{def}}{\equiv} m^{-1}k_x\dot{x}$, i.e., $d_x^{\text{unm}} \overset{\text{def}}{\equiv} \mathcal{P}_5\mathcal{P}_6\dot{x}$. Then, we can obtain the adequate control model, which is composed of a nominal part and an uncertain part as

$$\ddot{x} = -\mathcal{P}_5^{\mathcal{N}}(c\Phi s\theta c\psi + s\Phi s\psi)u_z + d_x^{\text{lum}}. \tag{23}$$

where the uncertain part represents the lumped disturbances, which are defined as

$$d_x^{\text{lum}} \overset{\text{def}}{\equiv} -\mathcal{P}_5^{\Delta}(c\Phi s\theta c\psi + s\Phi s\psi)u_z + \mathcal{P}_5\mathcal{P}_6\dot{x} - \mathcal{P}_5 d_x^{\text{ext}}. \tag{24}$$

Remark 3. The control performance and system's stability are not threatened while considering Assumption 1 since:

a. The nominal model has an acceptable level of fidelity and it is reliable for the control design because:

- The quadrotor in our study is intended to operate around a physically realizable maximum cruise speed. Also, the aircraft does not perform any aggressive maneuvers or flips (software limitation of the Euler angles and angular velocities, i.e., $\Phi^{\min} \le \Phi \le \Phi^{\max}$, $\theta^{\min} \le \theta \le \theta^{\max}$ and $p^{\min} \le p \le p^{\max}$, $q^{\min} \le q \le q^{\max}$, $r^{\min} \le r \le r^{\max}$). Thus, the aircraft will not be exposed to strong aerodynamic resistance. Hence, in such operating conditions the phenomenon relative to the aerodynamic and gyroscopic effects, e.g., $c_\Phi\dot{\Phi}^2 - J_{xx}^{-1}J_r\bar{\omega}\dot{\theta}$ and $m^{-1}k_x\dot{x}$, can be ignored in the modeling process. Many flight missions can be accomplished within this operating flight mode, such as; transportation, mapping, inspection, to mention a few. Such a flight scenario is adequate for our future application being collaborative payload transportation in an urban area using multiple quadrotors.
- The maximum tolerances on uncertainties are 30% bias for the moments of inertia and 20% bias for the mass. These tolerances are verified by simulation.

b. The lumped disturbances $d_\theta^{\text{lum}}, d_\xi^{\text{lum}}$ representing the uncertain part can be rejected by the robust control law which is based on an ADRC strategy. The ADRC includes a disturbance observer and a robust SMC controller.

c. Naturally, the SMC has strong robustness against parameters variations and model uncertainties.

Therefore, simplifying the model according to Assumption 1 is justifiable and is acceptable in the robust control law under discussion.

In order to elaborate an adequate control model of the quadrotor, state-space representation can be used to reformulate the mathematical model (12)-(13). Thus, considering Assumption 1, we get the following model

$$\begin{cases} \dot{x}_1 = x_2, \\ \dot{x}_2 = \mathcal{P}_1^{\mathcal{N},xx}x_4x_6 + \mathcal{P}_2^{\mathcal{N},xx}u_\Phi + d_\Phi^{\text{lum}}, \\ \dot{x}_3 = x_4, \\ \dot{x}_4 = \mathcal{P}_1^{\mathcal{N},yy}x_2x_6 + \mathcal{P}_2^{\mathcal{N},yy}u_\theta + d_\theta^{\text{lum}}, \\ \dot{x}_5 = x_6, \\ \dot{x}_6 = \mathcal{P}_1^{\mathcal{N},zz}x_2x_4 + \mathcal{P}_2^{\mathcal{N},zz}u_\psi + d_\psi^{\text{lum}}, \\ \dot{x}_7 = x_8, \\ \dot{x}_8 = -\mathcal{P}_5^{\mathcal{N}}(cx_1sx_3cx_5 + sx_1sx_5)u_z + d_x^{\text{lum}}, \\ \dot{x}_9 = x_{10}, \\ \dot{x}_{10} = -\mathcal{P}_5^{\mathcal{N}}(cx_1sx_3sx_5 - sx_1cx_5)u_z + d_y^{\text{lum}}, \\ \dot{x}_{11} = x_{12}, \\ \dot{x}_{12} = -\mathcal{P}_5^{\mathcal{N}}(cx_1cx_3)u_z + g + d_z^{\text{lum}}. \end{cases} \tag{25}$$

where $x \overset{\text{def}}{\equiv} \begin{bmatrix} \Phi & \dot{\Phi} & \theta & \dot{\theta} & \psi & \dot{\psi} & x & \dot{x} & y & \dot{y} & z & \dot{z} \end{bmatrix} \in \mathbb{R}^{12}$ is the state vector.

Remark 4. The quadrotor's model (25) is a dynamical system of six second-order subsystems, in which the first three

subsystems constitute the attitude dynamics and the succeeding subsystems establish the position dynamics. Also, the model is strongly coupled, nonlinear, underactuated, and multi-input multi-output. In addition, it is subjected to internal uncertainties and external disturbances. The states are the translational and rotational quantities, which are also the outputs. The inputs are thrust force and three torques. The nature of this aircraft's model brings a great difficulty and challenge in both theoretical development and practical implementation of the control algorithm.

From (25), it is evident that the dynamics of the Euler angles and the translational position can be assimilated to a perturbated second-order nonlinear system. Consequently, the design of the control law follows from the two models given below

$$\begin{cases} \dot{\chi}_1(t) = \chi_2(t), \\ \dot{\chi}_2(t) = f_\Theta^{\mathcal{N}}(\chi_2, \mathcal{P}_1^{\mathcal{N}}, t) + g_\Theta^{\mathcal{N}}(\mathcal{P}_2^{\mathcal{N}}) u_\Theta(t) + d_\Theta^{\text{lum}}(\mathcal{P}_1^{\Delta}, \mathcal{P}_2^{\Delta}, d_\Theta^{\text{ext}}, d_\Theta^{\text{unm}}, t), \\ \mathcal{Y}_1(t) = \chi_1(t). \end{cases} \tag{26}$$

and

$$\begin{cases} \dot{\chi}_3(t) = \chi_4(t), \\ \dot{\chi}_4(t) = F_\xi(\chi_1, \mathcal{P}_5^{\mathcal{N}}, t) + d_P^{\text{lum}}(\mathcal{P}_5^{\Delta}, \bar{\mathcal{P}}, d_\xi^{\text{ext}}, d_\xi^{\text{unm}}, t), \\ \mathcal{Y}_2(t) = \chi_4(t). \end{cases} \tag{27}$$

where $X_\Theta \overset{\text{def}}{=} [\chi_1 \quad \chi_2]^T \in \mathbb{R}^{3\times 2}$ is the vector of states, and $\chi_1 \overset{\text{def}}{=} \Theta = [\mathrm{x}_1 \quad \mathrm{x}_3 \quad \mathrm{x}_5]^T = [\Phi \quad \theta \quad \psi]^T$, $\chi_2 \overset{\text{def}}{=} \dot{\Theta} = \zeta = [\dot{\Phi} \quad \dot{\theta} \quad \dot{\psi}]^T = [\mathrm{x}_2 \quad \mathrm{x}_4 \quad \mathrm{x}_6]^T$ (by Remark 1), $u_\Theta \overset{\text{def}}{=} [u_\Phi \quad u_\theta \quad u_\psi]^T \in \mathbb{R}^3$ is the vector of control inputs, $\mathcal{Y}_1 \overset{\text{def}}{=} [\mathcal{Y}_1 \quad \mathcal{Y}_2 \quad \mathcal{Y}_3]^T = [\Phi \quad \theta \quad \psi]^T \in \mathbb{R}^3$ is the controlled output of the attitude loop, the uncertain function $d_\Theta^{\text{lum}} \overset{\text{def}}{=} [d_\Phi^{\text{lum}} \quad d_\theta^{\text{lum}} \quad d_\psi^{\text{lum}}]^T \in \mathbb{R}^3$ represents the lumped disturbances, and $\mathcal{P}_1^{\Delta} \overset{\text{def}}{=} [\mathcal{P}_1^{\Delta,xx} \quad \mathcal{P}_1^{\Delta,yy} \quad \mathcal{P}_1^{\Delta,zz}]^T$, $\mathcal{P}_2^{\Delta} \overset{\text{def}}{=} [\mathcal{P}_2^{\Delta,xx} \quad \mathcal{P}_2^{\Delta,yy} \quad \mathcal{P}_2^{\Delta,zz}]^T$, $\mathcal{P}_1^{\mathcal{N}} \overset{\text{def}}{=} [\mathcal{P}_1^{\mathcal{N},xx} \quad \mathcal{P}_1^{\mathcal{N},yy} \quad \mathcal{P}_1^{\mathcal{N},zz}]^T$, $\mathcal{P}_2^{\mathcal{N}} \overset{\text{def}}{=} [\mathcal{P}_2^{\mathcal{N},xx} \quad \mathcal{P}_2^{\mathcal{N},yy} \quad \mathcal{P}_2^{\mathcal{N},zz}]^T$. Also, $X_\xi \overset{\text{def}}{=} [\chi_3 \quad \chi_4]^T \in \mathbb{R}^{3\times 2}$ is the states' vector (the velocity χ_4 is not available for measurement), $\chi_3 \overset{\text{def}}{=} \xi = [\mathrm{x}_7 \quad \mathrm{x}_9 \quad \mathrm{x}_{11}]^T = [x \quad y \quad z]^T \in$, $\chi_4 \overset{\text{def}}{=} \dot{\xi} = \mathcal{V} = [\mathrm{x}_8 \quad \mathrm{x}_{10} \quad \mathrm{x}_{12}]^T = [\dot{x} \quad \dot{y} \quad \dot{z}]^T =$ $[v_x \quad v_y \quad v_z]^T$, and $\mathcal{Y}_2 \overset{\text{def}}{=} [\mathcal{Y}_4 \quad \mathcal{Y}_5 \quad \mathcal{Y}_6]^T = [x \quad y \quad z]^T \in \mathbb{R}^3$ is the controlled output of the position loop, and the uncertain function $d_\xi^{\text{lum}} \overset{\text{def}}{=} [d_x^{\text{lum}} \quad d_y^{\text{lum}} \quad d_z^{\text{lum}}]^T \in \mathbb{R}^3$ represents the lumped disturbances, where $\bar{\mathcal{P}} \overset{\text{def}}{=} [\mathcal{P}_6 \quad \mathcal{P}_7 \quad \mathcal{P}_8]^T$. The functions $f_\Theta^{\mathcal{N}}(\chi_2, \mathcal{P}_1^{\mathcal{N}}, t)$ and $g_\Theta^{\mathcal{N}}(\mathcal{P}_2^{\mathcal{N}}, t)$ are adequately smooth functions satisfying $f_\Theta^{\mathcal{N}}(\chi_2, \mathcal{P}_1^{\mathcal{N}}, 0) = 0$ and $g_\Theta^{\mathcal{N}}(\mathcal{P}_2^{\mathcal{N}}, t) \neq 0$ over the domain of definition. These can be written as

$$f_\Theta^{\mathcal{N}} \overset{\text{def}}{=} \begin{bmatrix} f_\Phi^{\mathcal{N}} \\ f_\theta^{\mathcal{N}} \\ f_\psi^{\mathcal{N}} \end{bmatrix} = \begin{bmatrix} (J_{xx}^{\mathcal{N}})^{-1}(J_{yy}^{\mathcal{N}} - J_{zz}^{\mathcal{N}})\dot{\theta}\dot{\psi} \\ (J_{yy}^{\mathcal{N}})^{-1}(J_{zz}^{\mathcal{N}} - J_{xx}^{\mathcal{N}})\dot{\Phi}\dot{\psi} \\ (J_{zz}^{\mathcal{N}})^{-1}(J_{xx}^{\mathcal{N}} - J_{yy}^{\mathcal{N}})\dot{\Phi}\dot{\theta} \end{bmatrix},$$

$$g_\Theta^{\mathcal{N}} \overset{\text{def}}{=} [g_\Phi^{\mathcal{N}} \quad g_\theta^{\mathcal{N}} \quad g_\psi^{\mathcal{N}}]^T = [(J_{xx}^{\mathcal{N}})^{-1} \quad (J_{yy}^{\mathcal{N}})^{-1} \quad (J_{zz}^{\mathcal{N}})^{-1}]^T.$$

The physical entity $F_\xi \neq 0$ describing the coupling between rotational and translational motions is defined as

$$F_\xi(\chi_1, \mathcal{P}_5^{\mathcal{N}}, t) \overset{\text{def}}{=} \begin{bmatrix} F_x \\ F_y \\ F_z \end{bmatrix} = \begin{bmatrix} -u_z(m^{\mathcal{N}})^{-1}(\mathrm{c}\Phi \mathrm{s}\theta \mathrm{c}\psi + \mathrm{s}\Phi \mathrm{s}\psi) \\ -u_z(m^{\mathcal{N}})^{-1}(\mathrm{c}\Phi \mathrm{s}\theta \mathrm{s}\psi - \mathrm{s}\Phi \mathrm{c}\psi) \\ -u_z(m^{\mathcal{N}})^{-1}(\mathrm{c}\Phi \mathrm{c}\theta) + \mathrm{g} \end{bmatrix}. \tag{28}$$

The following Definition 5 formulates the control problem of the study.

Definition 5. (Control problem of the study). The present study aims to design a reliable flight control algorithm with superior flight performance for the perturbated, nonlinear, and coupled quadrotor system (25). The flight controller is based on a position tracking controller $u_z(t)$ and attitude stabilization controller $u_\Theta(t) = [u_\Phi \quad u_\theta \quad u_\psi]^T$ to track a reference Cartesian trajectory in 3-D state-space. The controllers are implemented in a hierarchical scheme. The controllers are designed based on a robust fixed-time SMC control law. The control algorithm should satisfy the following points

(i) The attitude and position tracking errors are driven in a fixed-time to the origin, i.e., for $\forall e_1^\Theta(t) \overset{\text{def}}{=} \Theta(t) - \Theta_d(t), \forall e_1^\xi(t) \overset{\text{def}}{=} \xi(t) - \xi_d(t)$, there exist two constants T_Θ, T_ξ, such that

$$\begin{cases} \lim\limits_{t\to T_\Theta} e_1^\Theta(t) = 0, & \forall t > T_\Theta, \\ \lim\limits_{t\to T_\xi} e_1^\xi(t) = 0, & \forall t > T_\xi. \end{cases} \tag{29}$$

(ii) The controller should reject the lumped disturbances;
(iii) The control signal is chattering-free and nonsingular;
(iv) The stability of the overall feedback-loop system is ensured.

2.3 Motivation

Consider, for instance, the roll angle dynamics from the second-order attitude system (26) as

$$\begin{cases} \dot{\mathrm{x}}_1(t) = \mathrm{x}_2(t), \\ \dot{\mathrm{x}}_2(t) = f_{\mathrm{x}_1}^{\mathcal{N}}(\chi_2, \mathcal{P}_1^{\mathcal{N},xx}, t) + g_{\mathrm{x}_1}^{\mathcal{N}}(\mathcal{P}_2^{\mathcal{N},xx}) u_{\mathrm{x}_1}(t) + d_{\mathrm{x}_1}^{\text{lum}}(\mathcal{P}_1^{\Delta,xx}, \mathcal{P}_2^{\Delta,xx}, d_{\mathrm{x}_1}^{\text{ext}}, d_{\mathrm{x}_1}^{\text{unm}}, t), \\ \mathcal{Y}_1(t) = \mathrm{x}_1(t). \end{cases} \tag{30}$$

Let the control input $u_{\mathrm{x}_1}(t)$ of (30) be defined as

$$u_{\mathrm{x}_1}(t) \overset{\text{def}}{=} [g_{\mathrm{x}_1}^{\mathcal{N}}]^{-1}[\bar{u}_{\mathrm{x}_1}(t) - f_{\mathrm{x}_1}^{\mathcal{N}} - \hat{d}_{\mathrm{x}_1}^{\text{lum}}]. \tag{31}$$

Then, system (30) can be rewritten in the following form

$$\begin{cases} \dot{\mathrm{x}}_1(t) = \mathrm{x}_2(t), \\ \dot{\mathrm{x}}_2(t) = \bar{u}_{\mathrm{x}_1}(t), \\ \mathcal{Y}_1(t) = \mathrm{x}_1(t). \end{cases} \qquad x_0 \overset{\text{def}}{=} [\mathrm{x}_1(0) \quad \mathrm{x}_2(0)]^T \in \mathbb{R}^2 \tag{32}$$

The following control law, which is inspired from [44] has been designed in [59] for stabilizing a double-integrator system under the form of (32) in finite-time

$$\bar{u}_{\mathrm{x}_1}(t) \overset{\text{def}}{=} -k_1^{\mathrm{x}_1}\mathrm{sign}^{\gamma_1}(\mathrm{x}_1) - k_2^{\mathrm{x}_1}\mathrm{sign}^{\gamma_2}(\mathrm{x}_2). \tag{33}$$

where $k_1^{x_1}, k_2^{x_1}$ are positive constants and the exponents $\gamma_i, (i = \overline{1,n})$ for n-th order system are selected as follows: $\gamma_i \in (0,1)$ and γ_i should satisfy $\gamma_{i-1} = \gamma_i\gamma_{i+1}/(2\gamma_{i+1} - \gamma_i), i = \overline{2,n}$, $\gamma_{n+1} = 1$, and $\gamma_n = \gamma$, where $\gamma \in (1 - \varepsilon_1, 1)$ for a sufficiently small $\varepsilon_1 > 0$.

Remark 5. The work in [59] does not provide the estimation of the settling-time for the closed-loop system, including (31), (32), and (33). Moreover, the settling-time depends on the ICs $\boldsymbol{x_0}$ of system (32). The systems demonstrating finite-time stability exhibit superior performance as compared to their infinite-time counterparts, however, the finite-time control has an unavoidable drawback. The ICs deviating from the point of equilibrium result in unbounded growth of the convergence-time **[30]**. Besides, it is difficult and, in some cases, impossible to obtain the ICs of dynamic systems in practice.

The present work aims to:

(i) Estimate the settling-time of the feedback system (31)-(32);

(ii) Since the upper bound on the convergence-time of the feedback system (31)-(32) depends on the ICs of the system, we propose to design a novel fixed-time control law based on homogeneous SMC;

(iii) Next, it is proved that the upper-bound on the fixed settling-time of the proposed homogeneous SMC control law can be explicitly and uniformly estimated w.r.t. ICs;

(iv) Finally, a flight control algorithm is proposed for the quadrotor aircraft. The control algorithm includes an attitude stabilization controller and a position tracking controller.

(v) A corollary is proposed to extend the results of the current work to design fixed-time stabilization feedback controller for uncertain nonlinear high-order systems.

3 Main Results

3.1 Sliding Manifold Design and Convergence Analysis

The design of a control strategy based on SMC involves two steps: **(i)** The selection of a sliding manifold as per the desired motions of states trajectories in the system's state-space; **(ii)** The design of the control to ensure the existence of a sliding mode on this preselected manifold. The control aims to enforce the trajectories of the feedback system to reach and slide along the manifold toward the equilibrium point.

Consider the perturbated nonlinear second-order system (32). To ensure fixed-time stabilization at the origin of the states, the following NHCTSM, i.e., $\mathcal{S} = \{x_1, x_2 \in \mathbb{R}: s_{x_1}(t, x_1, x_2) = 0\}$, is proposed

$$s_{x_1}(t, x_1, x_2) \triangleq x_2(t) + \int_0^t [v(t) + w(t)]d\tau, \tag{34}$$

$$v(t) \triangleq -\bar{u}_{x_1}(t) = k_1^{x_1}\text{sign}^{\gamma_1}(x_1) + k_2^{x_1}\text{sign}^{\gamma_2}(x_2), \tag{35}$$

$$w(t) \triangleq \bar{k}_1^{x_1}\text{sign}^{\bar{\gamma}_1}(x_1) + \bar{k}_2^{x_1}\text{sign}^{\bar{\gamma}_2}(x_2). \tag{36}$$

where $s_{x_1}(t, x_1, x_2): \mathbb{R}_+ \times \mathbb{R} \times \mathbb{R} \to \mathbb{R}$ is a smooth function and the nonnegative parameters $\bar{k}_1^{x_1}, \bar{k}_2^{x_1}, \bar{\gamma}_1, \bar{\gamma}_2$ are tuned by following the guideline in Remark 10 given hereafter. The subsequent theorem shows that the proposed sliding manifold can drive the states (x_1, x_2) into the origin in a bounded fixed-time uniform w.r.t. ICs x_0 of system (32).

Theorem 1. For the system subject to lumped disturbances in (32), the sliding manifold $s_{x_1} = 0$ ensures the stabilization of the states $x(t) \triangleq [x_1(t) \quad x_2(t)]^T$ at the origin in bounded fixed settling-time T_x. The bound $T_x^{\max}$ on T_x is independent of the ICs $x_0 = [x_1(t_0) \quad x_2(t_0)]^T$ of system (32). An explicit expression of $T_x^{\max}$ can be also derived as

$$T_x \le T_x^{\max} \triangleq \frac{\gamma}{1-\gamma}\frac{\lambda_{\max}(P_1^x)}{\lambda_{\min}(Q_1^x)}\lambda_{\max}^{\frac{1-\gamma}{\gamma}}(P_1^x) + \frac{\bar{\gamma}}{\bar{\gamma}-1}\frac{\lambda_{\max}(P_2^x)}{\lambda_{\min}(Q_2^x)}\lambda_{\max}^{-\frac{\bar{\gamma}-1}{\bar{\gamma}}}(P_2^x).$$

Proof. By differentiating the sliding function (34) w.r.t. time, we get

$$\dot{s}_{x_1}(t) = \dot{x}_2(t) + v(t) + w(t). \tag{37}$$

After reaching the sliding manifold $s_{x_1} = 0$, the dynamics of $\dot{x}_2$ can be obtained from (37) as

$$\dot{x}_2(t) = -v(t) - w(t). \tag{38}$$

Then, the feedback-loop dynamics can be obtained from (32) and (38) as

$$\dot{x} \triangleq f(x): \begin{cases} \dot{x}_1 = x_2, \\ \dot{x}_2 = -k_1^{x_1}\text{sign}^{\gamma_1}(x_1) - k_2^{x_1}\text{sign}^{\gamma_2}(x_2) \\ \qquad -\bar{k}_1^{x_1}\text{sign}^{\bar{\gamma}_1}(x_1) - \bar{k}_2^{x_1}\text{sign}^{\bar{\gamma}_2}(x_2). \end{cases} \tag{39}$$

Lemma 4. ([31]). Consider the system (39). Suppose that $f(x)$ is a homogeneous vector field in the bi-limit with associated triples $(r_0, \kappa_0, f_0(x))$ and $(r_\infty, \kappa_\infty, f_\infty(x))$. If the origins of systems $\dot{x} = f(x), \dot{x}_0 = f_0(x)$ and $\dot{x}_\infty = f_\infty(x)$ GAS and the condition $\kappa_0 < 0 < \kappa_\infty$ holds true, then the origin of system (39) is fixed-time stable.

Remark 6. Lemma 4 has been used as the basis of many proofs for fixed-time stability of homogeneous dynamical systems such as the one in (39), e.g., [10] [11] [12] [41]. However, this lemma being based on the bi-limit homogeneity proof is limited since it cannot estimate the convergence-time or its upper bound. Thus, in the following, we conduct the stability analysis of the homogeneous system (39) based on LQF and ALE.

Remark 7. Note that the GAS of system (39) being derived from the proposed sliding function (34) can be verified by defining a radially unbounded positive definite Lyapunov function besides employing LaSalle's invariance theorem. The proof is presented in our previous work (proof of Theorem 2) [10].

System (39) can be written in the following state-space form

$$\dot{x}(t) = Ax(t) + Bu_x(t), \qquad x_0 = [\mathrm{x}_1(0) \quad \mathrm{x}_2(0)]^T. \tag{40}$$

where $u_x(t) \overset{\text{def}}{=} v(t) + w(t), u_x(t) \in \mathbb{R}$ is the input of the system (40) and $A = \begin{bmatrix} 0 & 1 \\ 0 & 0 \end{bmatrix}, B = \begin{bmatrix} 0 \\ 1 \end{bmatrix}$. The estimation of the convergence-time T_x is established in two steps. First, the closed-loop system (35)-(40) is analyzed to estimate the convergence-time under the finite-time control input (35). Second, the estimation of T_x is conducted.

Step 1. Applying the input $v(t)$ in (35) to system (40), we get

$$\dot{x}(t) = A_1 x(t) - B\left[k_1^{\mathrm{x}_1} \mathrm{sign}^{\gamma_1}(\mathrm{x}_1) + k_2^{\mathrm{x}_1} \mathrm{sign}^{\gamma_2}(\mathrm{x}_2)\right]. \tag{41}$$

Let the following LF be defined for system (41)

$$V_1(\Xi) = \Xi^T P_1^x \Xi, \qquad \Xi \overset{\text{def}}{=} \left[\mathrm{x}_1^{\gamma_1} \quad \mathrm{x}_2^{\gamma_2}\right]^T. \tag{42}$$

where the symmetric positive definite matrix P_1^x, i.e., $P_1^x = (P_1^x)^T > 0$, is the solution of ALE given as

$$P_1^x A_1 + A_1^T P_1^x = -Q_1^x, \tag{43}$$

where $Q_1^x > 0 \in \mathbb{R}^{n \times n}$ is an arbitrary symmetric positive definite matrix and A_1 is written accordingly to the controllable canonical form

$$A_1 = \begin{bmatrix} 0 & 1 \\ -k_1^{\mathrm{x}_1} & -k_2^{\mathrm{x}_1} \end{bmatrix}.$$

where $k_1^{\mathrm{x}_1}, k_2^{\mathrm{x}_1} > 0$ are such that the polynomial $s^2 + k_2^{\mathrm{x}_1} s + k_1^{\mathrm{x}_1}$ is Hurwitz, which implies that the matrix A_1 is certainly Hurwitz. Consequently, the system $\dot{x}(t) = A_1 x(t)$ is AS. Since P_1^x is a solution of the ALE in (43), the quadratic function $V_1(x) = x^T P_1^x x$, $x = [\mathrm{x}_1 \quad \mathrm{x}_2]^T$ is a Lyapunov candidate function for the system $\dot{x}(t) = A_1 x(t)$. Moreover, the following inequality is obtained for the time derivative of $V_1(x)$

$$\begin{aligned} \dot{V}_1(x) &= \dot{x}^T P_1^x x + x^T P_1^x \dot{x} = x^T (A_1^T P_1^x + P_1^x A_1) x \\ &= -x^T Q_1^x x < 0. \end{aligned} \tag{44}$$

If the following two conditions are satisfied, the inequality $\dot{V}_1(\Xi) < 0$ holds for $V_1(\Xi)$ given in (42): ***(i)*** The parameter γ is chosen in the interval $(1 - \varepsilon_1, 1)$, for a small positive number $\varepsilon_1 > 0$. ***(ii)*** $\dot{V}_1(\Xi)$ is obtained along with the trajectories of the closed-loop system (41). Therefore, $V_1(\Xi)$ is a LF for the system (41). Considering $\dot{V}_1(\Xi) < 0$, the system (41) is AS. It can be noted that the right-hand side of (41) is a homogeneous vector field of degree $\kappa_1 = [(\gamma - 1)/\gamma] < 0$ w.r.t. dilations (weights) $r_i = 1/\gamma_i, i = \overline{1,n}$. By using Lemma 2.2 of [60], the states of system (41) are guaranteed to be finite-time convergent to the equilibrium. By following the guidelines of Definition 4 given in Section 2.1.1 and Theorem 6.2 in [44], it can be verified that the LF $V_1(\Xi) = \Xi^T P_1^x \Xi$ is homogeneous in $x = [\mathrm{x}_1 \quad \mathrm{x}_2]^T$ of degree $l_1 = 1 > \max(-\kappa_1, 0)$, if γ is sufficiently close to 1, and its full-time derivative $\dot{V}_1(\Xi)$ is homogeneous in $x = [\mathrm{x}_1 \quad \mathrm{x}_2]^T$ of degree $l_1 + \kappa_1 = 1 + \kappa_1 > 0$, w.r.t. the same weights $r_i, i = \overline{1,n}$. Applying Lemma 2 with $V_2 = \dot{V}_1(\Xi)$, we get

$$\dot{V}_1(\Xi) \leq -c_1 V_1^{1+\kappa_1}(\Xi) = -c_1 V_1^{\frac{2\gamma-1}{\gamma}}(\Xi), \tag{45}$$

where $\frac{2\gamma-1}{\gamma} < 1$. According to Lemma 3, Rayleigh's inequalities can be applied to relations $V_1(x) = x^T P_1^x x$ and $\dot{V}_1(x) = x^T Q_1^x x$. Thus, we can obtain

$$\begin{cases} V_1(x) = \max\limits_{x \in \mathbb{R}^2 : x \neq 0} x^T P_1^x x \leq \lambda_{\max}(P_1^x) \|x\|^2, \\ \dot{V}_1(x) = \min\limits_{x \in \mathbb{R}^2 : x \neq 0} x^T Q_1^x x \leq -\lambda_{\min}(Q_1^x) \|x\|^2, \end{cases} \tag{46}$$

From the first inequality of (46), we get $\|x\|^2 \geq \frac{V_1(x)}{\lambda_{\max}(P_1^x)}$. Replacing $\|x\|^2$ by its expression in the second inequality of (46), we get $\dot{V}_1(x) \leq -\lambda_{\min}(Q_1^x) \frac{V_1(x)}{\lambda_{\max}(P_1^x)}$. Therefore, for an arbitrarily small positive number $\delta > 0$, we can get

$$\dot{V}_1(x) \leq \frac{\lambda_{\min}(Q_1^x)}{\lambda_{\max}(P_1^x)} V_1(x) < -\frac{(\lambda_{\min}(Q_1^x) - \delta)}{\lambda_{\max}(P_1^x)} V_1(x). \tag{47}$$

Considering the continuity of the right-hand side of (41) w.r.t. γ, the following inequality holds for $V_1(\Xi)$ given in (42)

$$\dot{V}_1(\Xi) < -\frac{(\lambda_{\min}(Q_1^x) - \delta)}{\lambda_{\max}(P_1^x)} V_1^{\frac{2\gamma-1}{\gamma}}(\Xi). \tag{48}$$

if the following two conditions are satisfied: ***(i)*** The parameter γ is chosen in the interval $(1 - \varepsilon_1, 1)$. ***(ii)*** $\dot{V}_1(\Xi)$ is obtained along with the trajectories of the closed-loop system (41). Since $\delta > 0$ is a small constant, the following expression can be obtained from (48)

$$\dot{V}_1(\Xi) < -\frac{\lambda_{\min}(Q_1^x)}{\lambda_{\max}(P_1^x)} V_1^{\frac{2\gamma-1}{\gamma}}(\Xi). \tag{49}$$

Hence, the constant c_1 can be assigned as $c_1 = \frac{\lambda_{\min}(Q_1^x)}{\lambda_{\max}(P_1^x)}$. The expression of the settling-time can be obtained via solving the differential equation (49). This can be achieved by utilizing the separation of variables method. Thus, by separating the variables and then integrating both sides of (49), we get

$$\int_{\Xi(0)}^{\Xi(t)} \frac{1}{V_1^{\frac{2\gamma-1}{\gamma}}} dV_1 \leq \int_0^t -\frac{\lambda_{\min}(Q_1^x)}{\lambda_{\max}(P_1^x)} dt$$

Then, the following expression is obtained

$$\frac{1}{\frac{1-\gamma}{\gamma}} \left[V_1^{\frac{1-\gamma}{\gamma}}(\Xi(t)) - V_1^{\frac{1-\gamma}{\gamma}}(\Xi(0)) \right] \leq -\frac{\lambda_{\min}(Q_1^x)}{\lambda_{\max}(P_1^x)} t$$

Finally, we can get

$$T_0(x_0) \leq T_0^{\max} \overset{\text{def}}{=} \frac{\gamma}{1-\gamma} \frac{\lambda_{\max}(P_1^x)}{\lambda_{\min}(Q_1^x)} V_1^{\frac{1-\gamma}{\gamma}}(\Xi(0)). \tag{50}$$

$T_0^{\max}$ is the upper bound on the convergence-time of the closed-loop system (35)-(40) having the finite-time control law designed in [59] as input. We can see that the estimate of $T_0^{\max}$ depend on the ICs of system (40).

Step 2. Applying the input term $\mathcal{w}(t)$ (36) to system (40), we get

$$\dot{x}(t) = A_2 x(t) - B\left[\bar{k}_1^{\mathrm{x}_1}\mathrm{sign}^{\bar{\gamma}_1}(\mathrm{x}_1) + \bar{k}_2^{\mathrm{x}_1}\mathrm{sign}^{\bar{\gamma}_2}(\mathrm{x}_2)\right]. \quad (51)$$

Let the following candidate LF be defined for system (51)

$$V_2(\Xi) = \Xi^T P_2^x \Xi, \qquad \Xi \stackrel{\text{def}}{=} \left[\mathrm{x}_1^{\bar{\gamma}_1} \quad \mathrm{x}_2^{\bar{\gamma}_2}\right]^T. \quad (52)$$

where the symmetric positive definite matrix P_2^x , i.e., $P_2^x = (P_2^x)^T > 0$, is the solution of ALE defined as

$$P_2^x A_2 + A_2^T P_2^x = -Q_2^x, \quad (53)$$

where $Q_2^x > 0 \in \mathbb{R}^{n\times n}$ is an arbitrary symmetric positive definite matrix and A_2 is in the controllable canonical form

$$A_2 = \begin{bmatrix} 0 & 1 \\ -\bar{k}_1^{\mathrm{x}_1} & -\bar{k}_2^{\mathrm{x}_1} \end{bmatrix}.$$

where $\bar{k}_1^{\mathrm{x}_1}, \bar{k}_2^{\mathrm{x}_1} > 0$ are such that the polynomial $s^2 + \bar{k}_2^{\mathrm{x}_1} s + \bar{k}_1^{\mathrm{x}_1}$ is Hurwitz. Given that the control gains $\bar{k}_1^{\mathrm{x}_1}, \bar{k}_2^{\mathrm{x}_1}$ form a Hurwitz polynomial $s^2 + \bar{k}_2^{\mathrm{x}_1} s + \bar{k}_1^{\mathrm{x}_1}$, the matrix A_2 is necessarily Hurwitz. A_2 is the matrix of the linear system obtained from (51). Therefore, the linear system $\dot{x}(t) = A_2 x(t)$ is AS and $V_2(x) = x^T P_2^x x$ is a LF for this system. Moreover, the following inequality is obtained for the time derivative of $V_2(x)$

$$\begin{aligned}\dot{V}_2(x) &= \dot{x}^T P_2^x x + x^T P_2^x \dot{x} = x^T (A_2^T P_2^x + P_2^x A_2) x \\ &= -x^T Q_2^x x < 0.\end{aligned} \quad (54)$$

Considering the continuity of the right-hand side of (51) w.r.t. $\bar{\gamma}$. If the following two conditions are satisfied, the inequality (54) holds for the function $V_2(\Xi) = \Xi^T P_2^x \Xi$ defined in (52): ***(i)*** The parameter $\bar{\gamma}$ is chosen within the interval $(1, 1+\varepsilon_2)$, for a small positive number $\varepsilon_2 > 0$. ***(ii)*** $\dot{V}_2(\Xi)$ is obtained along with the trajectories of closed-loop system (51). Consequently, $V_2(\Xi)$ is a LF for the system (51). Considering $\dot{V}_2(\Xi) < 0$, the system (51) is AS. It can be noted that the right-hand side of (51) is a homogeneous vector field of degree $\kappa_2 = [(\bar{\gamma} - 1)/\bar{\gamma}] > 0$ w.r.t. dilations (weights) $r_i = 1/\bar{\gamma}_i$, $i = \overline{1,n}$. We can verify that the LF $V_2(\Xi) = \Xi^T P_2^x \Xi$ is homogeneous in $x = [\mathrm{x}_1 \quad \mathrm{x}_2]^{\mathrm{T}}$ of degree $l_2 = 1 > \max(-\kappa_2, 0)$, $\dot{V}_2(\Xi)$ is homogeneous in $x = [\mathrm{x}_1 \quad \mathrm{x}_2]^T$ of degree $l_2 + \kappa_2 = 1 + \kappa_2$, w.r.t. the same weights $r_i, i = \overline{1,n}$. Applying Lemma 2 with $V_2 = \dot{V}_2(\Xi)$, we get

$$\dot{V}_2(\Xi) \le -c_2 V_2^{\frac{2\bar{\gamma}-1}{\bar{\gamma}}}(\Xi), \quad (55)$$

where $\frac{2\bar{\gamma}-1}{\bar{\gamma}} > 1$. Then, similarly to (49), the following inequality is obtained

$$\dot{V}_2(\Xi) \le -\frac{\lambda_{\min}(Q_2^x)}{\lambda_{\max}(P_2^x)} V_2^{\frac{2\bar{\gamma}-1}{\bar{\gamma}}}(\Xi), \quad (56)$$

Hence, the constant c_2 in (55) can be assigned as $c_2 = \frac{\lambda_{\min}(Q_2^x)}{\lambda_{\max}(P_2^x)}$. The expression of the settling-time can be obtained via solving the differential equation (56). This can be achieved by utilizing the separation of variables method. Thus, by separating the variables and then integrating both sides of (56), we get

$$\int_{\Xi(0)}^{\Xi(t)} \frac{dV_2}{V_2^{\frac{2\bar{\gamma}-1}{\bar{\gamma}}}} \le \int_0^t -\frac{\lambda_{\min}(Q_2^x)}{\lambda_{\max}(P_2^x)} dt,$$

Then the following expression can be obtained

$$\frac{1}{-\frac{\bar{\gamma}-1}{\bar{\gamma}}}\left[V_2^{-\frac{\bar{\gamma}-1}{\bar{\gamma}}}(\Xi(t)) - V_2^{-\frac{\bar{\gamma}-1}{\bar{\gamma}}}(\Xi(0))\right] \le -\frac{\lambda_{\min}(Q_2^x)}{\lambda_{\max}(P_2^x)} t,$$

Finally, the expression of t can be deduced as

$$t = \frac{\bar{\gamma}}{\bar{\gamma}-1}\frac{\lambda_{\max}(P_2^x)}{\lambda_{\min}(Q_2^x)}\left[V_2^{-\frac{\bar{\gamma}-1}{\bar{\gamma}}}(\Xi(t)) - V_2^{-\frac{\bar{\gamma}-1}{\bar{\gamma}}}(\Xi(0))\right],$$

Let □ be a positive number satisfying $V_2(\Xi(0)) >$ □. The time in which $V_2(\Xi)$ decreases and reaches the value □, i.e., $V_2(\Xi) \to$ □ can be given as

$$\begin{aligned} t &= \frac{\bar{\gamma}}{\bar{\gamma}-1}\frac{\lambda_{\max}(P_2^x)}{\lambda_{\min}(Q_2^x)}\left[V_2^{-\frac{\bar{\gamma}-1}{\bar{\gamma}}}(\Xi(t)) - V_2^{-\frac{\bar{\gamma}-1}{\bar{\gamma}}}(\Xi(0))\right] \\ &= \frac{\bar{\gamma}}{\bar{\gamma}-1}\frac{\lambda_{\max}(P_2^x)}{\lambda_{\min}(Q_2^x)}\left[\square^{-\frac{\bar{\gamma}-1}{\bar{\gamma}}} - V_2^{-\frac{\bar{\gamma}_0-1}{\bar{\gamma}_0}}(\Xi(0))\right] \\ &\le \frac{\bar{\gamma}}{\bar{\gamma}-1}\frac{\lambda_{\max}(P_2^x)}{\lambda_{\min}(Q_2^x)}\square^{-\frac{\bar{\gamma}-1}{\bar{\gamma}}} \stackrel{\text{def}}{=} T_1. \end{aligned}$$

We can obtain that $V_2(\Xi) \le \lambda_{\min}(P_2^x)\|\Xi\|^2$ thus $\|\Xi\|^2 \le \frac{V_2(\Xi)}{\lambda_{\min}(P_2^x)} \le \frac{\square}{\lambda_{\min}(P_2^x)} \le 1$. Then, the states of system (51) reach the following set where they stay confined $\Im \stackrel{\text{def}}{=} \left\{x: \|\Xi\|^2 \le \frac{\square}{\lambda_{\min}(P_2^x)}\right\}$ for $t > T_1$.

Step 3. In this step, the global settling-time for system (40) under the input $\mathcal{v}(t) + \mathcal{w}(t)$, i.e., (35) + (36) is analyzed as in [60]. Consider a positive real number □ satisfying $\forall$ □ $>$ $0, V_2(\Xi(0)) >$ □. The derivative of $V_2(\Xi)$ versus time along with trajectories of system (40) can be computed as

$$\begin{aligned} \dot{V}_2(\Xi) &= \frac{\partial V_2}{\partial x}(Ax + B\mathcal{w}) + \frac{\partial V_2}{\partial x}(B\mathcal{v}) \\ &\le \dot{V}_2(\Xi) - \frac{\partial V_2}{\partial x}\left(k_1^{\mathrm{x}_1}\mathrm{sign}^{\gamma_1}(\mathrm{x}_1) + k_2^{\mathrm{x}_1}\mathrm{sign}^{\gamma_2}(\mathrm{x}_2)\right) \\ &\le \dot{V}_2(\Xi) \le -\frac{\lambda_{\min}(Q_2^x)}{\lambda_{\max}(P_2^x)} V_2^{\frac{2\bar{\gamma}-1}{\bar{\gamma}}}(\Xi). \end{aligned}$$

According to Step 2 of the current proof, it can be shown that the states of system (51) reach the set $\Im = \left\{x: \|\Xi\|^2 \le \frac{\square}{\lambda_{\min}(P_2^x)} \le 1\right\}$ for $t \ge T_1 = \frac{\bar{\gamma}}{\bar{\gamma}-1}\frac{\lambda_{\max}(P_2^x)}{\lambda_{\min}(Q_2^x)}\lambda_{\max}^{-\frac{\bar{\gamma}-1}{\bar{\gamma}}}(P_2^x)$.

Similarly, the derivative of $V_1(\Xi)$ versus time along with trajectories of system (40) can be given as

$$\dot{V}_1(\Xi) = \frac{\partial V_1}{\partial x}(Ax + B\upsilon) + \frac{\partial V_1}{\partial x}(B\omega)$$
$$\leq \dot{V}_1(\Xi) - \frac{\partial V_1}{\partial x}\left(\bar{k}_1^{\mathrm{x}_1}\mathrm{sign}^{\bar{\gamma}_1}(\mathrm{x}_1) + \bar{k}_2^{\mathrm{x}_1}\mathrm{sign}^{\bar{\gamma}_2}(\mathrm{x}_2)\right)$$
$$\leq \dot{V}_1(\Xi) \leq -\frac{\lambda_{\min}(Q_1^x)}{\lambda_{\max}(P_1^x)} V_1^{\frac{2\gamma-1}{\gamma}}(\Xi).$$

From Step 1 of the proof, it is guaranteed that the input $\upsilon(t) + \omega(t)$ can stabilize system (40) at the origin in finite-time within a setting-time T_0 defined in (50). Without loss of generality, for all $t \geq T_1$, $\|\Xi\| = 1$ is applied for $V_1\big(\Xi(T_2)\big) \leq \lambda_{\max}(P_1^x)\|\Xi\|^2 = \lambda_{\max}(P_1^x)$. Hence, the upper bound on the global settling-time can be obtained as

$$T_x \leq T_x^{\max} \stackrel{\text{def}}{=} \frac{\gamma}{1-\gamma}\frac{\lambda_{\max}(P_1^x)}{\lambda_{\min}(Q_1^x)}\lambda_{\max}^{\frac{1-\gamma}{\gamma}}(P_1^x) + \frac{\bar{\gamma}}{\bar{\gamma}-1}\frac{\lambda_{\max}(P_2^x)}{\lambda_{\min}(Q_2^x)}\lambda_{\max}^{-\frac{\bar{\gamma}-1}{\bar{\gamma}}}(P_2^x). \tag{57}$$

Finally, the states of system (40) and thus (39) can be stabilized to zero $x = [\mathrm{x}_1 \quad \mathrm{x}_2]^T \to 0$ within fixed-time given in (57). ■

As mentioned in the first point of Section "*1.3 Theoretical and Practical Contributions*", the succeeding corollary with interesting results on fixed-time stabilization feedback controller and ISS can be deduced from Theorem 1.

Corollary 1. The following two results can be obtained from Theorem 1: **(i)** Fixed-time stabilization feedback controller for uncertain nonlinear high-order systems can be designed based on the proposed sliding surface (34). **(ii)** ISS is ensured in the presence of external bounded control input corrupted with matched nonlinear disturbances.

(i) Fixed-time stabilization feedback controller. Consider the following uncertain nonlinear n-th order system

$$\begin{cases} \dot{\bar{\mathrm{x}}}_1(t) = \bar{\mathrm{x}}_2(t), \\ \dot{\bar{\mathrm{x}}}_2(t) = \bar{\mathrm{x}}_3(t), \\ \quad\vdots \\ \dot{\bar{\mathrm{x}}}_{n-1}(t) = \bar{\mathrm{x}}_n(t), \\ \dot{\bar{\mathrm{x}}}_n(t) = f_{\bar{\mathrm{x}}}\big(\bar{\mathrm{x}}(t)\big) + g_{\bar{\mathrm{x}}}\big(\bar{\mathrm{x}}(t)\big)u_{\bar{\mathrm{x}}}(t) + d(t). \end{cases} \qquad \bar{\mathrm{x}}(0) = \bar{\mathrm{x}}_0, \tag{58}$$

where $\bar{\mathrm{x}} \stackrel{\text{def}}{=} [\bar{\mathrm{x}}_1, \bar{\mathrm{x}}_2, \dots, \bar{\mathrm{x}}_n]^{\mathrm{T}} \in \mathbb{R}^n$ is the state vector, $f_{\bar{\mathrm{x}}}^{\mathcal{N}}(\bar{\mathrm{x}})$ and $g_{\bar{\mathrm{x}}}^{\mathcal{N}}(\bar{\mathrm{x}}) \neq 0$ are smooth nonlinear functions representing the nominal dynamics of the system. The control input is denoted by $u_{\bar{\mathrm{x}}}(t) \in \mathbb{R}$ and $d(t) \in \mathbb{R}$ represents the lumped uncertainties. Consider the following sliding surface designed from (34) for the n-th order system (58)

$$\mathrm{s}(t) \stackrel{\text{def}}{=} \bar{\mathrm{x}}_n(t) + \sum_{i=1}^{n}\int_0^t \left[k_i^{\bar{\mathrm{x}}_i}\mathrm{sign}^{\gamma_i}(\bar{\mathrm{x}}_i) + \bar{k}_i^{\bar{\mathrm{x}}_i}\mathrm{sign}^{\bar{\gamma}_i}(\bar{\mathrm{x}}_i)\right]d\tau, \tag{59}$$

where $k_i^{\bar{\mathrm{x}}_i}, \bar{k}_i^{\bar{\mathrm{x}}_i} \in \mathbb{R}_+$. If the feedback $u_{\bar{\mathrm{x}}}$ is determined as $u_{\bar{\mathrm{x}}}(t) \stackrel{\text{def}}{=} \frac{1}{g_{\bar{\mathrm{x}}}^{\mathcal{N}}}\left[\sum_{i=1}^{n}\left[k_i^{\bar{\mathrm{x}}_i}\mathrm{sign}^{\gamma_i}(\bar{\mathrm{x}}_i) + \bar{k}_i^{\bar{\mathrm{x}}_i}\mathrm{sign}^{\bar{\gamma}_i}(\bar{\mathrm{x}}_i)\right] - f_{\bar{\mathrm{x}}}^{\mathcal{N}} - \hat{d}\right]$, where $\hat{d}$ is the estimate of d which is provided by a disturbance observer, the system (58) becomes as

$$\begin{cases} \dot{\bar{\mathrm{x}}}_1(t) = \bar{\mathrm{x}}_2(t), \\ \dot{\bar{\mathrm{x}}}_2(t) = \bar{\mathrm{x}}_3(t), \\ \quad\vdots \\ \dot{\bar{\mathrm{x}}}_{n-1}(t) = \bar{\mathrm{x}}_n(t), \\ \dot{\bar{\mathrm{x}}}_n(t) = -\sum_{i=1}^{n}\left[k_i^{\bar{\mathrm{x}}_i}\mathrm{sign}^{\gamma_i}(\bar{\mathrm{x}}_i) + \bar{k}_i^{\bar{\mathrm{x}}_i}\mathrm{sign}^{\bar{\gamma}_i}(\bar{\mathrm{x}}_i)\right]. \end{cases} \tag{60}$$

Thus, it follows that the states of the system (58) are stabilized at the zero-equilibrium point $\bar{\mathrm{x}} = 0$ in fixed-time from any arbitrary initial point $\bar{\mathrm{x}}_0 \neq 0$. The convergence-time is bounded as

$$T_{\bar{\mathrm{x}}} \leq T_{\bar{\mathrm{x}}}^{\max} \stackrel{\text{def}}{=} \frac{\gamma}{1-\gamma}\frac{\lambda_{\max}(P_1^{\bar{\mathrm{x}}})}{\lambda_{\min}(Q_1^{\bar{\mathrm{x}}})}\lambda_{\max}^{\frac{1-\gamma}{\gamma}}(P_1^{\bar{\mathrm{x}}}) + \frac{\bar{\gamma}}{\bar{\gamma}-1}\frac{\lambda_{\max}(P_2^{\bar{\mathrm{x}}})}{\lambda_{\min}(Q_2^{\bar{\mathrm{x}}})}\lambda_{\max}^{-\frac{\bar{\gamma}-1}{\bar{\gamma}}}(P_2^{\bar{\mathrm{x}}}).$$

(ii) ISS under external bounded control input corrupted with nonlinear disturbances. Consider the following nonlinear system

$$\dot{\bar{\mathrm{x}}} = f(\bar{\mathrm{x}}, d), \qquad \bar{\mathrm{x}} \in \mathbb{R}^n, d \in \mathbb{R}. \tag{61}$$

where $f : \mathbb{R}^n \times \mathbb{R} \to \mathbb{R}$ is a continuous vector field or Lipschitz continuous function that is homogeneous in the bi-limit and d is bounded exogenous disturbances. It should be noted that if the origins of the following systems

$$\dot{\bar{\mathrm{x}}} = f(\bar{\mathrm{x}}, 0), \qquad \dot{\bar{\mathrm{x}}} = f_0(\bar{\mathrm{x}}, 0), \qquad \dot{\bar{\mathrm{x}}} = f_\infty(\bar{\mathrm{x}}, 0).$$

are GAS equilibria, the system (61) is ISS w.r.t. the bounded matched disturbances d.

Remark 8. Corollary 1 presents a control design methodology for systems with high-integrator dynamics. The second-order system is a particular case where many fundamental physical systems in practice can be described by a double-integrator, such as the quadrotor dynamics representing the position and attitude of the aircraft. By following the guideline of the findings in Corollary 1, tracking controllers, i.e., FNHNTSMC can be designed for attitude and position loops. By so doing, the tracking controllers should be adequately designed to satisfy the conditions of Corollary 1, thus stabilizing the system.

3.2 Control Design

The obtained results in the previous subsection are exploited to derive and synthesize a trajectory tracking control law, i.e., FNHNTSMC, for the second-order attitude and position subsystems. To deal with the strong coupling and underactuation nature in the four-rotor dynamics, the hierarchical control framework consisting of attitude-position (inner-outer) loops is adopted. The block diagram of the feedback-loop control system is shown in Fig. 3. The desired trajectory can be generated by a trajectory generator algorithm such as B-spline [56]. The trajectory generator transforms some given waypoints to a time-parametrized path that is represented by a polynomial. The waypoints can be generated by a path planner, e.g., rapidly exploring random tree (RRT) or A* [2] [61].

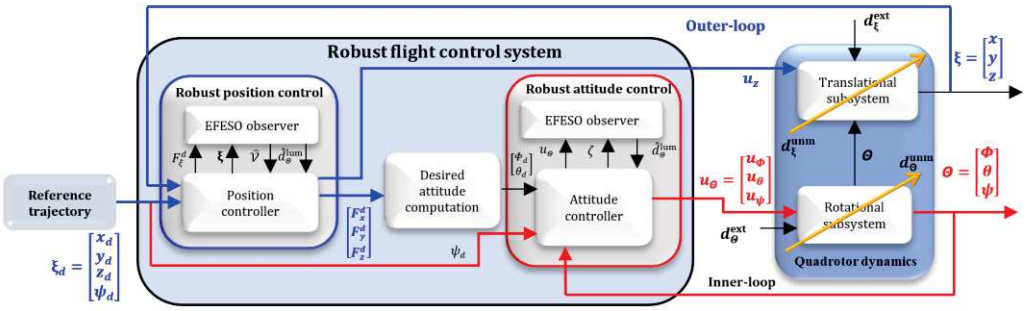

Fig. 3. Block diagram of the feedback-loop control system of the quadrotor aircraft. The orange arrows indicate parameters variation and unmodeled dynamics.

3.2.1 Attitude Tracking Controller

The proposed fixed-time sliding surface in Section 3.1 is used to derive and synthesize a new fixed-time feedback control law, i.e., FNHNTSMC. Consider the perturbated nonlinear attitude system (26). Let the attitude tracking error and its dynamics be defined as

$$\begin{cases} e_1^{\varTheta} \triangleq \varTheta - \varTheta_d, \\ e_2^{\varTheta} \triangleq \dot{\varTheta} - \dot{\varTheta}_d. \end{cases} \tag{62}$$

After differentiating (62), we get the errors dynamics as

$$\begin{cases} \dot{e}_1^{\varTheta} = e_2^{\varTheta}, \\ \dot{e}_2^{\varTheta} = \ddot{\varTheta} - \ddot{\varTheta}_d. \end{cases} \tag{63}$$

The sliding surface for the attitude tracking is defined based on (34) as

$$s_{\varTheta}(e_1^{\varTheta}, e_2^{\varTheta}, t) \triangleq e_2^{\varTheta}(t) + \int_0^t [\nu_{\varTheta}(t) + \iota\nu_{\varTheta}(t)]d\tau, \tag{64}$$

$$\nu_{\varTheta}(t) \triangleq k_1^{\varTheta}\text{sign}^{\gamma_1}(e_1^{\varTheta}) + k_2^{\varTheta}\text{sign}^{\gamma_2}(e_2^{\varTheta}), \tag{65}$$

$$\iota\nu_{\varTheta}(t) \triangleq \bar{k}_1^{\varTheta}\text{sign}^{\bar{\gamma}_1}(e_1^{\varTheta}) + \bar{k}_2^{\varTheta}\text{sign}^{\bar{\gamma}_2}(e_2^{\varTheta}). \tag{66}$$

We propose the following composite tracking control input that can establish fast reaching-time of the sliding surface $s_{\varTheta}$ and can achieve the sliding motion on $s_{\varTheta} = 0$

$$u_{\varTheta} \triangleq \frac{1}{g_{\varTheta}^{\mathcal{N}}}\left[u_{\text{r}}^{\varTheta} + u_{\text{eq}}^{\varTheta}\right]. \tag{67}$$

The proposed control scheme comprises two parts. The reaching control term $u_{\text{r}}^{\varTheta}$ is responsible for providing fast fixed-time convergence to the sliding manifold $s_{\varTheta}$ while the equivalent control term $u_{\text{eq}}^{\varTheta}$ is responsible for maintaining the system states on $s_{\varTheta}$ and suppresses the disturbances. The reaching law $u_{\text{r}}^{\varTheta}$ is appropriately designed to ensure fast fixed-time reaching of the sliding manifold as

$$u_{\text{r}}^{\varTheta} \triangleq -k_1^{s_{\varTheta}}\text{sign}^{\alpha}(s_{\varTheta}) - k_2^{s_{\varTheta}}\text{sign}^{\beta}(s_{\varTheta}). \tag{68}$$

The design of the $u_{\text{eq}}^{\varTheta}$ control is based on the sliding motion $s_{\varTheta} = 0, u_{\text{r}}^{\varTheta} = 0$. With $s_{\varTheta} = 0$, from (64), the sliding manifold dynamics is governed by

$$\dot{s}_{\varTheta} = \dot{e}_2^{\varTheta} + \nu_{\varTheta} + \iota\nu_{\varTheta} = 0, \tag{69}$$

From (26) and (63), we get

$$\dot{e}_2^{\varTheta} = f_{\varTheta}^{\mathcal{N}} + g_{\varTheta}^{\mathcal{N}}u_{\varTheta} + d_{\varTheta}^{\text{lum}} - \ddot{\varTheta}_d, \tag{70}$$

By putting the expression of $\dot{e}_2^{\varTheta}$ from (70) into (69) while considering $u_{\text{r}}^{\varTheta} = 0$ and $u_{\varTheta} \equiv u_{\text{eq}}^{\varTheta}$, yields

$$u_{\text{eq}}^{\varTheta} \triangleq -\nu_{\varTheta} - \iota\nu_{\varTheta} - f_{\varTheta}^{\mathcal{N}} + \ddot{\varTheta}_d - \hat{d}_{\varTheta}^{\text{lum}}. \tag{71}$$

Remark 9. It is pertinent to mention here that the proposed control law (67) avoids the singularity issue because the derivatives of the terms $\text{sign}^{\gamma_1}(\text{x}_1), \text{sign}^{\gamma_2}(\text{x}_2), \text{sign}^{\alpha}(s_{\text{x}_1})$ with fractional power $(\gamma_1, \gamma_2, \alpha < 1)$ are not involved in (67). Thus, the signal magnitude remains bounded. The singularity issue arises if the control signal has a term with a negative exponent. For instance, this issue arises if the derivative of $\text{sign}^{\gamma_1}(\text{x}_1)$ exists in the control law, i.e., $\lim_{\text{x}_1 \to 0} \frac{d(\text{sign}^{\gamma_1}(\text{x}_1))}{dt} = \lim_{\text{x}_1 \to 0} \gamma_1 |\text{x}_1|^{\gamma_1 - 1} = \infty$, since $\gamma_1 - 1 < 0$.

Remark 10. (Control parameters selection). Two classes of terms are used to design the fixed-time stabilization control law (71); one with power higher than 1, i.e., $\text{sign}^{\bar{\gamma}_1}(\text{x}_2), \text{sign}^{\bar{\gamma}_2}(\text{x}_2)$ and the other with power in fractions, i.e., $\text{sign}^{\gamma_1}(\text{x}_1), \text{sign}^{\gamma_2}(\text{x}_2)$. In contrast to the control structures reported in [59], [62], and [63], the proposed control structure in the present work can uniformly drive the system's states in fixed-time into a compact set w.r.t. the ICs. The exponents $\bar{\gamma}_i, (i = \overline{1,n})$ for n-th order system are selected as follows: $\bar{\gamma}_i > 1$ and $\bar{\gamma}_i$ should satisfy $\bar{\gamma}_{i-1} = \bar{\gamma}_i\bar{\gamma}_{i+1}/(2\bar{\gamma}_{i+1} - \bar{\gamma}_i), i = \overline{2,n}$, $\bar{\gamma}_{i+1} = 1$, and $\bar{\gamma}_n = \bar{\gamma}$, where $\bar{\gamma} \in (1, 1+\varepsilon_2)$ for a sufficiently small $\varepsilon_2 > 0$. The selection of $k_1^{\text{x}_1}, k_2^{\text{x}_1}$ is discussed above in Section 2.3.

3.2.2 Position Tracking Controller

Let the position tracking error be defined as

$$\begin{cases} e_1^{\xi} \triangleq \xi - \xi_d, \\ e_2^{\xi} \triangleq \dot{\xi} - \dot{\xi}_d. \end{cases} \tag{72}$$

The desired virtual controls $F_{\xi}^{d} \in \mathbb{R}^3, \xi = \{x, y, z\}$ of the position motion can be derived similarly to the attitude motion. Then, F_{ξ}^{d} are designed as

$$F_{\xi}^{d} \triangleq -\nu_{\xi} - w_{\xi} - \hat{d}_{\xi}^{\text{lum}} + \ddot{\xi}_d + u_{\text{r}}^{\xi}. \tag{73}$$

where $u_{\text{r}}^{\xi} \triangleq -k_1^{s_{\xi}}\text{sign}^{\alpha}(s_{\xi}) - k_2^{s_{\xi}}\text{sign}^{\beta}(s_{\xi})$, $s_{\xi}(t) \triangleq e_2^{\xi}(t) + \int_0^t [\nu_{\xi}(t) + w_{\xi}(t)]d\tau$, $\nu_{\xi}(t) \triangleq k_1^{\xi}\text{sign}^{\gamma_1}\left(e_1^{\xi}\right) + k_2^{\xi}\text{sign}^{\gamma_2}\left(e_2^{\xi}\right)$, and $w_{\xi}(t) \triangleq \bar{k}_1^{\xi}\text{sign}^{\bar{\gamma}_1}\left(e_1^{\xi}\right) + \bar{k}_2^{\xi}\text{sign}^{\bar{\gamma}_2}\left(e_2^{\xi}\right)$. Next, the lift control and the reference attitude signals need to be computed. Thus, by combining the expressions of F_{ξ} from (28) with those of F_{ξ}^{d} in (73), and after some manipulations, the lift control u_z and the desired roll and pitch angles (Φ_d, θ_d) can be obtained as: $u_z \triangleq m^{\mathcal{N}}\sqrt{\left(F_x^d\right)^2 + \left(F_y^d\right)^2 + \left(F_z^d - \text{g}\right)^2}$, $\Phi_d \triangleq \arcsin\left[-\frac{m^{\mathcal{N}}}{u_z}\left(F_x^d s\psi_d - F_y^d c\psi_d\right)\right]$, and $\theta_d \triangleq \arctan\left[\frac{1}{F_z^d - \text{g}}\left(F_x^d c\psi_d + F_y^d s\psi_d\right)\right]$.

3.3 Observer Design

The unknown disturbances $d_{\Theta}^{\text{lum}}, d_{\xi}^{\text{lum}}$ are considered sufficiently smooth (differentiable) uncertain functions where their first-time derivatives are bounded, as shown in the following assumption.

Assumption 2. The disturbances $d_{\Theta}^{\text{lum}}, d_{\xi}^{\text{lum}}$ are matched Lipschitz continuous, i.e., applied in the control channel with bounded derivatives satisfying $\left\|\dot{d}_{\Theta}^{\text{lum}}\right\| \leq \bar{d}_{\Theta}$ and $\left\|\dot{d}_{\xi}^{\text{lum}}\right\| \leq \bar{d}_{\xi}$ where $\bar{d}_{\Theta}, \bar{d}_{\xi} \in \mathbb{R}_+$ are known Lipschitz constants.

Remark 11. The observer designed for a surface vessel in [64] is inspired by the work conducted by Basin *et al.* in [65]. Although the interesting work [64] provides promising results, some shortcomings are found in the observer part of this work:

(i) Stability proof and convergence-time: A through stability proof for the convergence of the observer is not provided explicitly. Moreover, the stability analysis of the observer with the structure (13) in [64] cannot be conducted. The stability study should be conducted in two consecutive steps. Therefore, to achieve strict stability and convergence analyses, a switching function T_u is necessarily introduced in the observer dynamics. Thus, the convergence-time of the observer would be more accurate than the one given by expression (20) of [64];

(ii) Parameters selection: The condition on parameters tuning for the finite-time part of the observer is not provided in a strict way. These parameters are only assumed to satisfy that a given square matrix and its characteristic polynomial are Hurwitz. In contrast to that, we provide a tuning condition based on the bounds of the perturbation $\bar{d}_{\Theta}, \bar{d}_{\xi}$ given in Assumption 2, which is more practical.

(iii) Rejection of non-vanishing perturbation during the convergence: The introduction of the term $\Upsilon\text{sign}(\eta - \hat{\eta})$ in the right-hand side of equation 3 in expression (19) of [64] and [66] has not been justified by the authors. It might be used to cancel the disturbances. To reduce the chattering effect of the term $\Upsilon\text{sign}(\eta - \hat{\eta})$, the authors have replaced the sign function with a hyperbolic tangent function. However, this method does not seem to be very accurate in dealing with the non-vanishing perturbation d_{ξ}^{lum}. Non-vanishing means that the disturbances do not become zero when the error vanishes. In contrast to that, we have employed the Equivalent Control Method (ECM) to approximate and reject the non-vanishing perturbation during the convergence of the observer.

In the following, an Enhanced Fixed-time Extended State Observer (EFESO) is designed for the position dynamics. Similarly, another observer can be derived for the attitude system. Let the estimation error be defined as $e_1^{\text{ob}} \triangleq \xi - \hat{\xi}$. Given the perturbated translational dynamics described in (27), the EFESO is designed as

$$\begin{cases} \dot{\Gamma}_1^{\xi} = \Gamma_2^{\xi} + \rho_1^{\xi}\Lambda(t)\text{sign}^{\sigma_1}\left(e_1^{\text{ob}}\right) + \bar{\rho}_1^{\xi}\left(1 - \Lambda(t)\right)\text{sign}^{\varrho_1}\left(e_1^{\text{ob}}\right), \\ \dot{\Gamma}_2^{\xi} = \Gamma_3^{\xi} + \rho_2^{\xi}\Lambda(t)\text{sign}^{\sigma_2}\left(e_1^{\text{ob}}\right) + \bar{\rho}_2^{\xi}\left(1 - \Lambda(t)\right)\text{sign}^{\varrho_2}\left(e_1^{\text{ob}}\right) + F_{\xi}, \\ \dot{\Gamma}_3^{\xi} = \rho_3^{\xi}\Lambda(t)\text{sign}^{\sigma_3}\left(e_1^{\text{ob}}\right) + \bar{\rho}_3^{\xi}\left(1 - \Lambda(t)\right)\text{sign}^{\varrho_3}\left(e_1^{\text{ob}}\right) + \left[d_{\xi}^{\text{lum}}\right]_{\text{eq}}. \end{cases} \tag{74}$$

The term $\left[d_{\xi}^{\text{lum}}\right]_{\text{eq}}$ represents the approximation of the disturbances d_{ξ}^{lum} by the ECM. It is defined as

$$\left[d_{\xi}^{\text{lum}}\right]_{\text{eq}} \triangleq \left[\bar{d}_{\xi}\text{sign}\left(e_1^{\text{ob}}\right)\right]_{\text{eq}} \equiv d_{\xi}^{\text{lum}}, \tag{75}$$

where $\left[\bar{d}_{\xi}\text{sign}\left(e_1^{\text{ob}}\right)\right]_{\text{eq}}$ is an average value of the discontinuous function $\bar{d}_{\xi}\text{sign}\left(e_1^{\text{ob}}\right)$. For the implementation reason, $\left[d_{\xi}^{\text{lum}}\right]_{\text{eq}}$ can be approximated by a low-pass filter as

$$\left[\dot{d}_{\xi}^{\text{lum}}\right]_{\text{eq}} \approx \frac{1}{\bar{\tau}}\left(\bar{d}_{\xi}\text{sign}\left(e_1^{\text{ob}}\right) - \left[d_{\xi}^{\text{lum}}\right]_{\text{eq}}\right). \tag{76}$$

The exponents $\sigma_i, i = \overline{1,3}$ are selected as follows: $\sigma_i \in (0,1), i = \overline{1,3}$ satisfy the recurrent relations $\sigma_i = i\bar{\sigma} - (i-1), i = \overline{2,3}$, and $\sigma_1 = \bar{\sigma}$ where $\bar{\sigma} \in (1 - \varepsilon_3, 1)$ for a sufficiently small $\varepsilon_3 > 0$. The exponents $\varrho_i, i = \overline{1,3}$ are selected as follows: $\varrho_i > 1, i = \overline{1,3}$, satisfy the recurrent relations $\varrho_i = i\bar{\varrho} - (i-1), i = \overline{2,3}$, and $\varrho = \bar{\varrho}$ where $\bar{\varrho} \in (1, 1 + \varepsilon_4)$ for a small $\varepsilon_4 > 0$. The parameters $\rho_i^{\xi}, i = \overline{1,3}$ are selected based on the bound of the perturbation as $\rho_1^{\xi} = 2\bar{d}_{\xi}^{(1/3)}$, $\rho_2^{\xi} = 1.5\rho_3^{\xi}$, $\rho_3^{\xi} = 1.1\bar{d}_{\xi}$. $\bar{\rho}_i^{\xi}, i = \overline{1,3}$ are chosen such that the following matrix is Hurwitz

$$A_{\text{ob}}^{\xi} \triangleq \begin{bmatrix} -\bar{\rho}_1^{\xi} & 1 & 0 \\ -\bar{\rho}_2^{\xi} & 0 & 1 \\ -\bar{\rho}_3^{\xi} & 0 & 0 \end{bmatrix}.$$

Theorem 2. The observer (74) can precisely estimate the velocity $\mathcal{V}$ of the quadrotor system and the lumped disturbanceS

d_ξ^{lum} within a fixed-time, i.e., $\Gamma_3^\xi = \hat{d}_\xi^{\text{lum}} \equiv d_\xi^{\text{lum}}$ and $\Gamma_2^\xi = \hat{\mathcal{V}} \equiv \mathcal{V}$.

Proof. Define the observation errors as

$$\begin{cases} e_1^{\text{ob}} \overset{\text{def}}{=} \xi - \hat{\xi}, \\ e_2^{\text{ob}} \overset{\text{def}}{=} \mathcal{V} - \hat{\mathcal{V}}, \\ e_3^{\text{ob}} \overset{\text{def}}{=} d_\xi^{\text{lum}} - \hat{d}_\xi^{\text{lum}}, \end{cases} \tag{77}$$

After differentiating (77) versus time, we get the dynamics of the observation error as

$$\begin{cases} \dot{e}_1^{\text{ob}} = e_2^{\text{ob}} - \rho_1^\xi \Lambda \text{sign}^{\sigma_1}(e_1^{\text{ob}}) - \bar{\rho}_1^\xi (1-\Lambda)\text{sign}^{\varrho_1}(e_1^{\text{ob}}), \\ \dot{e}_2^{\text{ob}} = e_3^{\text{ob}} - \rho_2^\xi \Lambda \text{sign}^{\sigma_2}(e_1^{\text{ob}}) - \bar{\rho}_2^\xi (1-\Lambda)\text{sign}^{\varrho_2}(e_1^{\text{ob}}), \\ \dot{e}_3^{\text{ob}} = \dot{d}_\xi^{\text{lum}} - [d_\xi^{\text{lum}}]|_{\text{eq}} - \rho_3^\xi \Lambda \text{sign}^{\sigma_3}(e_1^{\text{ob}}) - \bar{\rho}_3^\xi (1-\Lambda)\text{sign}^{\varrho_3}(e_1^{\text{ob}}). \end{cases} \tag{78}$$

For $t \le T_u$, we have $\Lambda = 0$ and $[d_\xi^{\text{lum}}]|_{\text{eq}} \to \dot{d}_\xi^{\text{lum}}$. Thus, system (78) becomes

$$\begin{cases} \dot{e}_1^{\text{ob}} = e_2^{\text{ob}} - \bar{\rho}_1^\xi \text{sign}^{\varrho_1}(e_1^{\text{ob}}), \\ \dot{e}_2^{\text{ob}} = e_3^{\text{ob}} - \bar{\rho}_2^\xi \text{sign}^{\varrho_2}(e_1^{\text{ob}}), \\ \dot{e}_3^{\text{ob}} = -\bar{\rho}_3^\xi \text{sign}^{\varrho_3}(e_1^{\text{ob}}). \end{cases} \tag{79}$$

Similar to (40), the system (79) can be written in the following state-space form

$$\dot{z}(t) = A_z z(t) + B_z u_z(t). \tag{80}$$

where $z(t) = \left[e_1^{\text{ob}}(t) \quad e_2^{\text{ob}}(t) \quad e_3^{\text{ob}}(t)\right]^T$, $z_0 = \left[e_1^{\text{ob}}(0) \quad e_2^{\text{ob}}(0) \quad e_3^{\text{ob}}(0)\right]^T$ are ICs of the system, and A_z, B_z, u_z are given as

$$A_z = \begin{bmatrix} 0 & 1 & 0 \\ 0 & 0 & 1 \\ 0 & 0 & 0 \end{bmatrix}, B_z = \begin{bmatrix} 1 & 0 & 0 \\ 0 & 1 & 0 \\ 0 & 0 & 1 \end{bmatrix}, u_z = \begin{bmatrix} -\bar{\rho}_1^\xi \text{sign}^{\varrho_1}(e_1^{\text{ob}}) \\ -\bar{\rho}_2^\xi \text{sign}^{\varrho_2}(e_1^{\text{ob}}) \\ -\bar{\rho}_3^\xi \text{sign}^{\varrho_3}(e_1^{\text{ob}}) \end{bmatrix}.$$

We can select a LF as

$$V_z(\Xi_{z,1}) \overset{\text{def}}{=} \Xi_{z,1}^T(z) P_z^\xi \Xi_{z,1}(z). \tag{81}$$

where $\Xi_{z,1}(z) \overset{\text{def}}{=} \left[e_1^{\text{ob}} \quad (e_1^{\text{ob}})^{\frac{1}{\varrho_1}} \quad (e_1^{\text{ob}})^{\frac{1}{\varrho_2}}\right]^T$. The symmetric positive definite matrix P_z satisfies the ALE $P_z^\xi A_z + A_z^T P_z^\xi = -Q_z$ with Q_z being a positive definite matrix. Since the matrix A_z is Hurwitz, the linear system $\dot{z}(t) = A_z z(t)$ is AS. Since the matrix P_z^ξ is defined as the solution of $P_z^\xi A_z + A_z^T P_z^\xi = -Q_z^\xi$, the function $V_z(z) \overset{\text{def}}{=} z^T P_z^\xi z$ is a LF for system $\dot{z}(t) = A_z z(t)$. Moreover, the following inequality is obtained for the time derivative of $V_z(z)$

$$\begin{aligned} \dot{V}_z(z) &= \dot{z}^T P_z^\xi z + z^T P_z^\xi \dot{z} = z^T \left(A_z^T P_z^\xi + P_z A_z\right) z \\ &= -z^T Q_z^\xi z < 0. \end{aligned} \tag{82}$$

The inequality $\dot{V}_z(z) = -z^T Q_z^\xi z < 0$ remains valid for the function $V_z(\Xi_{z,1})$ given in (81). Hence, the system (80) is AS. The right-hand side of (80) is a homogeneous vector field of degree $\kappa_z = \bar{\varrho} - 1 > 0$ w.r.t. dilations $r_{i,z} = i\bar{\varrho} - (i-1), (i = \overline{1,n})$, which implies the uniform convergence of system (80) [67]. By following the guidelines of Definition 4 given above in Section 2.1.1 and Theorem 6.2 in [44], it can be obtained that the LF $V_z(\Xi_{z,1}) = \Xi_{z,1}^T(z) P_z^\xi \Xi_{z,1}(z)$ is homogeneous in $z = \left[e_1^{\text{ob}} \quad e_2^{\text{ob}} \quad e_3^{\text{ob}}\right]^T$ of degree $l_3 = 2 > \max(-\kappa_3, 0)$, if $\bar{\varrho}$ is sufficiently close to 1, and its full time derivative $\dot{V}_z(\Xi_{z,1})$ is homogeneous in $z = \left[e_1^{\text{ob}} \quad e_2^{\text{ob}} \quad e_3^{\text{ob}}\right]^T$ of degree $l_4 = l_3 + \kappa_z = 1 + \bar{\varrho} > 0$, w.r.t. the same weights $r_i, (i = \overline{1,n})$. Applying Lemma 2 with $V_2 = \dot{V}_z(\Xi_{z,1})$, we get

$$\dot{V}_z(\Xi_{z,1}) \le -c_z V_z^{\frac{\bar{\varrho}+1}{2}}(\Xi_{z,1}), \tag{83}$$

Considering the continuity of the right-hand side of (80) w.r.t. $\bar{\varrho}$, the following inequality holds

$$\dot{V}_z(\Xi_{z,1}) \le -\frac{\lambda_{\min}(Q_z^\xi)}{2\lambda_{\max}(P_z^\xi)} V_z^{\frac{\bar{\varrho}+1}{2}}(\Xi_{z,1}). \tag{84}$$

if $\bar{\varrho}$ is chosen in the interval $(1, 1+\varepsilon_4)$ for a small $\varepsilon_3 > 0$. Therefore, the constant c_z can be assigned as $c_z = \frac{\lambda_{\min}(Q_z^\xi)}{2\lambda_{\max}(P_z^\xi)}$.

When $t = T_u$, the LF $V_z(\Xi_{z,1})$ satisfies

$$\begin{aligned} V_z(T_u) &\le \left[\frac{\bar{\varrho}-1}{4} \frac{\lambda_{\min}(Q_z^\xi)}{\lambda_{\max}(P_z^\xi)} T_u + V_z^{\frac{1-\bar{\varrho}}{2}}(0)\right]^{\frac{2}{1-\bar{\varrho}}}, \\ &< \left[\frac{\bar{\varrho}-1}{4} \frac{\lambda_{\min}(Q_z^\xi)}{\lambda_{\max}(P_z^\xi)} T_u\right]^{\frac{2}{1-\bar{\varrho}}}. \end{aligned}$$

For $t > T_u$, we have $\Lambda = 0$ and system (78) becomes

$$\begin{cases} \dot{e}_1^{\text{ob}} = e_2^{\text{ob}} - \rho_1^\xi \text{sign}^{\sigma_1}(e_1^{\text{ob}}), \\ \dot{e}_2^{\text{ob}} = e_3^{\text{ob}} - \rho_2^\xi \text{sign}^{\sigma_2}(e_1^{\text{ob}}), \\ \dot{e}_3^{\text{ob}} = -\rho_3^\xi \text{sign}^{\sigma_3}(e_1^{\text{ob}}). \end{cases} \tag{85}$$

A LF can be selected as

$$V_z(\Xi_{z,2}) \overset{\text{def}}{=} \Xi_{z,2}^T(z) P_z^\xi \Xi_{z,2}(z). \tag{86}$$

where $\Xi_{z,2}(z) \overset{\text{def}}{=} \left[e_1^{\text{ob}} \quad (e_1^{\text{ob}})^{\frac{1}{\sigma_1}} \quad (e_1^{\text{ob}})^{\frac{1}{\sigma_2}}\right]^T$

The time derivative of $V_z(\Xi_{z,2})$ is given as

$$\dot{V}_z(\Xi_{z,2}) \le -\frac{\lambda_{\min}(Q_z^\xi)}{2\lambda_{\max}(P_z^\xi)} V_z^{\frac{\bar{\sigma}+1}{2}}(\Xi_{z,2}). \tag{87}$$

Since the exponent $\bar{\sigma}$ is smaller than 1, the LF (87) with the IC $V_z(T_u)$ is guaranteed to converge to zero in finite-time. Overall, system (85) can converge to the origin within fixed-time upper bounded as

$$T_{\mathrm{ob},\xi} \leq T_{\mathrm{ob},\xi}^{\max} = \frac{2\lambda_{\max}\left(P_z^{\xi}\right)}{\lambda_{\min}\left(Q_z^{\xi}\right)} \frac{2}{1-\bar{\sigma}} \left[\frac{\bar{\varrho}-1}{2} \frac{\lambda_{\min}\left(Q_z^{\xi}\right)}{2\lambda_{\max}\left(P_z^{\xi}\right)} T_u \right]^{\frac{1-\bar{\sigma}}{1-\bar{\varrho}}} + T_u. \tag{88}$$

Thus, completing the proof. ■

3.4 Stability Analysis of the Feedback-Loop Control System

In this subsection, the overall stability of the inner and outer tracking loops is investigated. Besides, the observer-controller dynamics are jointly analyzed to assure the UUB of all signals in the feedback system.

Theorem 3. Consider the nonlinear perturbated attitude system (27) and the designed control law u_Θ given in (67). Then, the attitude states reach the sliding surface s_Θ(64) in fixed-time and consequently converge to the origin in a uniformly bounded settling-time by sliding along $s_\Theta = 0$.

Proof. The first step proves that the reaching time is uniformly bounded, i.e., the states' trajectories reach the sliding manifold $s_\Theta = 0$ in fixed-time. After reaching the sliding surface, the second step demonstrates the fixed-time convergence of the tracking error to the origin, i.e., $e_1^\Theta(t) \to 0$ along with the sliding manifold $s_\Theta = 0$.

Step 1. Recalling the dynamic of s_Θ (64) from (69). Putting $\ddot{\Theta}$ from (26) into (69), we get

$$\dot{s}_\Theta = f_\Theta^{\mathcal{N}} + g_\Theta^{\mathcal{N}} u_\Theta + d_\Theta^{\mathrm{lum}} - \ddot{\Theta}_d + \nu_\Theta + \omega_\Theta, \tag{89}$$

Replacing the designed control law u_Θ by its expression given in (67) into (89), we get

$$\dot{s}_\Theta = u_{\mathrm{r}}^\Theta + d_\Theta^{\mathrm{lum}} - \hat{d}_\Theta^{\mathrm{lum}}, \tag{90}$$

Moreover, the lumped disturbances $\hat{d}_\Theta^{\mathrm{lum}}$ can be estimated by the EFESO, hence $d_\Theta^{\mathrm{lum}} - \hat{d}_\Theta^{\mathrm{lum}} = 0$. Thus, for $t \geq T_{\mathrm{ob}}$ we get

$$\dot{s}_\Theta = u_{\mathrm{r}}^\Theta = -k_1^{s_\Theta} \mathrm{sign}^{\alpha}(s_\Theta) - k_2^{s_\Theta} \mathrm{sign}^{\beta}(s_\Theta), \tag{91}$$

Defining the positive-definite LF as $V_\Theta(s_\Theta) \triangleq^{\mathrm{def}} s_\Theta^2/2$. After differentiating $V_\Theta(s_\Theta)$ and replacing (91), it yields

$$\begin{aligned} \dot{V}_\Theta(s_\Theta) &= s_\Theta \dot{s}_\Theta = s_\Theta \left[-k_1^{s_\Theta} \mathrm{sign}^{\alpha}(s_\Theta) - k_2^{s_\Theta} \mathrm{sign}^{\beta}(s_\Theta) \right], \\ &= -k_1^{s_\Theta} s_\Theta \mathrm{sign}^{\alpha}(s_\Theta) - k_2^{s_\Theta} s_\Theta \mathrm{sign}^{\beta}(s_\Theta), \end{aligned} \tag{92}$$

By noting that $s_\Theta \mathrm{sign}^{\alpha}(s_\Theta) = |s_\Theta||s_\Theta|^{\alpha}$ and $s_\Theta \mathrm{sign}^{\beta}(s_\Theta) = |s_\Theta||s_\Theta|^{\beta}$, we have

$$\begin{aligned} \dot{V}_\Theta(s_\Theta) &\leq -k_1^{s_\Theta} |s_\Theta|^{\alpha+1} - k_2^{s_\Theta} |s_\Theta|^{\beta+1} \\ &\leq -k_1^{s_\Theta} \left| 2\frac{1}{2} s_\Theta^2 \right|^{\frac{\alpha+1}{2}} - k_2^{s_\Theta} \left| 2\frac{1}{2} s_\Theta^2 \right|^{\frac{\beta+1}{2}} \\ &\leq -2k_1^{s_\Theta} V_\Theta^{\frac{\alpha+1}{2}} - 2k_2^{s_\Theta} V_\Theta^{\frac{\beta+1}{2}}. \end{aligned} \tag{93}$$

where the power rule is used in the second step. Let $\bar{\alpha} \triangleq^{\mathrm{def}} (\alpha+1)/2$ and $\bar{\beta} \triangleq^{\mathrm{def}} (\beta+1)/2$. Let $\alpha > 1$ and $\beta \in (0,1)$, thus $(\alpha+1)/2 > 1$ and $(\beta+1)/2 < 1$. By using Lemma 1, it results that the states' trajectories reach the sliding manifold $s_\Theta = 0$ in fixed-time upper bounded as $T_{\mathrm{r}} \leq T_{\mathrm{r}}^{\max} \triangleq^{\mathrm{def}} \frac{1}{2k_1^{s_\Theta}(\bar{\alpha}-1)} + \frac{1}{2k_2^{s_\Theta}(1-\bar{\beta})}$.

Step 2. In this step, we demonstrate the boundedness of all signals within the closed-loop system. Thus, we show that the observation error $e_3^{\mathrm{ob}} \triangleq^{\mathrm{def}} d_\Theta^{\mathrm{lum}} - \hat{d}_\Theta^{\mathrm{lum}}$, the sliding variable s_Θ, and the tracking errors will not drive the closed-loop system to instability, i.e., $(e_1^\Theta, e_2^\Theta) \nrightarrow \infty$. Recalling the errors dynamics given in (63). The dynamics of the feedback-loop can be written as

$$\begin{cases} \dot{e}_1^\Theta = e_2^\Theta, \\ \dot{e}_2^\Theta = f_\Theta^{\mathcal{N}} + g_\Theta^{\mathcal{N}} u_\Theta + d_\Theta^{\mathrm{lum}} - \ddot{\Theta}_d. \end{cases} \tag{94}$$

Considering the dynamics of the sliding surface designed in (64), the perturbated system (94) can be rewritten as

$$\begin{cases} \dot{e}_1^\Theta = e_2^\Theta, \\ \dot{e}_2^\Theta = \dot{s}_\Theta + e_3^{\mathrm{ob}} - \nu_\Theta - \omega_\Theta. \end{cases} \tag{95}$$

From this expression, we can note that the dynamics of the sliding function $\dot{s}_\Theta$ and the estimation error e_3^{ob} are part of the error dynamics $\dot{e}_2^\Theta$. Let the following candidate LF be defined for the feedback loop-system (95)

$$V(s_\Theta, e_1^\Theta, e_2^\Theta) \triangleq^{\mathrm{def}} \frac{1}{2}(s_\Theta^2 + e_1^\Theta + e_2^\Theta), \tag{96}$$

The time derivative of V along the trajectories of system (95) is obtained as

$$\begin{aligned} \dot{V} &\triangleq^{\mathrm{def}} s_\Theta \dot{s}_\Theta + e_1^\Theta \dot{e}_1^\Theta + e_2^\Theta \dot{e}_2^\Theta \\ &= s_\Theta \left[-k_1^{s_\Theta} \mathrm{sign}^{\alpha}(s_\Theta) - k_2^{s_\Theta} \mathrm{sign}^{\beta}(s_\Theta) \right] + e_1^\Theta e_2^\Theta + \\ &\left[e_2^\Theta \left(-k_1^{s_\Theta} \mathrm{sign}^{\alpha}(s_\Theta) - k_2^{s_\Theta} \mathrm{sign}^{\beta}(s_\Theta) \right) + e_2^\Theta e_3^{\mathrm{ob}} - \right. \\ &e_2^\Theta k_1^\Theta \mathrm{sign}^{\gamma_1}(e_1^\Theta) - e_2^\Theta k_2^\Theta \mathrm{sign}^{\gamma_2}(e_2^\Theta) - e_2^\Theta \bar{k}_1^\Theta \mathrm{sign}^{\bar{\gamma}_1}(e_1^\Theta) - \\ &\left. e_2^\Theta \bar{k}_2^\Theta \mathrm{sign}^{\bar{\gamma}_2}(e_2^\Theta) \right] \end{aligned}$$

$$\begin{aligned} &\leq -k_1^{s_\Theta}|s_\Theta| - k_1^{s_\Theta}|s_\Theta||s_\Theta| - k_2^{s_\Theta}|s_\Theta| - k_2^{s_\Theta}|s_\Theta||s_\Theta| + |e_1^\Theta||e_2^\Theta| - \\ &k_1^{s_\Theta}|e_2^\Theta| - k_1^{s_\Theta}|e_2^\Theta||s_\Theta| - k_2^{s_\Theta}|e_2^\Theta| - k_2^{s_\Theta}|e_2^\Theta||s_\Theta| + |e_2^\Theta||e_3^{\mathrm{ob}}| - \\ &k_1^\Theta|e_2^\Theta| - k_1^\Theta|e_1^\Theta||e_2^\Theta| - k_2^\Theta|e_2^\Theta| - k_2^\Theta|e_2^\Theta||e_2^\Theta| - \bar{k}_1^\Theta|e_2^\Theta| - \\ &\bar{k}_1^\Theta|e_1^\Theta||e_2^\Theta| - \bar{k}_2^\Theta|e_2^\Theta| - \bar{k}_2^\Theta|e_2^\Theta||e_2^\Theta|, \end{aligned}$$

By employing Young's inequality, it yields

$$\begin{aligned} \dot{V} \leq &-k_1^{s_\Theta} \frac{1+s_\Theta^2}{2} - k_1^{s_\Theta} \frac{2s_\Theta^2}{2} - k_2^{s_\Theta} \frac{1+s_\Theta^2}{2} - k_2^{s_\Theta} \frac{2s_\Theta^2}{2} + \frac{(e_1^\Theta)^2+(e_2^\Theta)^2}{2} - \\ &k_1^{s_\Theta} \frac{1+(e_2^\Theta)^2}{2} - k_1^{s_\Theta} \frac{(e_2^\Theta)^2+s_\Theta^2}{2} - k_2^{s_\Theta} \frac{1+(e_2^\Theta)^2}{2} - k_2^{s_\Theta} \frac{(e_2^\Theta)^2+s_\Theta^2}{2} + \\ &\frac{(e_2^\Theta)^2+(e_3^{\mathrm{ob}})^2}{2} - k_1^\Theta \frac{1+(e_2^\Theta)^2}{2} - k_1^\Theta \frac{(e_1^\Theta)^2+(e_2^\Theta)^2}{2} - k_2^\Theta \frac{1+(e_2^\Theta)^2}{2} - \end{aligned}$$

$$k_2^{\Theta}\frac{\left(e_2^{\Theta}\right)^2+\left(e_2^{\Theta}\right)^2}{2}-\bar{k}_1^{\Theta}\frac{1+\left(e_2^{\Theta}\right)^2}{2}-\bar{k}_1^{\Theta}\frac{\left(e_1^{\Theta}\right)^2+\left(e_2^{\Theta}\right)^2}{2}-\bar{k}_2^{\Theta}\frac{1+\left(e_2^{\Theta}\right)^2}{2}-\bar{k}_2^{\Theta}\frac{\left(e_2^{\Theta}\right)^2+\left(e_2^{\Theta}\right)^2}{2}$$

$$\leq\left\{-3k_1^{s\Theta}-3k_2^{s\Theta}-k_1^{s\Theta}-k_2^{s\Theta}\right\}\frac{s_{\Theta}^2}{2}+\left\{1-k_1^{\Theta}-\bar{k}_1^{\Theta}\right\}\frac{\left(e_1^{\Theta}\right)^2}{2}+\left\{-2k_1^{s\Theta}-2k_2^{s\Theta}+2-2k_1^{\Theta}-3k_2^{\Theta}-2\bar{k}_1^{\Theta}-3\bar{k}_2^{\Theta}\right\}\frac{\left(e_2^{\Theta}\right)^2}{2}+\frac{-2k_1^{s\Theta}-2k_2^{s\Theta}+\left(e_3^{\mathrm{ob}}\right)^2-k_1^{\Theta}-k_2^{\Theta}-\bar{k}_1^{\Theta}-\bar{k}_2^{\Theta}}{2}$$

$$\leq -K_V V+L_V. \tag{97}$$

where $K_V \triangleq \max\{1-k_1^{\Theta}-\bar{k}_1^{\Theta},-2k_1^{s\Theta}-2k_2^{s\Theta}+2-2k_1^{\Theta}-3k_2^{\Theta}-2\bar{k}_1^{\Theta}-3\bar{k}_2^{\Theta},-3k_1^{s\Theta}-3k_2^{s\Theta}-k_1^{s\Theta}-k_2^{s\Theta}\}\in\mathbb{R}_+$, and $L_V \triangleq \max\left\{\frac{-2k_1^{s\Theta}-2k_2^{s\Theta}+\left(e_3^{\mathrm{ob}}\right)^2-k_1^{\Theta}-k_2^{\Theta}-\bar{k}_1^{\Theta}-\bar{k}_2^{\Theta}}{2}\right\}<\infty$. The expression (97) can be associated with a first-order linear differential equation with constant coefficients. It can be verified that the solution of (97) is given as

$$\begin{aligned}V(t)&\leq \exp\left(-K_V(t-t_0)\right)V(t_0)+L_V\exp(-K_V t)\int_{t_0}^{t}\exp(K_V\tau)d\tau\\&=\exp\left(-K_V(t-t_0)\right)V(t_0)+\frac{L_V\exp(-K_V t)}{K_V}\left(\exp(K_V t)-\exp(K_V t_0)\right)\\&=\exp\left(-K_V(t-t_0)\right)V(t_0)+\frac{L_V}{K_V}\left(1-\exp\left(-K_V(t_0-t)\right)\right).\end{aligned}$$

Then by calculating the limit of $V(t)$ we get $\lim_{t\to\infty}V(t)\leq\frac{L_V}{K_V}$. Thus $V(t)$ is convergent to a finite bounded value $\frac{L_V}{K_V}\in[0,\infty)$. Consequently, it can be concluded that $V(s_{\Theta},e_1^{\Theta},e_2^{\Theta})$ and so $s_{\Theta},e_1^{\Theta},e_2^{\Theta}$ will not escape to infinity. Hence, it follows that the tracking error is UUB, which ensures the boundedness of the signals of the feedback system.

Step 3. When the sliding motion occurs (i.e., $s_{\Theta}=0$), we have $\dot{s}_{\Theta}=0$. Hence, the control input in (67) becomes

$$u_{\Theta}=\frac{1}{g_{\Theta}^{\mathcal{N}}}\left[-\mathcal{V}_{\Theta}-\mathcal{W}_{\Theta}-f_{\Theta}^{\mathcal{N}}+\ddot{\Theta}_d-\hat{d}_{\Theta}^{\mathrm{lum}}\right]. \tag{98}$$

Given the dynamics of the tracking error from (94) and substituting (98) into them, we get

$$\begin{cases}\dot{e}_1^{\Theta}=e_2^{\Theta},\\ \dot{e}_2^{\Theta}=-\mathcal{V}_{\Theta}-\mathcal{W}_{\Theta}.\end{cases} \tag{99}$$

By utilizing the proposed Corollary 1, it can be concluded that the error dynamics (99) settle at the zero equilibrium, i.e., $(e_1^{\Theta},e_2^{\Theta})\to 0$, during the sliding motion $s_{\Theta}=0$ in a fixed sliding-time T_s. The upper bound on the global settling-time is given as $T_{\Theta}\leq T_{\Theta}^{\max}\triangleq T_{\mathrm{ob},\Theta}+T_{\mathrm{r}}+T_{\mathrm{sm}}$, where $T_{\mathrm{ob},\Theta}$ is the convergence-time of the observer, T_{r} is the reaching-time of the sliding manifold during the reaching phase, and T_{sm} is the sliding time during the sliding mode (phase). $T_{\mathrm{ob},\Theta},T_{\mathrm{r}},T_{\mathrm{sm}}$ are defined as

$$\begin{cases}T_{\mathrm{ob},\Theta}\leq T_{\mathrm{ob},\Theta}^{\max}\triangleq\frac{2\lambda_{\max}(P_z^{\Theta})}{\lambda_{\min}(Q_z^{\Theta})}\frac{2}{1-\bar{\sigma}}\left[\frac{\bar{\varrho}-1}{2}\frac{\lambda_{\min}(Q_z^{\Theta})}{2\lambda_{\max}(P_z^{\Theta})}T_u\right]^{\frac{1-\bar{\sigma}}{1-\bar{\varrho}}}+T_u,\\ T_{\mathrm{r}}\leq T_{\mathrm{r}}^{\max}\triangleq\frac{1}{2k_1^{s\Theta}(\bar{\alpha}-1)}+\frac{1}{2k_2^{s\Theta}(1-\bar{\beta})},\\ T_{\mathrm{sm}}\leq T_{\mathrm{s}}^{\max}\triangleq\frac{\gamma}{1-\gamma}\frac{\lambda_{\max}(P_1^{\Theta})}{\lambda_{\min}(Q_1^{\Theta})}\lambda_{\max}^{\frac{1-\gamma}{\gamma}}(P_1^{\Theta})+\frac{\bar{\gamma}}{\bar{\gamma}-1}\frac{\lambda_{\max}(P_2^{\Theta})}{\lambda_{\min}(Q_2^{\Theta})}\lambda_{\max}^{\frac{\bar{\gamma}-1}{\bar{\gamma}}}(P_2^{\Theta}).\end{cases}$$

Thus, completing the proof. ■

Remark 12. By following the same arguments in the proof of Theorem 3, it can be demonstrated that the tracking errors of the position system settle at the origin $e_1^{\xi}=\left[e_1^x\quad e_1^y\quad e_1^z\right]^T\to 0$ along $s_{\xi}=0$ within fixed-time upper bounded as $T_{\xi}\leq T_{\xi}^{\max}$. Furthermore, it is worth to mention that the reported works on homogeneous-SMC of quadrotor system do not provide an explicit estimation of the sliding time $\boldsymbol{T_{\mathrm{sm}}}$, i.e., [8] [9] [10] [11] [12]. The convergence proofs of these works are based on the bi-limit homogeneity approach, which cannot estimate the settling-time or its upper bound.

4 Simulation Results and Discussions

To demonstrate the effectiveness of the developed controller, a processor-in-the-loop (PIL) simulation is performed. In the PIL scheme, the C++ code of the controller runs onboard the Pixhawk® autopilot hardware, while the aircraft model is simulated in Simulink® in the host computer (see Fig. 28). The nominal physical parameters of the quadrotor are summarized in Table 1. The moments of inertia have been estimated by the bifilar pendulum experiment, as depicted in Fig. 4 [10]. The control parameters are chosen based on Remark 10 as follows:

(i) Attitude controller: $k_1^{\Phi}=k_1^{\theta}=\bar{k}_1^{\Phi}=\bar{k}_1^{\theta}=4, k_1^{\psi}=3, k_2^{\Phi}=k_2^{\theta}=\bar{k}_2^{\Phi}=\bar{k}_2^{\theta}=3, k_2^{\psi}=2$, $k_1^{s\Phi}=k_1^{s\theta}=k_2^{s\Phi}=k_2^{s\theta}=8, k_1^{s\psi}=k_2^{s\psi}=4$.

(ii) Position controller: $k_1^x=k_1^y=1.75, k_1^z=3.2, k_2^x=k_2^y=2.28, k_2^z=1.2, k_1^{sx}=k_1^{sy}=k_1^{sz}=k_2^{sx}=k_2^{sy}=k_2^{sz}=1.2$.

The parameters tuning is as follows: for instance, the larger the value of $k_1^{\Phi}=\bar{k}_1^{\Phi}$ the faster is the rise time, but more overshoot and oscillations appear during the response's transient phase, leading to larger settling-time. The parameters $k_2^{\Phi}=\bar{k}_2^{\Phi}$ act as oscillations damper. Thus, a tradeoff should be made to attain the best response behavior.

The exponents are chosen as:

(i) Reaching control: $\alpha=1.2,\beta=0.8$.

(ii) Equivalent control: $\varepsilon_1=0.25,\gamma=0.75,\gamma_1=0.6,\gamma_2=0.75,\varepsilon_2=0.25,\bar{\gamma}=1.25,\bar{\gamma}_1=1.67,\bar{\gamma}_2=1.25$.

The parameters of the observer are selected to be: $\varepsilon_3=0.3,\varepsilon_4=0.2,\bar{\sigma}=0.7,\bar{\varrho}=1.2,T_u=0.1,\rho_1^{\xi}=4.3,\rho_2^{\xi}=6.96,\rho_3^{\xi}=11,\bar{\rho}_i^{\xi}=5,\bar{\rho}_i^{\xi}=10,\bar{\rho}_i^{\xi}=12,\bar{d}_{\xi}=10$.

Table 1. Nominal parameters of the vehicle.

Parameter	Value	Unit
$m^{\mathcal{N}}$	1.80	kg
l	0.225	m
g	9.81	m/s^2
$J_{xx}^{\mathcal{N}}$	0.0232	$kg.m^2$
$J_{yy}^{\mathcal{N}}$	0.0249	$kg.m^2$
$J_{zz}^{\mathcal{N}}$	0.0342	$kg.m^2$

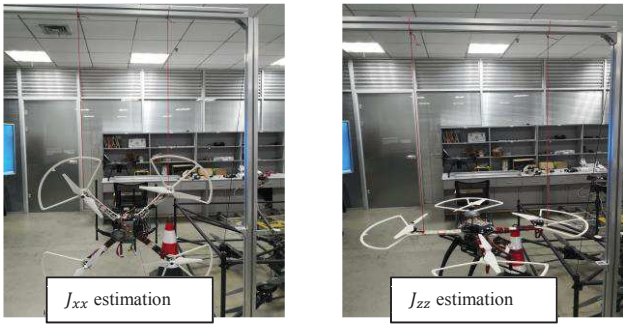

Fig. 4. Bifilar pendulum setup for estimating the moments of inertia.

4.1 Validation of the Fixed-Time Convergence

To confirm the theoretical findings regarding the fixed-time convergence of the designed controller, two scenarios for different initial positions of the quadrotor are considered as *Case 1:* $\xi_0 = [20 \quad 30 \quad 0]_E^T$ m; *Case 2:* $\xi_0 = [-50 \quad -60 \quad 8]_E^T$ m. Simultaneously, initial states of quadrotors are chosen as $\mathcal{V}_0 = [0 \quad 0 \quad 0]_E^T$ m/s, $\Theta_0 = [0 \quad 0 \quad 0]_B^T$ deg, $\zeta_0 = [0 \quad 0 \quad 0]_B^T$ deg/s. To illustrate the improvement attained with the proposed fixed-time control approach, we have conducted a comparative study with some of the recently proposed fast fixed/finite time convergent controllers, i.e., [9] [59] and [68]. The gains of the controllers are tuned as best as possible according to the conditions that guarantee a good transient response, precise reference tracking, and quick disturbance rejection.

Unlike the comparative study in [9], we have considered the measurement noise (Fig. 8) and parameters variations in the simulation process. This aims to make the simulation process closer to reality so as to better assess the performance of the controllers. First, the validation of the fixed-time convergence is conducted for the nominal case of the system's parameters. Second, parameters uncertainties and noise are considered.

4.1.1 Fixed-Time Convergence Under Nominal Values of the System's Parameters

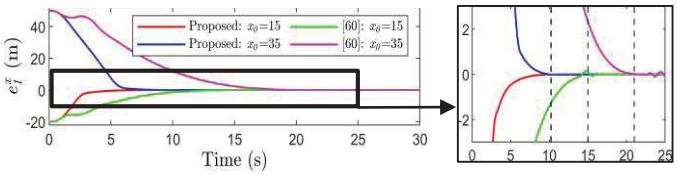

Fig. 5. Convergence of position tracking error under nominal values.

From Fig. 5, it is observed that the tracking error is stabilized at the origin in the same settling-time even different initial positions are set for the quadrotor. This result confirms the valuable fixed-time convergence property of the developed control law. The convergence-time of the quadrotor to the desired position is not affected by its initial positions or how far it is from the desired set-point. However, in practice, convergence-time is still constrained by the maximum admissible physical velocities of the motors (see Remark 13 below). A comparison between our controller and the controllers [9] [59] [68] regarding the settling-time is displayed in Table 2. Compared to the finite-time controllers [59] [67], the proposed controller exhibits enhanced performance since *(i)* the convergence rate has been reduced considerably, *(ii)* the settling-time remains almost the same and it shows weak dependence on the ICs. Compared to the fixed-time controller [9], the convergence-time has been improved. These results verify the prominent feature of the presented control algorithm in terms of an enhanced and uniform convergence rate. The estimations of lumped disturbances in both translational and rotational subsystems are depicted in Fig. 6 and Fig. 7, respectively. The observer can precisely estimate the disturbances besides reconstructing the unmeasured velocity.

Remark 13. A faster settling-time for larger initial positions is achieved at the expense of the larger velocity of the multirotor. This can surpass the admissible physical constraints imposed on the motors' velocities. In practice, a tradeoff should be made between velocity/motors constraints and a fast convergent-time since no physical system has infinite velocity.

Table 2. Convergence-time for different initial positions of the quadrotor.

Control strategy	Convergence rate	Initial positions	Performance index: Convergence-time (s)
Controller [59]	Finite-time	*Case 1*	15
		Case 2	21
		Difference	6
Controller [68]	Finite-time	*Case 1*	12
		Case 2	14
		Difference	2
Controller [9][1]	Fixed-time	*Case 1*	12
		Case 2	
Proposed	Fixed-time	*Case 1*	**10.22**
		Case 2	

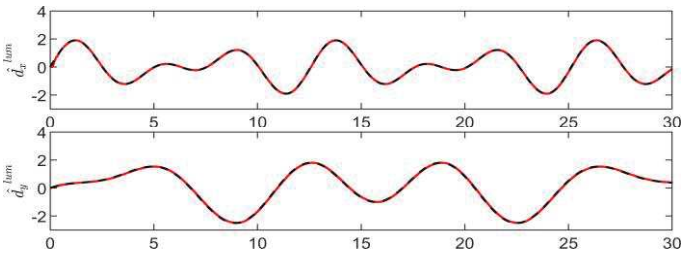

[1] Data related to [9] and [68] is taken from Table 2 of [9].

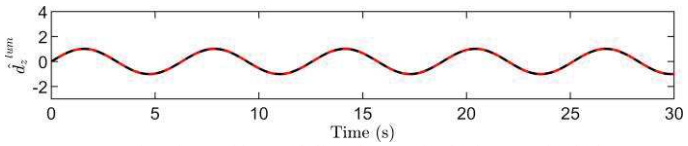

Fig. 6. Estimations of lumped disturbances in the inner attitude-loop.

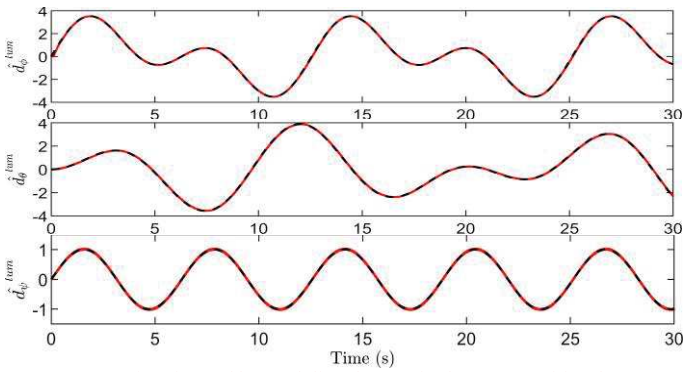

Fig. 7. Estimations of lumped disturbances in the outer position-loop.

4.1.2 Fixed-Time Convergence Under Parameters Variations and Measurement Noise

a) Parametric uncertainties: To verify the claims of Assumption 1 and Remark 3, uncertainties of 20% and 30% are considered on the mass and the moments of inertia as: $m^{\Delta} = +0.2m^{N}$, $J_{xx}^{\Delta} = +0.3J_{xx}^{N}$, $J_{yy}^{\Delta} = -0.3J_{yy}^{N}$, $J_{zz}^{\Delta} = +0.3J_{zz}^{N}$, i.e., $m = 2.16$ kg, $J_{xx} = 0.0302$ kg m^2, $J_{yy} = 0.0174$ kg m^2, $J_{zz} = 0.0445$ kg m^2.

b) Measurement noise:

b.1) Gyroscope signal: $\zeta(t) = \tilde{\zeta}(t) + \zeta_{\text{mb}} + N(t)$ rad/s, where $\zeta = [p \quad q \quad r]_B^T$ rad/s is the final signal used in control, $\tilde{\zeta}$ is the true measurement in rad/s, ζ_{mb} is the measurement bias in rad/s, $N(t)$ is a random noise with the standard deviation N_{sd} in rad/s and the mean 0, i.e., $N = N_{\text{sd}}\text{rand}(\cdot)$, where $\text{rand}(\cdot)$ generates a random number in the interval (0,1).

b.2) GPS and barometer signals: $\xi(t) = \tilde{\xi}(t) + \text{rand}(\cdot)\xi_e$ m, where $\tilde{\xi}$ is the real measurement and ξ_e is the position deviation error.

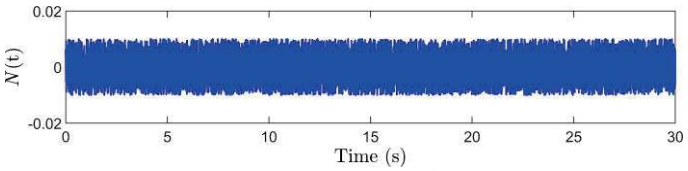

Fig. 8. Measurement noise.

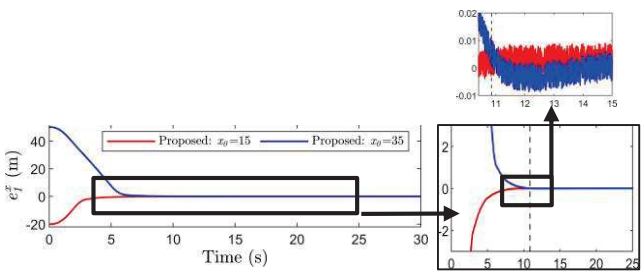

Fig. 9. Convergence of position tracking error under parameters variations and measurement noise.

The evolution of the position tracking error in the presence of sensors' noise and parameters variations is depicted in Fig. 9. The convergence-time of the proposed control algorithm remains almost the same with a small reasonable increase of 0.63 s compared to the convergence-time in Table 2, i.e., 10.22 s. This confirms that the convergence-time of the proposed control law is not largely affected by measurement noise and parametric uncertainties of 20% on the mass and 30% on the moments of inertia. However, large variation beyond these limits may lead to a significant increase in the convergence-time.

4.1.3 Fixed-Time Convergence of the Attitude States

To better illustrate the fixed-time feature for the rotational subsystem of the quadrotor, three scenarios for different initial states of the roll motion are considered as *Case 1:* $\{\Phi_0 = 10 \text{ deg}, p_0 = -70 \text{ deg/s}\}$; *Case 2:* $\{\Phi_0 = -30 \text{ deg}, p_0 = 300 \text{ deg/s}\}$; *Case 3:* $\{\Phi_0 = -50 \text{ deg}, p_0 = 0 \text{ deg/s}\}$. A Comparison of convergence-time between our controller and the controller in [59] is displayed in Fig. 10. This figure indicates that the convergence-time of the finite-time control law given in [59] grows with the increase in the values of the ICs or deviation of the values from the origin. Hence, the ICs dictate the upper limit on the convergence time of the finite-time stable control law under discussion. We can notice the ability of the designed fixed-time control law in terms of convergence of the state. Compared to the control law [59], it is observed that the convergence-time remains fixed at 1.12 s for different ICs even the control parameters for both control schemes are set to demonstrate the best performance. A comparison between our controller and the controller [59] regarding the settling-time is displayed in Table 3. Similar to the previous comparative study on translational position, the proposed control algorithm exhibits faster fixed convergence-time of the roll angle within the physical limits on the angular velocity of the quadrotor. The plot of the phase portrait of the plant states Φ, p is depicted in Fig. 11, while the time evolution of the states Φ, p, and the sliding surface s_{Φ} is displayed in Fig. 12. It can be seen from these two figures that the states and the sliding surface converge to zero. Hence the states' trajectories reach the sliding manifold $s_{\Phi} = 0$ where they are confined and then driven to the origin by sliding along s_{Φ}.

Table 3. Convergence-time for different ICs of the roll states.

Control strategy	Convergence rate	Initial positions	Performance index: Convergence-time (s)
Controller [59]	Finite-time	*Case 1*	1.81
		Case 2	2.45
		Case 3	2.79
Proposed	Fixed-time	*Case 1*	**1.12**
		Case 2	
		Case 3	

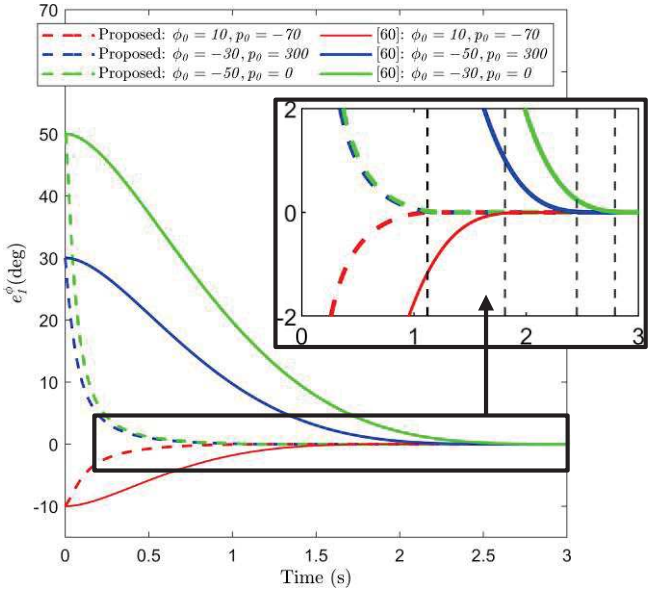

Fig. 10. Comparisons of convergence-time of the roll angle for different ICs.

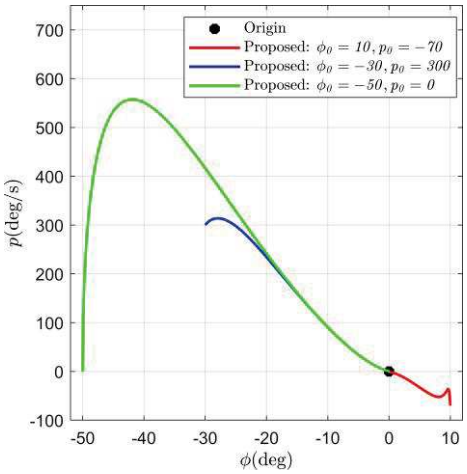

Fig. 11. Phase portrait of the roll states $\boldsymbol{\Phi}$ and $\boldsymbol{p}$.

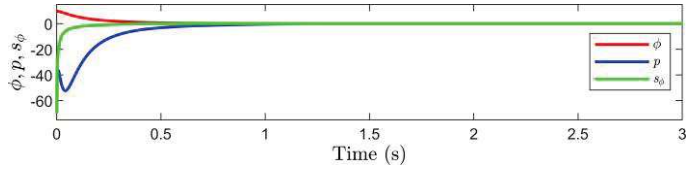

Fig. 12. Time evolution of the states Φ, p, and sliding surface s_{Φ}: *Case 1*.

4.2 Robustness Evaluation in Cartesian Trajectory Tracking

To evaluate the robustness and disturbance rejection capabilities of the proposed flight control systems (FCS), a comparative study is performed by considering four FCSs (see Table 4). FCS 1 is a commercially available flight controller of the Pixhawk® autopilot. FCS 2 [21] combines the classical linear SMC and the backstepping technique. FCS 3 combines two finite-time controllers, namely, Continuous Nonsingular Terminal Sliding Mode Control (CNTSMC) from [59] and a Continuous Twisting Controller (CTC) from [14]. FCS 4 is the proposed flight controller being based on the FNHNTSMC.

Table 4. Different FCSs used in Cartesian trajectory tracking.

FCS	Position controller	Attitude controller
FCS 1 (Pixhawk® autopilot)	PID	PID
FCS 2 [21]	IBSMC	IBSMC
FCS 3 [59] + [14]	CNTSMC [59]	CTC [14]
FCS 4	FNHNTSMC	FNHNTSMC

The Cartesian reference trajectory is as follows

$$\xi_d = [x_d \quad y_d \quad z_d]_E^T = [6\sin(0.2t) \quad 6\sin(0.2t)0.5\cos(0.2t) \quad 8 + 2\sin(0.2t)]_E^T \text{ m}.$$

In Order to test the FCSs in the most challenging situation that could be encountered in a real flight scenario, disturbances, uncertainties, measurement noise, and measurement errors are simultaneously considered in the numerical simulation as:

a) External disturbances: We suppose that the aircraft enters a windy area at $t = 32$ s during the flight mission. The external perturbations d_{ξ}^{ext} affecting the position states are generated by a more realistic Dryden wind model compared to the ordinary $\sin(\cdot)$ wave-based models. The components d_{ξ}^{ext} along the three axes $\xi \in \{x, y, z\}$ are expressed as [69]

$$d_{\xi}^{\text{ext}}(t) \triangleq -k_d^{\xi}\left[v_{\xi}(t) - v_{w,\xi}(t)\right]^2 \text{sign}\left[v_{\xi}(t) - v_{w,\xi}(t)\right].$$

A specific MATLAB® bloc can generate the Dryden wind, i.e., "*Dryden Wind Turbulence Model (Continuous)*". Since the quadrotor has coupled dynamics, the attitude states are inevitably affected by the Dryden wind being applied to the position dynamics. Fig. 13 presents the wind velocities. At maximum, the wind gusts can reach a velocity of 12 m/s, which is reasonable in practice.

b) Internal disturbances: b.1) ***Nonparametric uncertainties:*** This is represented by the unmodeled dynamics accordingly to Assumption 1. **b.2)** ***Parametric uncertainties:*** Similar to 4.1.2.

c) Measurement noise: Similar to 4.1.2.

The simulation results are presented from Fig. 14 to Fig. 25. Fig. 14 presents the 3-D flight trajectory tracking for the quadrotor with different FCSs, and the corresponding 2-D trajectory tracking profiles are depicted in Fig. 15. The responses of the position variables are depicted in Fig. 16. A preliminary analysis of the graphs in Fig. 14, Fig. 15, and Fig. 16 shows that the proposed FCS enjoys better tracking capabilities compared to the other FCSs. However, the difference may still be unclear from these graphs. Therefore, by inspecting the position tracking errors in Fig. 17, it can be observed that the suggested FCS exhibits accurate tracking and better disturbance rejection than the other FCSs. Noticeable ripples can be seen in the graphs of the FCS 3. This can be explained by the existence of the term $(\eta + T|\mathcal{U}_n|)\text{sign}(s)$ in the control law (35)-(38) of [59]. Since the author of [59] did not provide the tuning conditions of the parameters $\eta, T \in \mathbb{R}_+$,

we noticed that the larger are η, T, the robust is the system, but this leads to an undulatory behavior in the position states. Thus, the tuning of these two parameters should be made by considering a robustness-chattering tradeoff. FCS 2 [21] is found to be sensitive to large external disturbances. This controller provided excellent results for wind speed less than 2 m/s, as shown in simulation Scenario III of [21]. However, in the actual challenging flight conditions in the presence of other perturbations such as parameters variation, the controller being not observer-based, it cannot counteract the strong lumped disturbances. Moreover, from Fig. 5(c) of [21], the controller does not accurately track the pitch angle. This is due to the sensitivity of the backstepping technique to the matched uncertainties even it compensates theoretically exactly uncertainties decreasing together with the state variables (good attenuation of unmatched disturbances). The Pixhawk® controller (FCS 1) is more affected by disturbances with large tracking errors compared to the other FCSs. Overall, the proposed FCS provides an enhanced disturbance rejection feature. This improved robustness is due to the adopted AADC that integrates a robust SMC law and a disturbance observer. The Integral-Square-Error (ISE) and the Root-Mean-Square Error (RMSE) are calculated to deliver an accurate quantitative evaluation. These indexes are given as

$$\text{RMSE} = \sqrt{\frac{1}{N}\sum_{i=1}^{N}\left|\left(e_1^{\xi}\right)_i\right|^2}, \qquad \text{ISE} = \int_{t_i}^{t_f} e_1^{\xi}(\tau)^2\, d\tau.$$

where $\xi = \{x, y, z\}$, N is the dimension of the e_1^{ξ} array. The ISE and RMSE results are given in Table 5. Compared to the other controllers, the analysis of these results demonstrates that the proposed controller assures accurate tracking for all translational states of the quadrotor. This result confirms the superiority and effectiveness of the suggested control method regarding precision and disturbance rejection. For better understanding, the results of Table 5 are represented by bar graphs in Fig. 18 (ISE) and (RMSE) Fig. 19.

Table 5. Analysis of RMSE and ISE for the trajectory tracking (Simulation results).

FCS	Performance index					
	RMSE			ISE		
	e_1^x	e_1^y	e_1^z	e_1^x	e_1^y	e_1^z
FCS 1 (Pixhawk® autopilot)	0.350	0.238	0.410	9.800	4.549	13.43
FCS 2 [21]	0.211	0.122	0.200	3.575	0.819	3.216
FCS 3 [18], [59]	0.164	0.101	0.178	2.171	1.198	2.544
FCS 4 (Proposed)	**0.113**	**0.074**	**0.100**	**1.029**	**0.438**	**0.813**

The responses of the attitude variables of the proposed FNHNTSMC are depicted in Fig. 20. It follows from this figure that the designed attitude controller ensures precise tracking of the reference signals.

The observation outputs are displayed in Fig. 21, Fig. 22, and Fig. 23, respectively. Fig. 21 and Fig. 22 display the estimated lumped disturbances along the three axes of translational and rotational systems. It is evident from these figures that the perturbations have been timely identified, and thus enhancing the robustness of the control system against strong lumped disturbances. It can be observed from Fig. 23 that the observer delivers an accurate estimation of the linear velocity in a short time. Along with the estimation of the velocities, an output-feedback control is achieved. Thus, the proposed control scheme relying on unmeasurable velocities is robust against the accelerometer's faults. This important finding resulting from the developed velocity-free control circumvents the deficiency of the full-state feedback-based controllers. Fig. 24 and Fig. 25 display the angular velocities of the motors for FCS 4 (proposed) and FCS 2, respectively. These velocities are related to the control inputs by expression (9). Thus, they indicate the chattering propagation from the control signals to the physical actuators (brushless motors). Owing to the designed continuous-SMC control law, the angular velocities related to the proposed control signal are less corrupted by the chattering compared to the FCS 2 being based on the classical SMC (Fig. 25). Such a control law allows to significantly alleviate the high frequencies in the control signal, avoiding the undesirable shaking of the quadrotor, which may lead to instability. It can be observed from the plot of Fig. 25 that the FCS 2 demonstrates a high oscillatory motors' signal in comparison with the proposed continuous-SMC control law. Further characterization of the performance comparison among the controllers under discussion is based on the Integral of the Absolute value of the Derivative of the input u (IADU). This criterion is defined as $\text{IADU} = \int_{t_i}^{t_f}\left|\frac{du_z(\tau)}{d\tau}\right| d\tau$. The IADU index for the thrust force u_z of FCS 2 and FCS 4 is as follows: $\text{IADU}[(u_z)_{\text{FCS 2}}] = 5.12$, $\text{IADU}[(u_z)_{\text{FCS 4}}] = 1.15$. To precisely quantify the chattering alleviation, the Relative Percentage Difference (RPD) criterion is employed to characterize the IADU criterion. The RPD is defined as

$$\text{RDP}_{\text{FCS 4}}^{u_z} \triangleq \frac{|\text{IADU}_{\text{FCS 2}} - \text{IADU}_{\text{FCS 4}}|}{\text{IADU}_{\text{FCS 2}}} 100\ \%\ \downarrow.$$

The RDP indicates that the disrupting chattering of traditional SMC in the IBSMC of FCS 2 has been noticeably alleviated by the proposed continuous-SMC scheme ($\text{RDP}_{\text{FCS 4}}^{u_z} = 77.53\%\ \downarrow$).

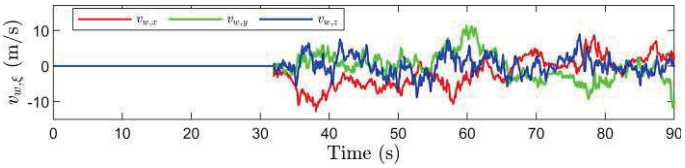

Fig. 13. Dryden wind model represented by the velocities along the three axes.

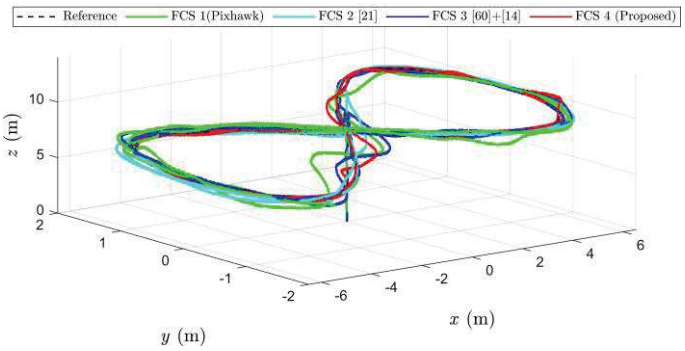

Fig. 14. 3-D trajectory tracking for different FCSs.

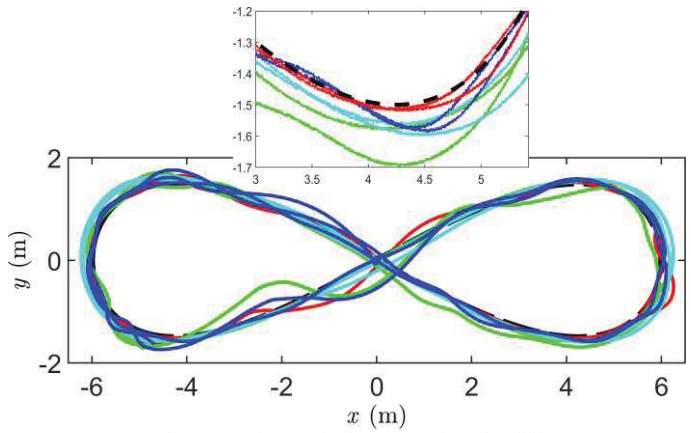

Fig. 15. Quadrotor's trajectory in the $x-y$ plane for different FCSs.

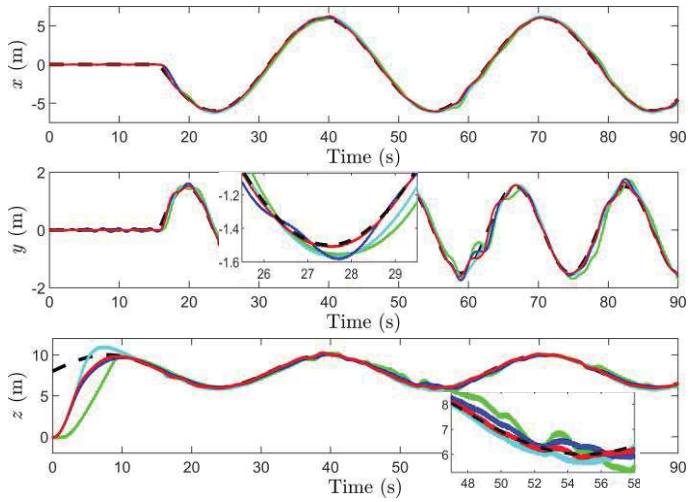

Fig. 16. Responses of the translational position states (x, y, z).

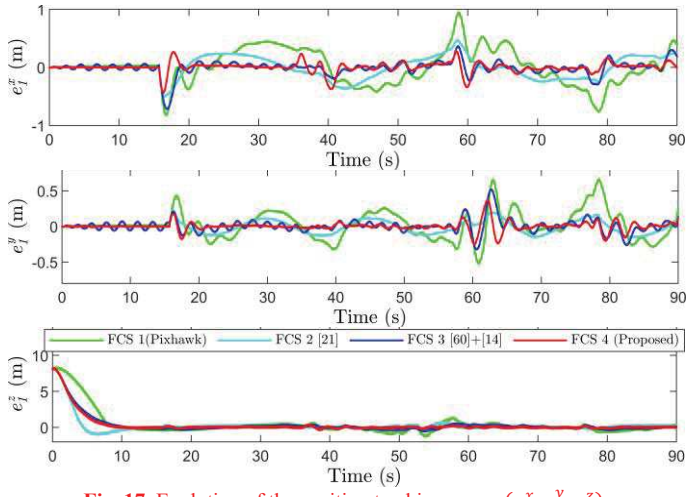

Fig. 17. Evolution of the position tracking errors (e_1^x, e_1^y, e_1^z).

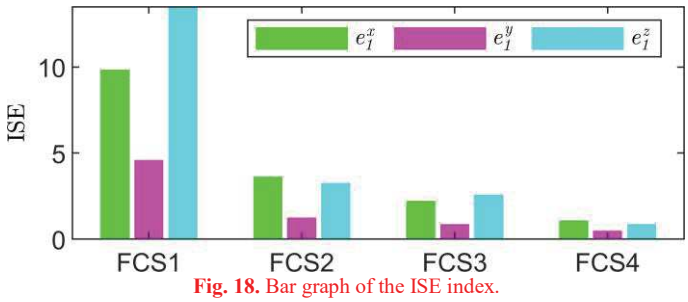

Fig. 18. Bar graph of the ISE index.

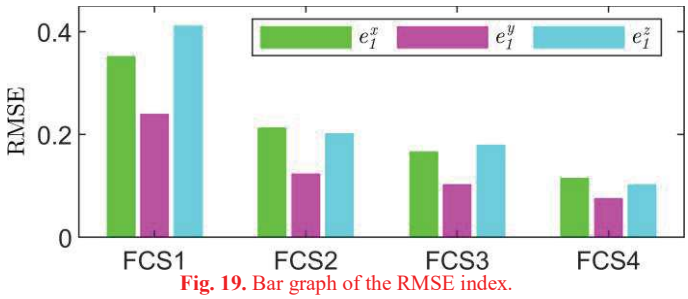

Fig. 19. Bar graph of the RMSE index.

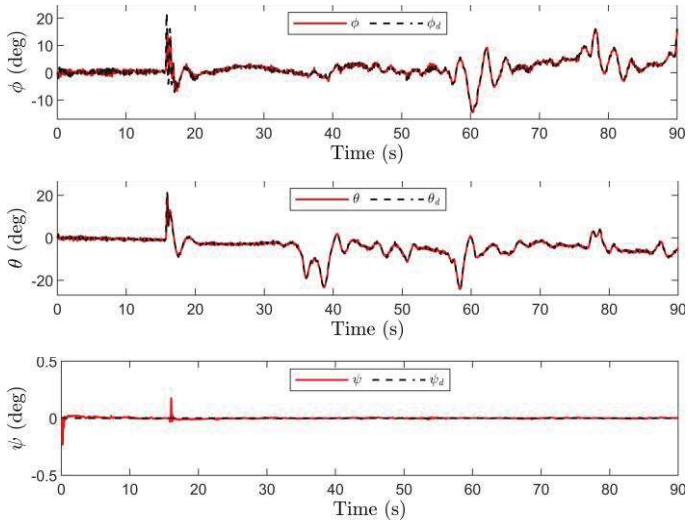

Fig. 20. Responses of the rotational attitude states (Φ, θ, ψ).

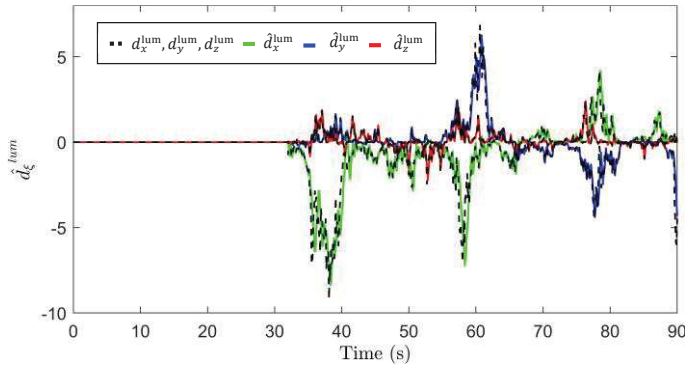

Fig. 21. The estimated lumped disturbances in the translational position.

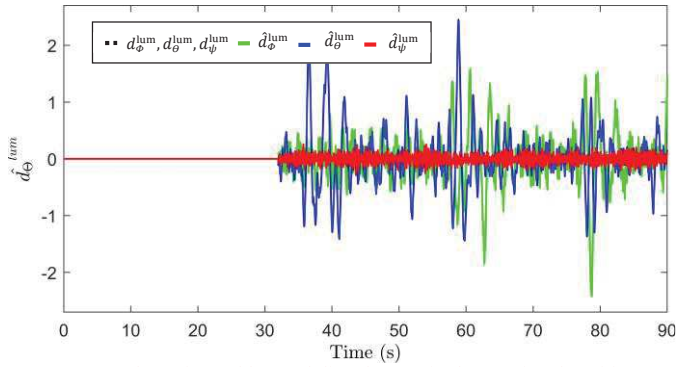

Fig. 22. The estimated lumped disturbances in the rotational position.

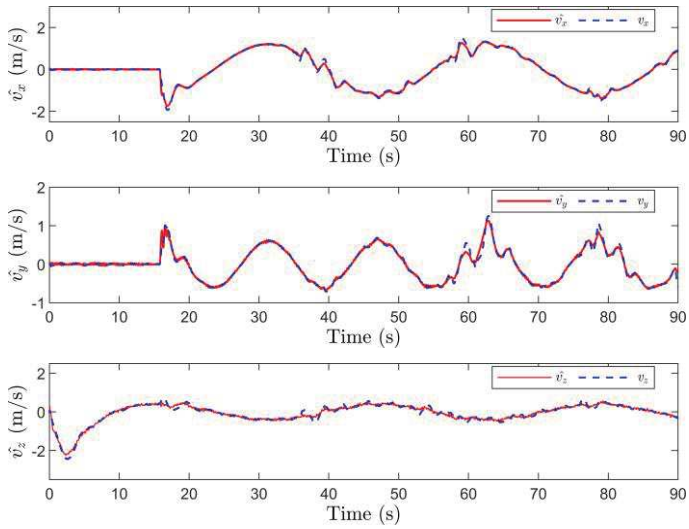

Fig. 23. The estimated velocities of the quadrotor $(\hat{v}_x, \hat{v}_y, \hat{v}_z)$.

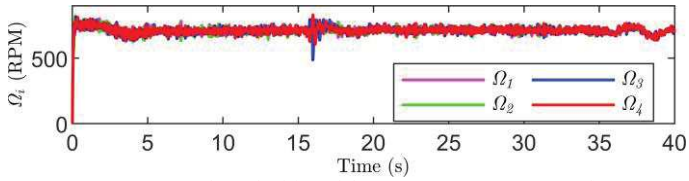

Fig. 24. Angular velocities of the motors: FCS 4 (Proposed).

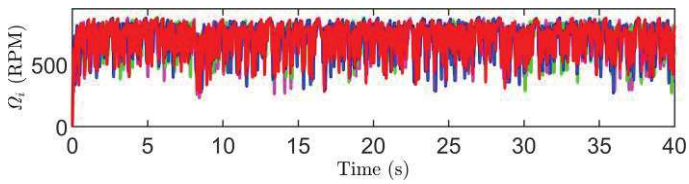

Fig. 25. Angular velocities of the motors: FCS 2.

5 Experimental Results and Discussions

Real-time experiments are performed to validate the proposed control strategy better. To verify the feasibility of the developed controller besides ensuring the safety of individuals and equipment, the experiment is divided into two parts. First, the attitude controller is validated separately on the ground. Second, an outdoor flight experiment is carried out to check Cartesian trajectory tracking in a 3-D flight environment.

Remark 14. Scientific literature has reported few works on robust fixed-time control of quadrotors, i.e., [8] [9] [36] [37] [38]. However, these studies demonstrate evidence of the control performance in a simulation environment only. Unlike these studies, the present research presents a concrete and complete investigation on the subject topic, including but not limited to; design, simulation, and realization of a proposed control algorithm on real hardware, thus completing the study.

5.1 Attitude Experiment

Detailed experimental scenarios, including origin stabilization, attitude tracking, and attitude regulation, are conducted. The block diagram of the proposed attitude control scheme is depicted in Fig. 26. In addition, a comparative study is performed to show the improvement attained by the designed controller. Firstly, a stabilization experiment is introduced to assess the capability of the proposed controller in stabilizing the attitude from any random initial configuration to the origin. Secondly, regulation and tracking experiments that are more commonly encountered in practice are performed. This aims to better show the robust control law's effectiveness and workability in the presence of abrupt changes of references and time-varying trajectory. To experimentally characterize the performance of the proposed controller, a convenient Model-Based Design (MBD) framework is established. MBD approach is very popular in the control community to design controllers and to validate them in real-time owing to its attracting salient features like reliability, robustness against errors in code, and ability to offer time-saving.

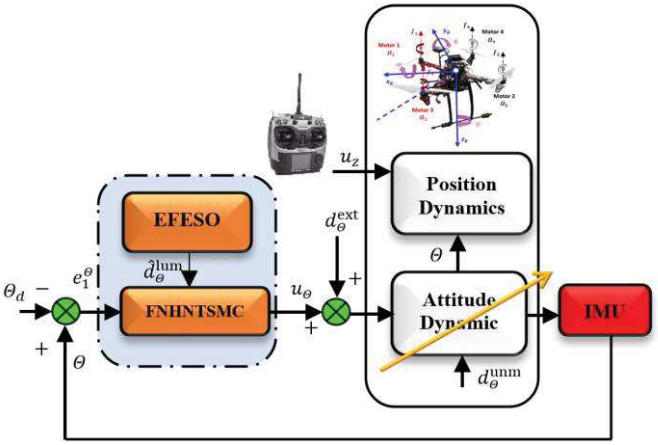

Fig. 26. The proposed attitude control scheme – Block diagram. The orange arrow indicates parameters variation and unmodeled dynamics.

5.1.1 Experimental Setup

The quadrotor-based setup illustrated in Fig. 27 has been used to conduct the real-time tests. The aircraft is attached to a 3-DoF spherical joint in the developed test-bed. Mechanically, the experimental setup is centered on a DJI 450 frame. For more hardware descriptions, the reader can refer to reference [10].

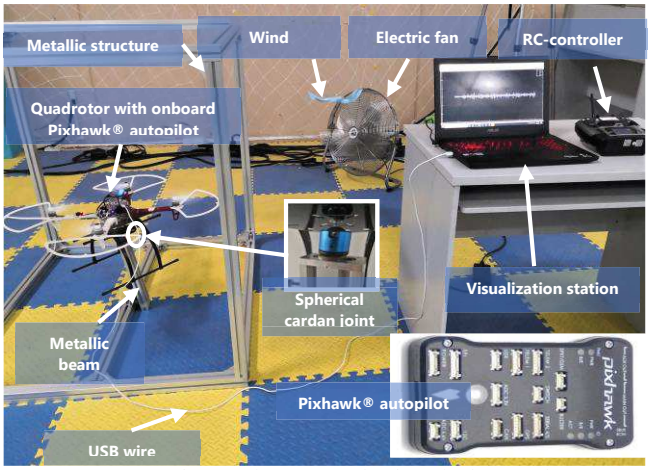

Fig. 27. The experiment setup for the attitude control.

The presented control scheme has been validated using the MBD, which is illustrated in Fig. 28. The validation procedure consists of two steps; the first step involves simulation of the control law in R2019b MATLAB®/Simulink®, which is interfaced with an open-source FlightGear® simulator (2018.3.1 version). FlightGear® offers a realistic rendering and dynamic simulation environment for the visualization of states of a quadrotor. In the second step, a C++ code realizes the control law in the real autopilot to experimentally characterize the control performance based on real-time tests. Simulink® toolbox "*UAV Toolbox Support Package for PX4® Autopilots*" (The recently released version: "*UAV Toolbox Support Package for PX4® Autopilots*") facilitated the realization procedure by automatically converting the source MATLAB® code to a readily-deployable C++ code. Moreover, the toolbox offered to communicate between the quadrotor and MATLAB® for visualization of data and monitoring purpose. The external mode of Simulink® is used for connecting the target autopilot to MATLAB®. The control performance is based on analysis of data logged on a controller-interfaced SanDisk Ultra micro-SD card of 8GB capacity.

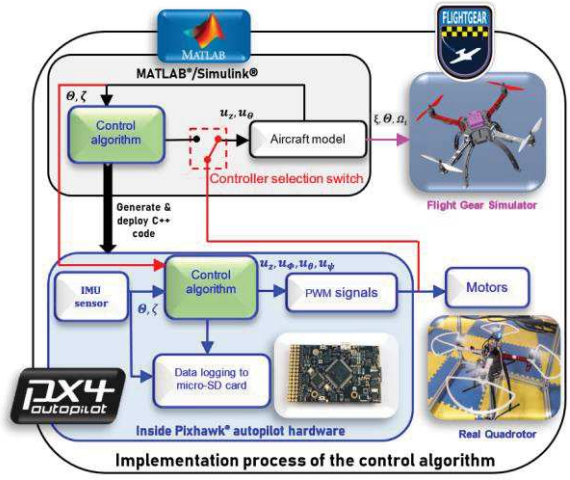

Fig. 28. MBD framework structure and interconnection of various elements to realize simulation and hardware implementation.

5.1.2 Stabilization Experiment

This experiment aims to validate the fixed-time feature of the presented controller. Therefore, two scenarios with different initial states of the roll and pitch angles are considered as *Case 1:* $\{\Phi_0 = 15 \text{ deg}, \theta_0 = -15 \text{ deg}\}$; *Case 2:* $\{\Phi_0 = 8 \text{ deg}, \theta_0 = -8 \text{ deg}\}$. In practice, this scenario may correspond to a hovering flight for taking photos or recording videos. The attitude response is depicted in Fig. 29 and the phase portrait is presented in Fig. 30. It can be observed that the controller can drive the states to the origin in fast convergence-time. The states converge to the origin almost in the same settling-time for different ICs. The difference is still reasonable and small, i.e., 22 ms. This can be explained by the adopted simplification of SAA in Remark 1 besides the considered simplifications in the dynamics of the attitude system (Assumption 1 and Remark 2). Overall, these practical interesting results validate the theoretical finding of fixed-time stability as demonstrated by simulation in Fig. 10 and Fig. 11.

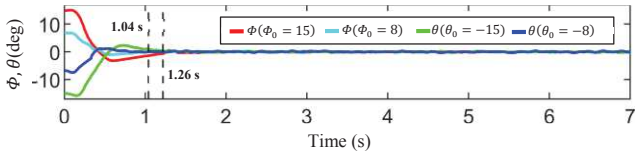

Fig. 29. Convergence of the states to the origin.

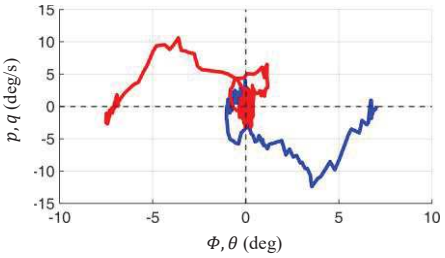

Fig. 30. Phase portrait of attitude's states.

5.1.3 Robustness and Disturbance Rejection Experiments

Series of comparative experiments are conducted to characterize the performance of the presented control law by considering four different robust controllers, i.e., FNHNTSMC-EFESO (proposed), Robust Backstepping Sliding Mode Controller (RBSSMC) [21], CTC [14] and Robust Adaptive Nonsingular Fast Terminal SMC (RANFTSMC) [70]. Moreover, the experiments have been carried out while considering the external disturbances (load perturbations and wind gusts). Additionally, considering Assumption 1, the unmodeled dynamics also exist as disturbances. Besides, parametric uncertainties are inevitably present as additional perturbations due to the estimation inaccuracy.

5.1.3.1 Comparative Experiment Under Load Disturbances

A 140 g load is attached to the quadrotor's front left arm, as mentioned in Fig. 31. Fig. 32 shows that all the control methods

guarantee the convergence of the states to the reference set-points. The orientation errors are shown in Fig. 33, which confirms the proposed control law's ability to eliminate the steady-state error, even if the vehicle is affected by lumped disturbances. Fig. 34 displays the control inputs. Owing to the designed continuous-SMC control law, the proposed control signal is less corrupted by the chattering compared to the rest of the controllers. Such a control law allows to significantly alleviate the high frequencies in the control signal, avoiding the undesirable shaking of the quadrotor, which may lead to instability. It can be observed from the graphs of Fig. 34 that the BSSMC demonstrates a high oscillatory control signal in comparison with other counterparts. Further characterization of the performance comparison among the controllers under discussion is based on the ISE and IADU criteria. ISE and IADU are computed and presented in Table 6.

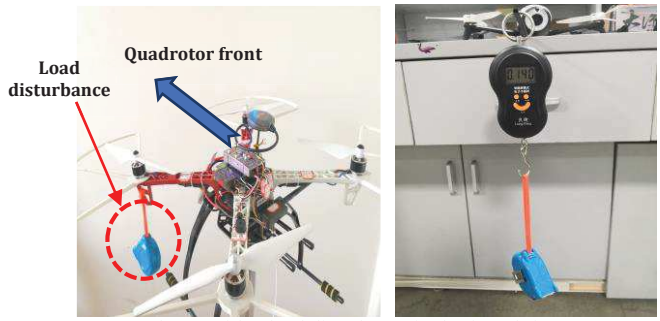

Fig. 31. Quadrotor with a load disturbance in the front left arm.

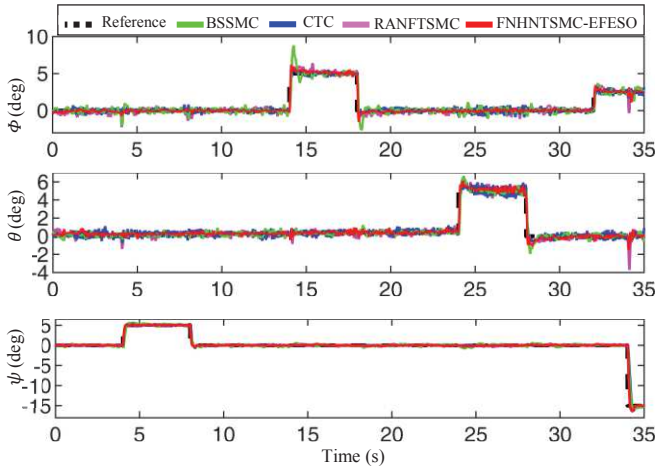

Fig. 32. Orientation (Φ, θ, ψ): Comparison under load disturbance.

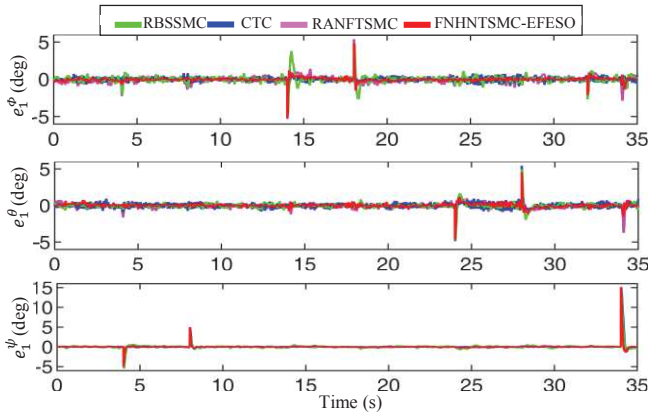

Fig. 33. Orientation errors $(e_1^{\Phi}, e_1^{\theta}, e_1^{\psi})$: Comparison under load disturbance.

Table 6. Performance comparison of the attitude controllers based on ISE and IADU criteria.

Control strategy	Performance index					
	ISE			IADU		
	e_1^{Φ}	e_1^{θ}	e_1^{ψ}	e_1^{Φ}	e_1^{θ}	e_1^{ψ}
CTC [14]	0.089	0.076	0.023	3.02	1.82	0.81
RBSSMC [21]	0.091	0.082	0.035	4.92	2.18	1.01
RANFTSMC [70]	0.048	0.034	0.013	1.52	1.35	0.65
FNHNTSMC-EFESO	**0.033**	**0.032**	**0.012**	**1.12**	**1.33**	**0.25**

It is evident that the proposed control law based on FNHNTSMC-EFESO has improved the control precision for all the states. The superiority of the proposed controller is explained by the adopted ADRC approach, where the estimation of the lumped disturbances has significantly improved the robustness of the controller. Also, the control smoothness is enhanced by the suggested controller for all the control signals comparably to other SMC-based controllers. Fig. 35 displays the estimated disturbances by the EFESO where it can be noticed that the oscillations and swinging caused by the slung load are well estimated. The identified disturbances are fed to the FNHNTSMC controller, which timely compensates them.

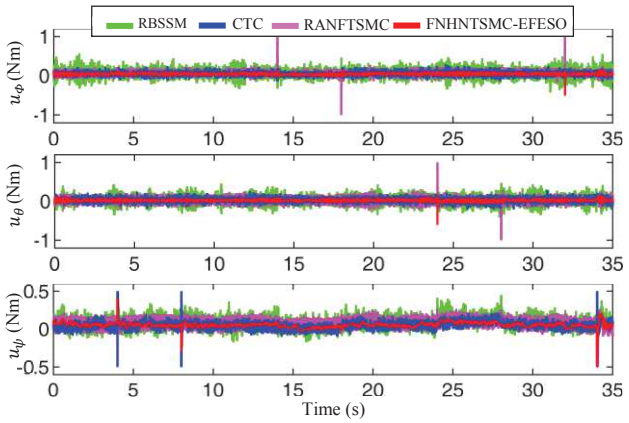

Fig. 34. Control torques $(u_{\Phi}, u_{\theta}, u_{\psi})$: Comparison under load disturbance.

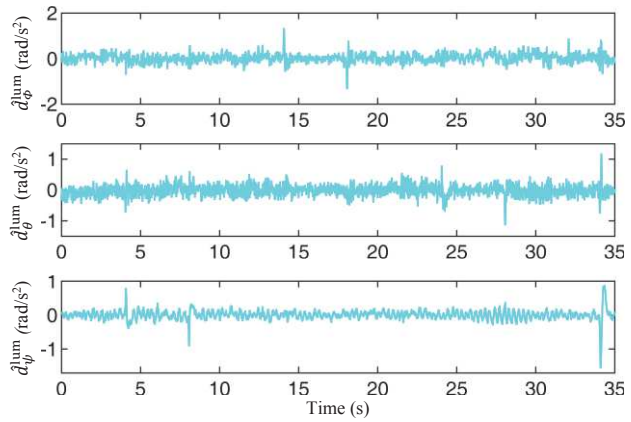

Fig. 35. Estimates of the disturbances $\left(\hat{d}_{\Phi}^{\text{lum}}, \hat{d}_{\theta}^{\text{lum}}, \hat{d}_{\psi}^{\text{lum}}\right)$.

5.1.3.2 Comparative Experiment Under Wind Disturbances

The wind is generated at the beginning of the experiment, i.e., from $t = 0$s, using a 140W industrial electric fan of 0.5m diameter. The desired time-varying trajectory for testing the attitude states is written as: $\Phi_d = -5\sin(2\pi f t), \theta_d = 5\sin(2\pi f t), \psi_d = 7.5\cos(2\pi f t)$, where f is the frequency in Hz. Fig. 36 illustrates footage of the experiment. It is evident from Fig. 37 and Fig. 38 that the proposed attitude controller exhibits better disturbance rejection capability, which ensures accurate tracking of the reference trajectory with the smallest tracking error compared to the other controllers. The control torques are depicted in Fig. 39. Similar to the previous case, the chattering is significantly reduced in the continuous control signal of the proposed control law.

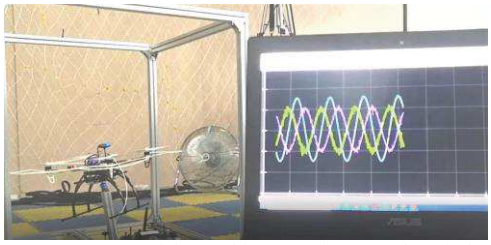

Fig. 36. Footage of the tracking experiment under wind gusts.

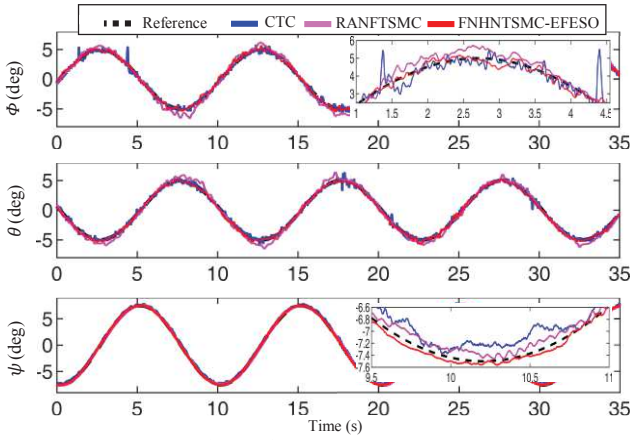

Fig. 37. Orientation (Φ, θ, ψ): Comparison under wind disturbance.

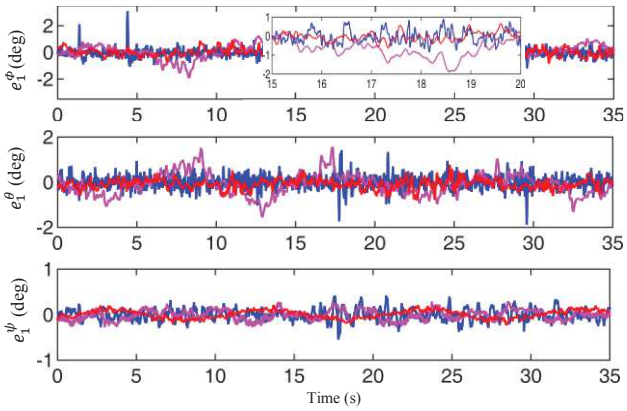

Fig. 38. Orientation errors $\left(e_1^{\Phi}, e_1^{\theta}, e_1^{\psi}\right)$: Comparison under wind disturbance.

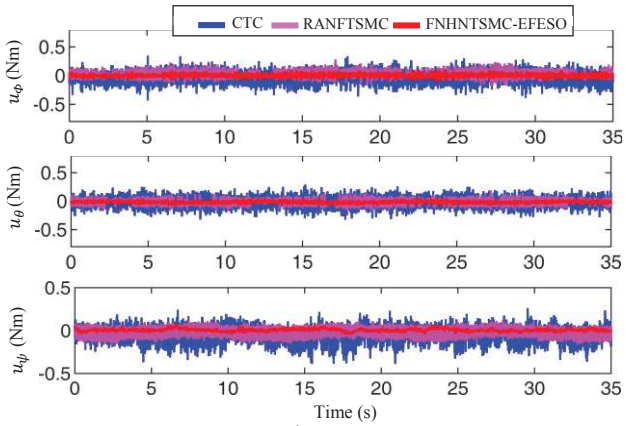

Fig. 39. Orientation errors $\left(e_1^{\Phi}, e_1^{\theta}, e_1^{\psi}\right)$: Comparison under wind disturbance.

5.2 Outdoor Trajectory Tracking Experiment

5.2.1 Hardware and Software Configuration

After conducting a Robot Operating System (*ROS*)/Gazebo simulation not presented here for the sake of space, a real outdoor flight experiment is performed. The complete experimental setup is shown in Fig. 1 in Section 2.2.1. The overall hardware and software configuration built for the quadrotor control in our experiment is depicted in Fig. 41. An onboard companion computer (Nvidia Jetson Nano computer (NJNC)) is connected through the Universal Asynchronous Receiver-Transmitter (UART) serial port to the Pixhawk® autopilot. The NJNC is running Ubuntu Bionic 18.04 operating system while the Pixhawk® autopilot is flashed by the PX4 firmware version 1.11.3. The autopilot communicates with other hardware using "*MAVLink*" protocol. The NJNC exchanges the data with the autopilot through a ROS package called "*MAVROS*". This package is the officially supported bridge between ROS and the "*MAVLink*" protocol. It enables "*MAVLink*" extendable communication between computers running "*ROS*" and "*MAVLink*" enabled autopilots. The control algorithm is implemented in the NJNC using ROS-melodic/C++ code. TP-LINK TL-AP1201P AC1200 dual-band outdoor wireless Wi-Fi router with omnidirectional antenna covering

200 m radius is used to create a wireless network. The quadrotor has been set to connect to this network using a USB Wi-Fi dongle automatically. An ASUS computer with the following specifications is used in the ground base station; Intel(R) Core (TM) i5-7300HQ CPU @ 2.50GHz 2.50 GHz, 20.0 GB RAM, and the operating system is Windows 10 Pro 64-bit. The ground computer can remotely access the onboard companion computer, i.e., NJNC, through its IP address over the Wi-Fi network using "*Putty*" software version 0.70 through SSH connection. This allows manually running the control algorithms by taping a shell command that initiates a ".launch" script that executes a C++ file containing the controller codes. For the sake of safety, the data monitoring, e.g., battery level, flight modes, localization, sensors of the quadrotor need to be displayed in real-time. To this end, radio telemetry modules are used to transmit the states of the quadrotor to "*QGroundControl*" software version 4.1.3 installed on the ground computer. The horizontal position (x, y) of each quadrotor is provided by M8N GPS module while the vertical position z is measured by a Benewake TF02-Pro 40m IP65 lidar. The attitude variables, i.e., $(\Phi, \theta, \psi), (p, q, r)$, are provided by the Inertial Measurement Unit (IMU) of the Pixhawk®. It is to be noted that a radio controller can also be used to control the quadrotor manually. Fig. 40 presents the hardware and software configuration layers in our experiment. Fig. 41 describes the implementation procedure of the proposed trajectory tracking controller for the quadrotor. The controller's outputs are the desired angular velocities which are sent to the Pixhawk® autopilot in "*Offboard Flight Mode* (OFM)". OFM is one of the automatic flight control modes of the Pixhawk® autopilot.

The trajectory tracking results of our proposed controller are presented from Fig. 42 to Fig. 44. In this experiment, the proposed FCS 4 is compared with the commercially available FCS 1 described in Table 4. The way in which the quadrotor follows the reference flight trajectory is presented in the 3-D state-space in Fig. 42. It is evident from this figure that the Cartesian trajectory is tracked accurately by FCS 4. Fig. 43 depicts the translational variables and Fig. 44 displays the profiles of the tracking errors for the Cartesian position. As illustrated in these two figures, the suggested FCS allows to precisely maintain the vehicle on the reference time-varying Cartesian trajectory compared to FCS 1. These practical results confirm the simulation findings drawn above in Section 4.2. The tracking errors are converging to the origin, where they steadily maintain their values in the close vicinity. Both ISE and RDP are computed and represented in Table 7. As a result, compared to the FCS 1, the tracking error has been considerably reduced as $(e_1^x \downarrow 68.17\%, e_1^y \downarrow 92.94\%, e_1^z \downarrow 50.69\%)$.

Table 7. Analysis of the ISE performance index for the trajectory tracking using the RDP criterion (Experimental results).

FCS	Performance index		
	ISE		
	e_1^x	e_1^y	e_1^z
FCS 1 (Pixhawk®)	5.97	6.24	2.59
FCS 4 (proposed)	**1.90**	**0.44**	**1.27**
Improvement (RDP) (%)	68.17	92.94	50.69

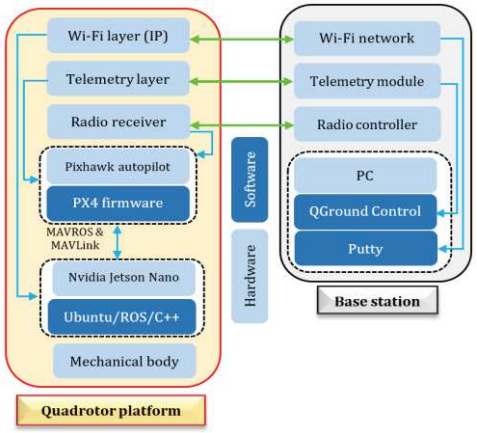

Fig. 40. Control system architecture, including hardware and software configuration layers in our experiment.

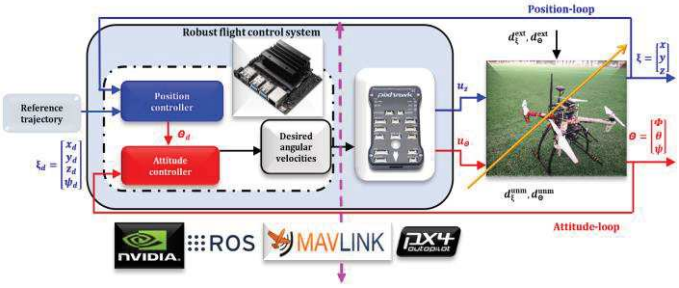

Fig. 41. Block diagram of the implementation procedure of the proposed trajectory tracking controller. The controller is implemented in the NJNC using ROS/C++ code. The orange arrow indicates parameters variation and unmodeled dynamics.

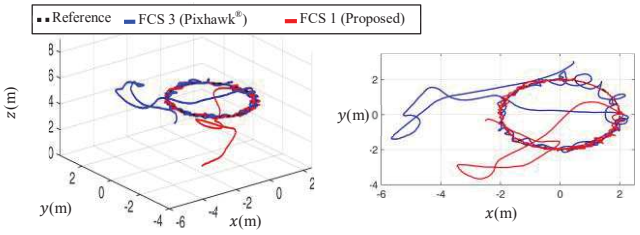

Fig. 42. 3-D trajectory tracking of the quadrotor.

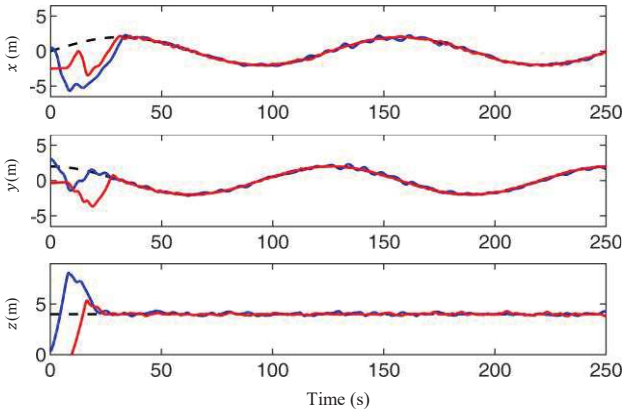

Fig. 43. Profiles of the position of the quadrotor (x, y, z).

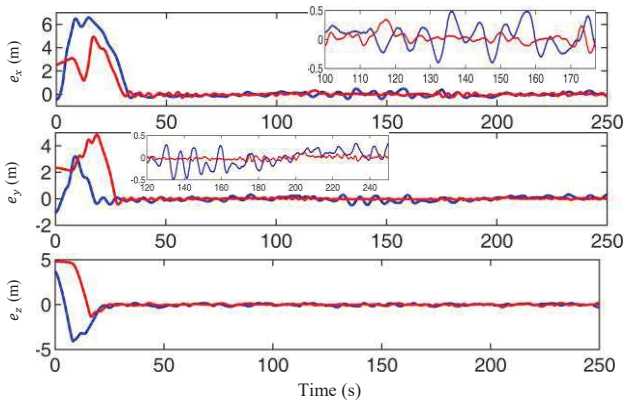

Fig. 44. Evolution of the position tracking errors (e_1^x, e_1^y, e_1^z).

6 Conclusion

In this study, the robust fixed-time tracking control problem for the multirotor system in the presence of various disturbances has been investigated. A Corollary that presents a control design methodology for systems with high-integrator dynamics has been established. Following this design procedure, a new observer-based control scheme has been proposed for the position and attitude loops within a hierarchical control framework. The developed control scheme drives the states of the system to the desired references in fixed-time uniformly w.r.t. the values of the ICs. Moreover, the control signal is nonsingular and smooth without switching frequencies. The convergence proofs of the developed fixed-time convergent algorithms have been analyzed based on proper LQF and ALE. Numerical simulations and real outdoor flight experiments have demonstrated the superiority of the designed controller in terms of performance improvements compared to other related controllers.

Further work could extend our results on fixed-time control of a single quadrotor to the fixed-time cooperative control of a group of quadrotors. This distinguishing feature is potentially vital in practical scenarios of the cooperative control of multi-agent systems, particularly those involving formation control of the quadrotors that are required to converge to the desired formation pattern in a short time.

Declaration of Competing Interest

The authors declare that there is no competing interest to disclose.

Acknowledgment

The authors would like to express their sincerest gratitude to the Co-Editor-in-Chief, Dr. Michael V. Basin, the Associate Editor, and the anonymous reviewers. Their insightful comments have helped to improve the quality of this paper noticeably.

Funding

This study is supported by the Fundamental Research Funds for the Central Universities under Grants No. ZYGX2018KYQD211 and No. ZYGX2019J084, the National Natural Science Foundation of China under Grant No. 61803075.

References

[1] O. Mechali, J. Iqbal, X. Xie, L. Xu and A. Senouci, "Robust finite-time trajectory tracking control of quadrotor aircraft via terminal sliding mode-based active antidisturbance approach: A PIL experiment," *International Journal of Aerospace Engineering,* Vols. 2021, Article ID 5522379, pp. 1-28, 2021.

[2] O. Mechali, X. Limei, W. Mingzhu, G. Fan and A. Senouci, "A rectified RRT* with efficient obstacles avoidance method for UAV in 3D environment," in *IEEE 9th Annual International Conference on CYBER Technology in Automation, Control, and Intelligent Systems (CYBER)*, Suzhou, China, 2019.

[3] F. Guo, M. Wei, M. Ye, J. Li, O. Mechali and Y. Cao, "An unmanned aerial vehicles collaborative searching and tracking scheme in three-dimension space," in *IEEE 9th Annual International Conference on CYBER Technology in Automation, Control, and Intelligent Systems (CYBER)*, Suzhou, China, 2019.

[4] O. Elhaki and K. Shojaei, "A novel model-free robust saturated reinforcement learning-based controller for quadrotors guaranteeing prescribed transient and steady state performance," *Aerospace Science and Technology,* vol. 119, pp. 1-29, 2021.

[5] S. Ullah, Q. Khan, M. Adeel, S. A. M. Kirmani and O. Mechali, "Neuro-adaptive fast integral terminal sliding mode control design with variable gain robust exact differentiator for under-actuated quadcopter UAV," *ISA Transactions,* 2021.

[6] M. A. Lotufo, L. Colangelo, C. Perez-Montenegro, E. Canuto and C. Novara, "UAV quadrotor attitude control: An ADRC-EMC combined approach," *Control Engineering Practice,* vol. 84, pp. 13-22, 2019.

[7] B. Ning, Q.-L. Han and Q. Lu, "Fixed-time leader-following consensus for multiple wheeled mobile robots," *IEEE Transactions on Cybernetics,* vol. 50, no. 10, pp. 4381-4392, 2020.

[8] S. Shao, S. Wang and Y. Zhao, "Fixed time robust trajectory tracking control for quadrotor UAV with disturbances," in *39th Chinese Control Conference (CCC)*, Shenyang, China, 2020.

[9] X. Shao, B. Tian and W. Yang, "Fixed-time trajectory following for quadrotors via output feedback," *ISA Transactions,* vol. 110, pp. 213-224, 2021.

[10] O. Mechali, L. Xu, Y. Huang, M. Shi and X. Xie, "Observer-based fixed-time continuous nonsingular terminal sliding mode control of quadrotor aircraft under uncertainties and disturbances for robust trajectory tracking: Theory and experiment," *Control Engineering Practice,* vol. 111, pp. 1-23, 2021.

[11] Z. Wang, Y. Su and L. Zhang, "Fixed-time attitude tracking control for rigid spacecraft," *IET Control Theory & Applications,* vol. 14, no. 5, pp. 790-799, 2020.

[12] H. Hou, X. Yu, L. Xu, K. Rsetam and Z. Cao, "Finite-time continuous terminal sliding mode control of Servo motor systems," *IEEE Transactions on Industrial Electronics,* vol. 67, no. 7, pp. 5647-5656, 2020.

[13] E. Reyes-Valeria, R. Enriquez-Caldera, S. Camacho-Lara and J. Guichard, "LQR control for a quadrotor using unit quaternions: Modeling and simulation," in *23rd International Conference on Electronics, Communications and Computing*, Cholula, Puebla, Mexico, 2013.

[14] O. Mechali, L. Xu, A. Senouci, X. Xie, C. Xin and A. Mechali, "Finite-time observer-based robust continuous twisting control for the attitude of

an uncertain quadrotor UAV subjected to disturbances," in *IEEE International Conference on Mechatronics and Automation (IEEE ICMA 2020)*, Beijing, China, 2020.

[15] J. Wang, X. Ma, H. Li and B. Tian, "Self-triggered sliding mode control for distributed formation of multiple quadrotors," *Journal of the Franklin Institute,* vol. 357, no. 17, pp. 12223-12240, 2020.

[16] C. A. Martínez-Fuentes, R. Seeber, L. Fridman and J. A. Moreno, "Saturated Lipschitz continuous sliding mode controller for perturbed systems with uncertain control coefficient," *IEEE Transactions on Automatic Control,* vol. 66, no. 8, pp. 3885-3891, 2021.

[17] V. Utkin, A. Poznyak, Y. Orlov and A. Polyakov, Road map for sliding mode control design, Switzerland: Springer Nature, 2020.

[18] O. Mechali, J. Iqbal, A. Mechali, X. Xie and L. Xu, "Finite-time attitude control of uncertain quadrotor aircraft via continuous terminal sliding-mode-based active anti-disturbance approach," in *IEEE International Conference on Mechatronics and Automation (ICMA)*, Takamatsu, Japan, 2021.

[19] F. Chen, R. Jiang, K. Zhang, B. Jiang, S. Member and G. Tao, "Robust backstepping sliding-mode control and observer-based fault estimation for a quadrotor UAV," *IEEE Transactions on Industrial Electronics,* vol. 63, no. 8, pp. 5044-5056, 2016.

[20] Z. Jia, J. Yu, Y. Mei, Y. Chen, Y. Shen and X. Ai, "Integral backstepping sliding mode control for quadrotor helicopter under external uncertain disturbances," *Aerospace Science and Technology,* vol. 68, pp. 299-307, 2017.

[21] D. J. Almakhles, "Robust backstepping sliding mode control for a quadrotor trajectory tracking application," *IEEE Access,* vol. 8, pp. 5515-5525, 2020.

[22] L. Fridman, J. A. Moreno, B. Bandyopadhyay, S. Kamal and A. Chalanga, "Continuous nested algorithms : The fifth generation of sliding mode controllers," in *Recent advances in sliding modes: From control to intelligent mechatronics*, Switzerland, Springer International Publishing, 2015, pp. 5-35.

[23] M. Boukattaya, H. Gassara and T. Damak, "A global time-varying sliding-mode control for the tracking problem of uncertain dynamical systems," *ISA Transactions,* vol. 97, pp. 155-170, 2020.

[24] Q. Guo, Q. Wang and X. Li, "Finite-time convergent control of electrohydraulic velocity servo system under uncertain parameter and external load," *IEEE Transactions on Industrial Electronics,* vol. 66, no. 6, pp. 4513-4523, 2019.

[25] L. Ding, Q.-L. Han, B. Ning and D. Yue, "Distributed resilient finite-time secondary control for heterogeneous battery energy storage systems under denial-of-service attacks," *IEEE Transactions on Industrial Informatics,* vol. 16, no. 7, pp. 4909-4919, 2020.

[26] B. Ning, X. Yu, G. Wen and Z. Cao, "Finite-time bipartite tracking control for double-integrator networked systems with cooperative and antagonistic interactions," *IEEE Transactions on Circuits and Systems I: Regular Papers,* vol. 67, no. 12, pp. 5223-5232, 2020.

[27] N. Wang, Q. Deng, G. Xie and X. Pan, "Hybrid finite-time trajectory tracking control of a quadrotor," *ISA Transactions,* vol. 90, pp. 278-286, 2019.

[28] D. Ma, Y. Xia, G. Shen, Z. Jia and T. Lib, "Flatness-based adaptive sliding mode tracking control for a quadrotor with disturbances," *Journal of the Franklin Institute,* vol. 355, no. 14, pp. 6300-6322, 2018.

[29] Y. E. Houm, A. Abbou, M. Labbadi and M. Cherkaoui, "Optimal new sliding mode controller combined with modified supertwisting algorithm for a perturbed quadrotor UAV," *International Journal of Aerospace Engineering ,* Vols. Volume 2020, Article ID 9753870, 10 pages, 2020.

[30] Z. Zuo, B. Tian, M. Defoort and Z. Ding, "Fixed-time consensus tracking for multi-agent systems with high-order integrator dynamics," *IEEE Transactions on Automatic Control,* vol. 63, no. 2, pp. 563-570, 2018.

[31] V. Andrieu, L. Praly and A. Astolfi, "Homogeneous approximation, recursive observer design, and output feedback," *SIAM Journal of Control and Optimization,* vol. 47, no. 4, pp. 1814-1850, 2008.

[32] A. Polyakov, "Nonlinear feedback design for fixed-time stabilization of linear control systems," *IEEE Transactions on Automatic Control,* vol. 57, no. 8, pp. 2106-2110, 2012.

[33] O. Mechali, J. Iqbal, J. Wang, X. Xie and L. Xu, "Distributed leader-follower formation control of quadrotors swarm subjected to disturbances," in *IEEE International Conference on Mechatronics and Automation (ICMA)*, Takamatsu, Japan, 2021.

[34] B. Ning, Q.-L. Han and Z. Zuo, "Practical fixed-time consensus for integrator-type multi-agent systems: A time base generator approach," *Automatica,* vol. 105, pp. 406-414, 2019.

[35] B. Ning, Q.-L. Han and Z. Zuo, "Distributed optimization for multiagent systems: An edge-based fixed-time consensus approach," *IEEE Transactions on Cybernetics ,* vol. 49, no. 1, pp. 122-132, 2019.

[36] M. Wang, B. Chen and C. Lin, "Fixed-time backstepping control of quadrotor trajectory tracking based on neural network," *IEEE Access,* vol. 8, pp. 177092-177099, 2020.

[37] W. Gong, K. Luo, B. Li, Y. Yang and H. Ban, "Fixed-time attitude tracking control for quadrotor UAVs under actuator failures," in *International Conference on Sensing and Instrumentation in IoT Era (ISSI)*, Lisbon, Portugal, 2019.

[38] X. Ai and J. Yu, "Fixed-time trajectory tracking for a quadrotor with external disturbances: A flatness-based sliding mode control approach," *Aerospace Science and Technology,* vol. 89, pp. 58-76, 2019.

[39] D. Ma, Y. Xia, G. Shen, H. Jiang and C. Hao, "Practical fixed-time disturbance rejection control for quadrotor attitude tracking," *IEEE Transactions on Industrial Electronics,* vol. 68, no. 8, pp. 7274-7283, 2021.

[40] M. Basin, Y. Shtessel and F. Aldukali, "Continuous finite- and fixed-time high-order regulators," *Journal of the Franklin Institute,* vol. 353, no. 18, pp. 5001-5012, 2016.

[41] B. Tian, H. Lu, Z. Zuo and H. Wang, "Fixed-time stabilization of high-order integrator systems with mismatched disturbances," *Nonlinear Dynamic,* vol. 94, pp. 2889-2899, 2018.

[42] A. Filippov, Differential equations with discontinuous right-hand side, Springer Science and Business Media Dordrecht, 1988.

[43] E. Bernuau, D. Efimov, W. Perruquetti and A. Polyakov, "On homogeneity and its application in sliding mode control," *Journal of the Franklin Institute,* vol. 351, no. 4, pp. 1866-1901, 2014.

[44] S. P. Bhat and D. S. Bernstein, "Geometric homogeneity with applications to finite-time stability," *Mathematics of Control, Signals and Systems,* vol. 17, pp. 101-27, 2005.

[45] R. A. Hor and C. R. Johnson, Matrix analysis, Cambridge University Press, 1990.

[46] L. N. Trefethen and D. B. III, NUmerical linear algebra, SIAM, 1997.

[47] Y. Wang and J. Hu, "Robust control for a quadrotor aircraft with small overshoot and high-precision position tracking performance," *Journal of the Franklin Institute,* vol. 357, no. 18, pp. 13386-13409, 2020.

[48] L. Rodolfo, G. Carrillo, A. E. D. López, R. Lozano and C. Pégard, Quad rotorcraft control, London U.K: Springer, 2013.

[49] Q. Quan, Introduction to multicopter design and control, Singapore: Springer Nature, 2017.

[50] A. Castillo, R. Sanz, P. Garcia, W. Qiu, H. Wang and C. Xu, "Disturbance observer-based quadrotor attitude tracking control for aggressive maneuvers," *Control Engineering Practice,* vol. 82, pp. 14-23, January 2019.

[51] N. V. Hien, V.-T. Truong and N.-T. Bui, "An object-oriented systems engineering point of view to develop controllers of quadrotor unmanned aerial vehicles," *International Journal of Aerospace Engineering,* vol. Article ID 8862864, 2020.

[52] M. Plesha, G. Gray and F. Costanzo, Engineering mechanics: Statics and dynamics: Second edition, New York: McGraw-Hill Higher Education, 2012.

[53] X. Shao, J. Liu and H. Wan, "Robust back-stepping output feedback trajectory tracking for quadrotors via extended state observer and sigmoid

tracking differentiator," *Mechanical Systems and Signal Processing,* vol. 104, pp. 631-741, 2018.

[54] N. Wanga, Q. Deng, G. Xie and X. Pan, "Hybrid finite-time trajectory tracking control of a quadrotor," *ISA Transactions,* vol. 90, pp. 278-286, 2019.

[55] H. Oleynikova, M. Burri, Z. Taylor, J. Nieto, R. Siegwart and E. Galceran, "Continuous-time trajectory optimization for online UAV replanning," in *2016 IEEE/RSJ International Conference on Intelligent Robots and Systems (IROS)*, Daejeon, South Korea, 2016.

[56] G. Rousseau, C. S. Maniu, S. Tebbani, M. Babel and N. Martin, "Minimum-time B-spline trajectories with corridor constraints. Application to cinematographic quadrotor flight plans," *Control Engineering Practice,* vol. 89, pp. 190-203, 2019.

[57] Q. Guo and Z. Chen, "Neural adaptive control of single-rod electrohydraulic system with lumped uncertainty," *Mechanical Systems and Signal Processing,* vol. 146, pp. 1-17, 2021.

[58] Q. Guo, Z. Zuo and Z. Ding, "Parametric adaptive control of single-rod electrohydraulic system with block-strict-feedback model," *Automatica,* vol. 113, pp. 1-9, 2020.

[59] H. Rabiee, M. Ataei and M. Ekramian, "Continuous nonsingular terminal sliding mode control based on adaptive sliding mode disturbance observer for uncertain nonlinear systems," *Automatica,* vol. 109, pp. 1-7, 2019.

[60] Z. Zuo, Q. Han and B. Ning, Fixed-time cooperative control of multi-agent systems, Switzerland: Springer Nature , 2019.

[61] W. Wu, X. Xie, M. Wei, M. Omar and L. Xu, "Planetary rover path planning based on improved A* algorithm," in *International Conference on Intelligent Robotics and Applications (ICIRA)*, 2019.

[62] V. Torres-González, T. Sanchez, L. M.Fridman and J. A.Morenob, "Design of continuous twisting algorithm," *Automatica,* vol. 80, pp. 119-126, 2017.

[63] R. Falcón, H. Ríos and A. Dzul, "Comparative analysis of continuous sliding-modes control strategies for quad-rotor robust tracking," *Control Engineering Practice,* vol. 90, pp. 241-256, 2019.

[64] J. Zhang, S. Yu and Y. Yan, "Fixed-time output feedback trajectory tracking control of marine surface vessels subject to unknown external disturbances and uncertainties," *ISA Transactions,* vol. 93, pp. 145-155, 2019.

[65] M. Basin, P. Yu and Y. Shtessel, "Finite- and fixed-time differentiators utilising HOSM techniques," *IET Control Theory & Applications,* pp. 1144-1152, 2017.

[66] L. Zhang, C. Wei, RongWu and N. Cui, "Fixed-time extended state observer based non-singular fast terminal sliding mode control for a VTVL reusable launch vehicle," *Aerospace Science and Technology,* Vols. 82-83, pp. 70-79, 2018.

[67] J. Ni, L. Liu, M. Chen and C. Liu, "Fixed-time disturbance observer design for Brunovsky systems," *IEEE Transactions on Circuits and Systems II: Express Briefs,* vol. 65, no. 3, pp. 341-345, 2018.

[68] B. Tian, L. Liu, H. Lu, Z. Zuo, Q. Zong and Y. Zhang, "Multivariable finite time attitude control for quadrotor UAV: Theory and experimentation," *IEEE Transactions on Industrial Electronics,* vol. 65, no. 3, pp. 2567-2577, 2018.

[69] A. Aboudonia, A. El-Badawy and R. Rashad, "Disturbance observer-based feedback linearization control of an unmanned quadrotor helicopter," *Proceedings of the Institution of Mechanical Engineers, Part I: Journal of Systems and Control Engineering,* vol. 230, no. 9, pp. 877-891, 2016.

[70] M. Labbadi and M. Cherkaoui, "Robust adaptive nonsingular fast terminal sliding mode tracking control for an uncertain quadrotor UAV subjected to disturbances," *ISA Transactions,* vol. 99, pp. 290-304, 2020.

[71] J. Ni, L. Liu, C. Liu, X. Hu and T. Shen, "Fixed-time dynamic surface high-order sliding mode control for chaotic oscillation in power system," *Nonlinear Dynamics,* vol. 86, pp. 401-420, 2016.